

**SOLID-STATE  $^{31}\text{P}$  NMR SPECTROSCOPY  
OF BACTERIOPHAGE M13 AND  
TOBACCO MOSAIC VIRUS**

Ontvangen.

23 FEB. 1995

UB-CARDEX



CENTRALE LANDBOUWCATALOGUS

0000 0611 3647

40951

**Promotor:**        **dr. T.J. Schaafsma**  
                         **hoogleraar in de moleculaire fysica**

**Co-promotor:**   **dr. M.A. Hemminga**  
                         **universitair hoofddocent bij de vakgroep Moleculaire Fysica**

**Pieter Magusin**

**SOLID-STATE  $^{31}\text{P}$  NMR SPECTROSCOPY  
OF BACTERIOPHAGE M13 AND  
TOBACCO MOSAIC VIRUS**

**Proefschrift**

ter verkrijging van de graad van doctor  
in de landbouw- en milieuwetenschappen  
op gezag van de rector magnificus,  
dr. C.M. Karssen,  
in het openbaar te verdedigen  
op woensdag 8 maart 1995  
des namiddags te vier uur in de Aula  
van de Landbouwuniversiteit te Wageningen

92-3

BIBLIOTHEEK  
LANDBOUWUNIVERSITEIT  
WAGENINGEN

CIP-GEGEVENS KONINKLIJKE BIBLIOTHEEK, DEN HAAG

Magusin, Pieter

Solid-state  $^{31}\text{P}$  NMR spectroscopy of bacteriophage M13 and  
tobacco mosaic virus / Pieter Magusin. - [S.l. : s.n.] -

III.

Proefschrift Landbouw Universiteit Wageningen. - Met lit.  
opg. - Met samenvatting in het Nederlands.

ISBN 90-5485-355-7 geb.

Trefw.: vaste-stof kernspinresonantie / spectroscopie /  
virussen.

## STELLINGEN

1. Zonder rekening te houden met de gereflecteerde lichtcomponent, loopt men bij de analyse van absorptie-metingen met gepolariseerd licht het risico de dichroïsche verhouding verkeerd te interpreteren in termen van moleculaire oriëntatie.

Azumi, R., Matsumoto, M. en Kawabata, Y. (1993) *J. Phys. Chem.* 97, 12862-12869

2. Dat toevoeging van Nod signaalmolekulen van de bacterie *Rhizobium meliloti* aan suspensies van *Medicago microcallus* cellen na 5 en 72 uur een verhoging van het aantal celkernen in de S-fase tot gevolg heeft, zou even goed kunnen wijzen op een blokkering, als op de door Savouré et al. gesuggereerde stimulering van de celdeling.

Savouré, A., Magyar, Z., Pierre, M., Brown, S., Schultze, M., Dudits, D., Kondorosi, A. & Kondorosi, E., (1994) *EMBO J.* 13, 1093-1102

3. De door Crespi et al. berekende hoge stabiliteit van de secundaire structuur van het 700 bp transcript van het *enod40* gen in *Medicago* planten sluit niet uit, dat een deel van dit transcript toch voor een klein eiwit codeert.

Crespi, M., Jurkevitch, E., Poiret, M., d'Aubenton-Carafa, Y., Petrovics, G., Kondorosi, E. & Kondorosi, A. (1994) *EMBO J.* 13, 5099-5112

4. Gezien de kleine atoomstraal en de hoge gyromagnetische verhouding van de helium isotoop  $^3\text{He}$ , verdient het aanbeveling het NMR-onderzoek aan poreuze materialen met  $^3\text{He}$ -gas in plaats van het meer gebruikelijke  $^{129}\text{Xe}$ -gas uit te voeren.

Seydoux, R., Diehl, P., Mazitov, R.K. & Jokisaari, J. (1993), *J. Magn. Reson.* 101, 78-83

5. Bij de bestudering van planteweefsels met behulp van NMR microscopie dient men voor een betrouwbare interpretatie van de resultaten rekening te houden met het effect van intercellulaire luchtholtes.

6. De veronderstelling dat door langzame beweging veroorzaakte transversale NMR relaxatie in het algemeen gekarakteriseerd wordt door een relaxatietijd in de orde van grootte van de correlatietijd van de beweging, gaat niet op voor rotationele diffusie

Alam, T.M. & Drobny, G.P. (1991) *Chem. Rev.* 91, 1945-1590; dit proefschrift.

7. De aanname van een ladder van rotor energienivo's om rotor resonantie effecten bij MAS NMR spectroscopie te verklaren, is slechts bij benadering in overeenstemming met de uit de quantum mechanica af te leiden energienivo's van een vrije macroscopische rotor.
8. Kennis over de glasovergang van voedingsmiddelen is van belang voor het nauwkeurig vaststellen van de optimale bewaarcondities.  
  
van den Berg, C. (1992) Carbohydrates in The Netherlands 8, 23-25
9. Indien te ver doorgevoerd, leidt de binnen een ministerie gebruikelijke interne controle om ervoor te zorgen dat openbare middelen worden uitgegeven aan waarvoor ze bedoeld zijn, juist tot het gebruik van andere openbare middelen voor waarvoor ze niet bedoeld zijn.
10. De Centraaleuropese volken hebben elkaar in de loop der eeuwen op cultureel gebied meer beïnvloed, dan menigeen ter plekke volmondig zou willen erkennen.
11. De promotie is de bevalling na een lastige zwangerschap.

Stellingen behorende bij het proefschrift:

"Solid-state  $^{31}\text{P}$  NMR spectroscopy of bacteriophage M13 and Tobacco Mosaic Virus"

P.C.M.M. Magusin

Wageningen, 8 maart 1995

**If you cannot - in the long run - tell everyone  
what you have been doing, your doing has been worthless.**

**Erwin Schrödinger**

**Aan Jiska en mijn ouders**

**cover figure:** the left first-order sideband in a magic-angle-spinning phase-sensitive two-dimensional exchange phosphorus nuclear-magnetic-resonance spectrum of 60% (w/w) M13 recorded at a resonance frequency of 202.5 MHz using a mixing time of 1 ms (unpublished). Inhomogeneous broadening causes the ridge-like shape of the sideband. Its approximately gaussian shape presumably reflects a continuous distribution of phosphodiester conformations (Chapter 4).



## Voorwoord

In dit proefschrift breng ik verslag uit van het onderzoek dat ik in het kader van een door de Stichting van Biofysica gefinancierd project heb uitgevoerd bij de vakgroep Moleculaire Fysica. Verschillende medewerkers van de vakgroep waren met raad en daad bij het project betrokken. Graag wil ik op deze plaats een aantal van hen met name bedanken: Tjeerd Schaafsma voor zijn bereidheid op te treden als mijn promotor, en Marcus Hemminga, mijn co-promotor, voor zijn geduldige begeleiding in al die jaren. Hartelijk dank ik Ruud Spruijt en Cor Wolfs voor de isolatie van de benodigde grote hoeveelheden virus-materiaal, Adri de Jager voor assistentie op het technische vlak en Gerrit Polder, Cornelis Schillemans en Frank Vergeldt voor hun hulp bij het oplossen van computerproblemen. Verder wil ik Arno Kentgens en Gerda Nachtegaal van de SON-faciliteit in Nijmegen bedanken voor hun hulp bij de vaak intensieve meetsessies aldaar. Verschillende studenten hebben in het kader van hun vakgroep-stage een waardevolle bijdrage geleverd aan mijn onderzoek: Leon ter Beek, Lucie van der Steeg en Jan-Jaap ter Horst, dank jullie wel! Mijn kamergenote op kamer 127 in het Transitorium, Marinette van der Graaf, dank ik voor haar prettige gezelschap. Bedankt ook Rik Leenders, Werner Stolle en Henk Franssen voor de talrijke keren dat ik met jullie mee kon rijden naar Wageningen en terug. Tenslotte wil ik mijn ouders en Jiska, mijn vrouw, bedanken voor hun morele steun in de verschillende stadia van mijn promotie-onderzoek en de afronding ervan in de vorm van dit proefschrift.

Pieter

# **CONTENTS**

<b>Chapter 1</b>	<b>1</b>
General Introduction	
<b>Chapter 2</b>	<b>12</b>
A theoretical study of rotational diffusion models for rod-shaped viruses. The influence of motion on $^{31}\text{P}$ nuclear magnetic resonance lineshapes and transversal relaxation. (published in 1993, Biophys. J. 64 , 1851-1860)	
<b>Chapter 3</b>	<b>23</b>
Analysis of $^{31}\text{P}$ nuclear magnetic resonance lineshapes and transversal relaxation of bacteriophage M13 and tobacco mosaic virus (published in 1993, Biophys. J. 64 , 1861-1868)	
<b>Chapter 4</b>	<b>32</b>
Analysis of $^{31}\text{P}$ MAS NMR spectra and transversal relaxation of bacteriophage M13 and tobacco mosaic virus (published in 1994, Biophys. J. 66 , 1197-1208)	
<b>Chapter 5</b>	<b>45</b>
2D-Exchange $^{31}\text{P}$ NMR spectroscopy of bacteriophage M13 and tobacco mosaic virus (published in 1995, Biophys. J. 68, final manuscript version)	
<b>Appendix</b>	<b>57</b>
Naming of the binding sites in TMV	
<b>Summary</b>	<b>61</b>
<b>Samenvatting</b>	<b>63</b>
<b>Curriculum Vitae</b>	<b>65</b>

## **CHAPTER 1**

### **General Introduction**

## General Introduction

### TMV: infection, structure and assembly

Although a series of related plant viruses is actually classified as tobacco mosaic viruses or tobamoviruses, the name tobacco mosaic virus (TMV) is generally used to refer specifically to the common and most investigated Vulgare (or U1) strain (Butler, 1979). In this thesis, this common practice will be followed. TMV is a single-stranded RNA virus, which can be isolated with relatively high yield from infected plants (1-5 g/kg) (Hwang et al., 1994). Little is known about the early events in infection of tobacco plants with TMV (Wilson, 1985). This is largely due to the fact that plant infection is a complex, slow and asynchronous process. Some form of wounding of the plant protoplasts is required for initiating a synchronous infection in a population of host plants (Hwang et al., 1994), indicating that TMV infects by direct penetration via local, transient wounding of the plasma membrane (Burgess et al., 1973a, Burgess et al., 1973b; Kassanis et al., 1977). However, another mechanism similar to the disassembly of bacteriophage

M13 in the bacterial membrane has also been suggested (Durham, 1978): upon membrane attachment, the TMV virion would become destabilized by protein-lipid interactions and the release of  $\text{Ca}^{2+}$  from the virion core. The uncoating of the destabilized virus would then be driven by the translation of the viral RNA by the ribosomes, as the RNA enters the host cell. In contrast to M13 coat protein, however, TMV coat protein does not insert into the membrane (Datema, 1987). The viral RNA encodes for four proteins (Goelet et al., 1982; Ohno et al., 1984). Two of these proteins are involved in the replication of the RNA (Ishikawa et al., 1986), a third one plays a role in the cell-to-cell movement of TMV to adjacent cells through the plasmodesmata (Tomenius et al., 1987), and the fourth is the coat protein necessary for the formation of virus particles, which are probably also involved in the long-distance movement of TMV between distant parts of the infected plant (Saito et al., 1990). After synthesis in the cytoplasm, the coat protein

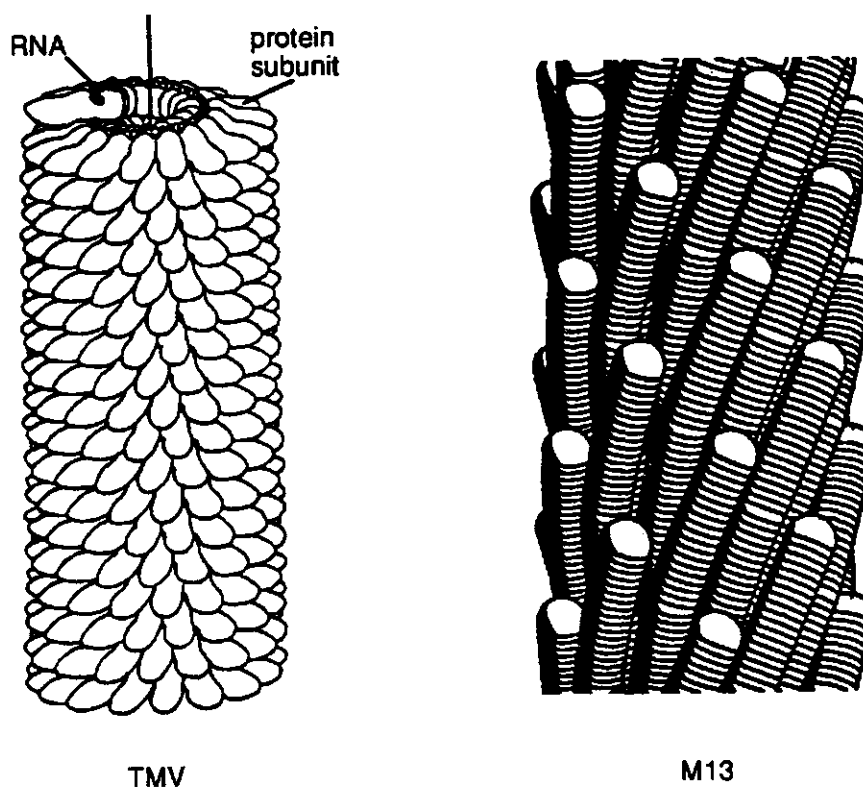


FIGURE 1: Schematic drawing of a virus particle of TMV (left) and M13 (right) (from Butler, 1984, and Marvin, 1990, respectively). TMV: The protein subunits are arranged in a one start helix of 49 subunits per three turns. Also indicated is part of the RNA molecule, which is bound with three nucleotides per protein subunit. M13: The  $\alpha$ -helical coat proteins, drawn as gently-curved rods almost parallel to the virion axis, are arranged in a five-start helix overlapping each other as scales of a fish.

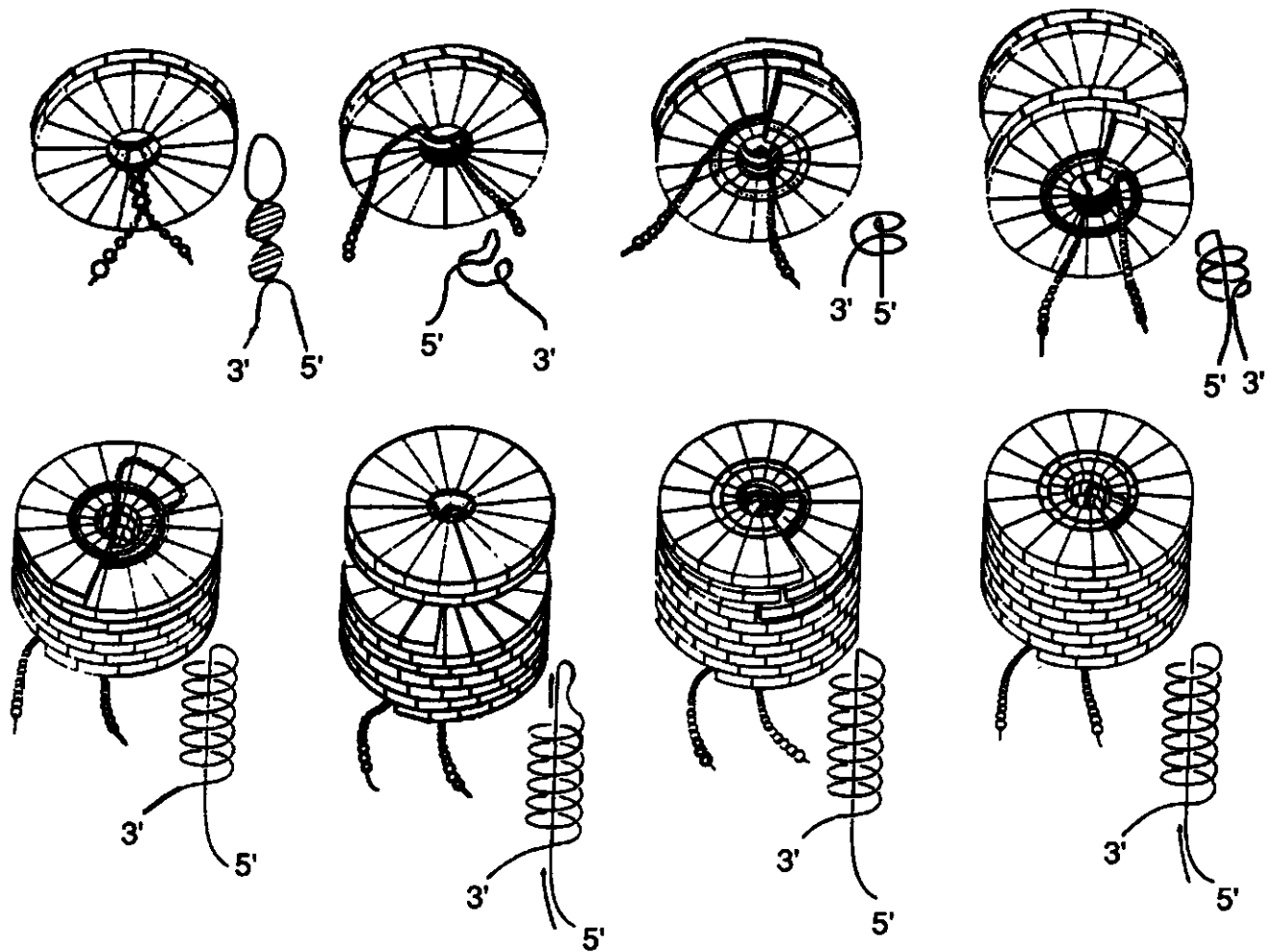


FIGURE 2: Possible scheme for nucleation and elongation in TMV assembly (see text) (from Butler, 1984).

accumulates in the chloroplasts and interacts with the light-harvesting photosystems (especially PSII) in thylakoids, giving rise to the disease phenotype after which the virus is named (Reinero and Beachy, 1989).

TMV particles have the shape of a rod with a length of 300 nm and an outer diameter of 18 nm (Fig. 1a). The protein coat is formed by 2,130 subunits ( $M=17,500$  Da) arranged in a helix with 49 subunits per three turns. The structure of the RNA molecule, which consists of 6,395 nucleotides, has been well determined. It is buried within the coat between layers of subunits, following the protein helix with three nucleotides per protein subunit and the phosphates at a radius of  $\sim 4$  nm (Stubbs et al., 1977). Various sorts of binding between RNA and protein subunits inside TMV have been suggested: electrostatic interactions between phosphodiester and arginine residues, hydrophobic interactions between the nucleotide bases and the left radial  $\alpha$ -helix of the subunits, and hydrogen bridges (Stubbs and Stauffacher, 1981). As a consequence of the strong correlation between the geometry of the protein coat and the encapsulated RNA, three types of phosphates can be distinguished in the nucleic acid backbone. One of these three phosphate types has a relatively high level of disorder (Cross et al., 1983a). Indeed, in RNA-protein interaction models for TMV, two phosphates are generally interacting closely

with arginine residues, whereas no arginine is close to a third one (see Appendix).

Dissociated coat subunits and RNA of TMV spontaneously reassemble under suitable conditions into virus particles (Fraenkl-Conrat and Williams, 1955). Numerous *in vitro* studies have resulted in a detailed model for TMV self-assembly *in vivo* (Fig. 2). At physiological pH, TMV coat proteins form disc-shaped aggregates with two ring-like layers of 17 proteins each (Butler and Klug, 1978). The subunits in the protein disc largely have a well-defined structure including four  $\alpha$ -helices connected by a strip of  $\beta$ -sheet (Bloomer et al., 1978). A stretch of 24 amino residues, however, is highly mobile (Jardetzky et al., 1978; de Wit et al., 1979), forming a flexible loop located within a radius of 4.0 nm in the central core of the protein disc. The assembly of a virion is initiated by selective interaction of a protein disc with a specific part of the viral RNA molecule, the origin-of-assembly sequence (OAS). The uncoated OAS region probably forms a RNA hairpin, which can insert into the central hole of the protein disc. The loop of the hairpin then intercalates between the two layers of the protein disc. Among other nucleoprotein interactions, the residues Arg90 and Arg92 in the flexible loops of the protein units make salt-bridges with the RNA phosphates. As a result, the flexible loops of the protein units in the disc become immobilized forming the

so-called V-columns ("V" for vertical) (Stubbs et al., 1977). The close interactions between V-columns of adjoining subunits probably force the disc to transform into a helix of two turns, the so-called lock washer. At this stage, both the 3' and 5'-RNA tail protrude from the same side of the lock washer. A second protein disk approaches from the opposite side and interacts with the RNA. It pulls up the 5'-tail and transforms into a lock washer, as well. Additional disks then add to the nucleoprotein complex in a similar way, and the complex elongates to a specific length. The lock washers stack on top of each other, forming a continuous protein helix of several turns. This elongation process is repeated until the 5'-tail of the RNA has been completely encapsulated. Meanwhile, the 3'-tail becomes covered much more slowly, perhaps by the binding of smaller aggregates of coat proteins (Butler, 1979).

### Filamentous bacteriophages: life cycle and structure

Filamentous bacteriophages (Inovirus) form a large group of related virus strains with similar morphology and life cycle (Rasched and Oberer, 1986). They infect gram-negative bacteria by adsorbing to the tip of specific bacterial pili. Some of the strains, like M13, fd, f1, Ike, I2-2 and If1, share *Escherichia coli* as a host, but differ in the specificity for its pili. For instance, M13, fd and f1 infect *E. coli* via its F-pili. Other examples are Pf1, Pf2 and Pf3, which infect *Pseudomonas aeruginosa*, and Xf, a virus of the plant pathogen *Xanthomonas oryzae*. Upon adsorption, the protein coat of the Inovirus virion dissolves into the inner cell membrane (Marvin, 1989), and the circular, single-stranded DNA consisting of ~ 6500 nucleotides ( $\pm 10\%$ ) (Day et al., 1988) enters the host cell, while being converted into the double-stranded replicative form. This DNA synthesis probably drives the disassembly of the virion (Marco et al., 1974). Inside the host cell, new single-stranded DNA is synthesized off the replicative form by the "rolling circle" mechanism (Gilbert and Dressler, 1968). The new progeny viral DNA is covered by the DNA-binding protein g5p encoded by the viral gene-5, resulting in an intra-cellular rod-shaped nucleoprotein complex, morphologically similar to the virion outside the cell, but less stable. In contrast to most bacterial viruses, which are released from the host by cell lysis, the filamentous bacteriophages are continuously assembled and extruded through the bacterial membrane without killing the host cell. During this phage extrusion, g5p is exchanged by the major coat protein encoded by the viral gene 8, also called gene-8 protein (g8p). The negative charge of the headgroups of the lipid molecules in the bacterial membrane may play a role in the release of g5p (Butler, 1979). A model for assembly of the virion at membrane adhesions has been suggested on the basis of the "telescoping" behaviour of the virions in certain organic solutions *in vitro* (Marvin, 1989).

Outside the host cell, Inovirus exists as rod-shaped nucleoprotein particles with a diameter of ~ 6 to 9 nm and a length between ~ 700 and 2000 nm, depending on the strain and relative humidity (Day et al., 1988; Dunker et al., 1974). Their protein coat mainly consists of several thousand (2000 - 7000) copies of g8p, a protein

of ~ 50 amino acids (Day et al., 1988). Although the actual amino acid sequence of g8p differs among various Inovirus strains, its geometry is essentially a slightly curved  $\alpha$ -helix for all of them. Strong homology also exists at the level of charge distribution along the protein: there is a collection of acidic and basic residues near the N-terminus and C-terminus, respectively, and a hydrophobic stretch between the two charged ends. Subunits in the protein coat of Inovirus virions are oriented with their helical axis roughly parallel to the virion axis, thereby partly overlapping one another as scales of a fish (Fig. 1b) (Marvin, 1990). They form a tubular protein shell with the acidic N-termini at the outside and the basic C-termini at the inside of the tube. X-ray diffraction studies have established two different classes on the basis of the protein coat structure. The symmetry of the protein coat of Class I phages, which include the strains Ff (fd, f1 and M13), If1 and Ike, involves a 5-fold rotation axis combined with a 2-fold screw axis of pitch 32 Å (Fig. 1b) (Banner et al., 1981; Marvin, 1990; Marvin et al., 1994). In Class II phages (Pf1, Pf3 and Xf), the subunits of the protein coat are arranged according to a one-start helix with 15 Å pitch and 22 units per five turns (Marvin et al., 1974; Marvin, 1990). Protein products of other genes are located at the two ends of the virion. The virion end, which emerges first from the host cell, contains the gene-7 and gene-9 proteins, without which virus particles are hardly formed (Russel, 1991). The four or five copies of gene-3 protein and gene-6 protein at the other virion end, are required, respectively, for adsorption and penetration, and for locking the tube into place (Russel, 1991).

In contrast to the structure of the protein coat, little is known about the geometry of the DNA molecule encapsulated in the virion, other than that the DNA molecule seems to be located inside the virion within a core of less than 2.5 nm wide (Banner et al., 1981; Russel, 1991), where it is immobilized by interactions with the protein coat (DiVerdi and Opella, 1981b; Cross et al., 1983b). For Class I viruses, these nucleoprotein interactions are predominantly of an electrostatic, non-specific nature. Each g8p subunit has four positively charged residues at conserved positions in the C-terminal facing the inside of the protein shell, which are able to neutralize the negative charges of the phosphodiester in the encapsulated DNA. Replacement of one positively charged residue (Lys48) by a neutral residue results in mutant virions that are 33% longer than wild-type virions (Hunter et al., 1987). There are no indications for any interaction between aromatic g8p residues and the bases of the encapsulated DNA. In Ff-virions, the nucleotides interact among themselves by base stacking (Day, 1973), but the estimated interbase distance of 3.4 Å is difficult to reconcile with the mean axial rise of 2.7 Å per nucleotide expected for homogeneous distribution of DNA along the inside of the protein coat, as commonly assumed (Day et al., 1979; Banner et al., 1981). Although nucleoside sugar pucker and glycosyl torsion are similar as for A-DNA, only 20% of the viral DNA at most seems to have the regular phosphodiester backbone found in A-DNA (Thomas et al., 1988). In fact, the DNA backbone mainly has phosphodiester with B-type conformation (Fritzsche et al., 1981), or may even be

largely disordered (Cross et al., 1983b). Based on the generally non-integral ratio between the number of subunits and nucleotides, e.g. 1 : 2.4 for Ff-viruses, helical double-stranded DNA models have been suggested for Class-I viruses with the bases directed inward, but not necessarily forming (canonical) base-pairs. In these models, the symmetry of the DNA-helix and the protein coat differ, so that consecutive phosphodiester in the nucleic acid backbone interact differently with the protein coat. Such complex phosphodiester inhomogeneity could perhaps explain the lack of experimental evidence for any regular geometry of the encapsulated DNA molecule. A similar DNA-model with the bases facing inward has also been proposed for the Class-II virus Xf. For Pf1 and Pf3, other members of Class-II, "bases-out" models have been suggested with the nucleotide bases of the encapsulated DNA interacting with the tyrosine residues of the coat protein subunits (Day et al., 1979; Kostrikis et al., 1994). In Pf1, the DNA structure would be sufficiently open, for lysine and arginine side chains to reach into the virion core and neutralize the negative charge of the nucleic acid phosphates located at a 2.5-Å distance from the virion axis (Liu and Day, 1994; Day et al., 1988; Day et al., 1979). In Pf3, the negative charge of the DNA backbone is perhaps balanced by the presence of metal cations, like  $\text{Ca}^{2+}$  or  $\text{Mg}^{2+}$ , in the virion core. In this thesis, we have studied bacteriophage M13, well-known for its use as a DNA-packaging vehicle in biochemistry, as an example for Inovirus in general, and Ff-viruses, more specifically.

### **$^{31}\text{P}$ NMR studies of nucleic acids and nucleoprotein complexes**

Phosphorus ( $^{31}\text{P}$ ) nuclear magnetic resonance (NMR) spectroscopy is a powerful technique for obtaining information about structure and dynamics of nucleic acids and nucleic acid complexes in solution or gel. At present, it is commonly accepted that conformational heterogeneity exists in nucleic acid structures. Structure variations in long DNA duplexes have largely been established by x-ray crystallography. NMR spectroscopy has especially provided detailed knowledge about local structures in oligonucleotides, such as e.g. hairpins and pseudo-knots. Novel two-dimensional (2D) and three-dimensional (3D)  $^1\text{H}/^{31}\text{P}$  NMR methods have made it possible to assign the  $^{31}\text{P}$  NMR spectrum of oligonucleotides with a length up to 14 basepairs (Schröder et al., 1987), so that specific information on the conformation of each of the phosphodiester in the nucleic acid backbone can be obtained in these molecules. Relatively large variations in phosphodiester conformation are found (van de Ven and Hilbers, 1988). Moreover, molecular dynamics calculations suggest that the structures arising from x-ray and NMR studies still represent time-averaged structures only and that an even larger variety of conformations temporarily exist at a time-scale of picoseconds (Scheek, 1994).

Because the electron distribution surrounding a phosphorus nucleus in a nucleic acid molecule is far from spherical, its  $^{31}\text{P}$  chemical shift measured by NMR spectroscopy, in principle, depends on the molecular orientation with respect to the external magnetic field.

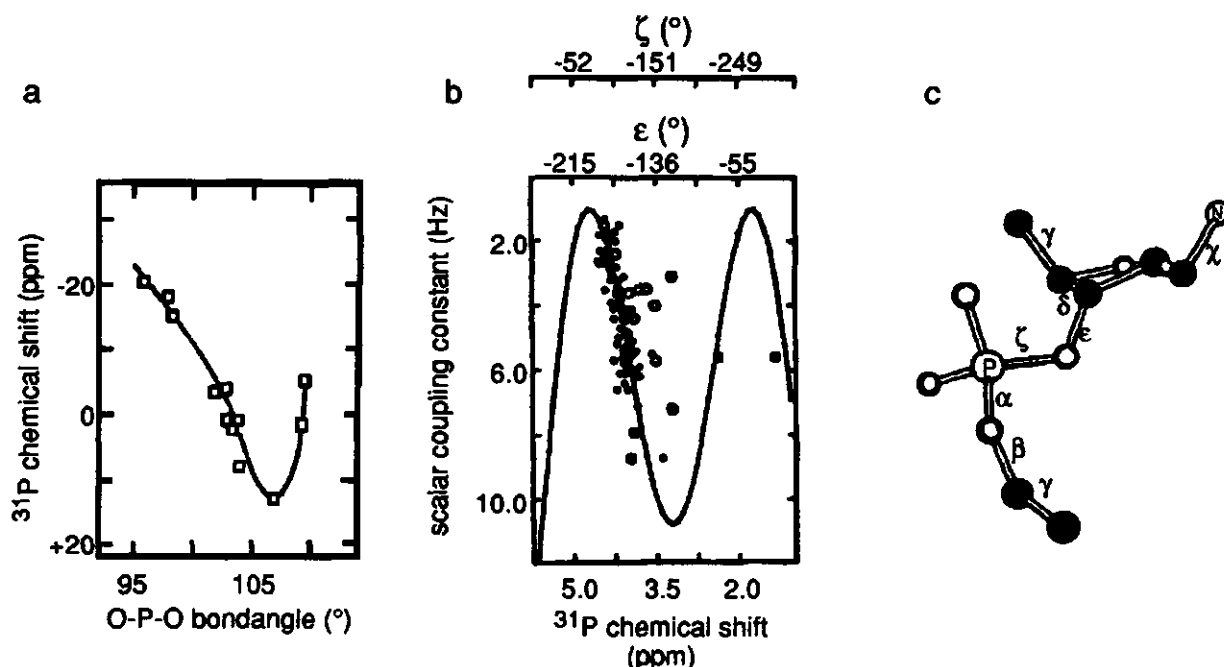


FIGURE 3: Dependence of  $^{31}\text{P}$  chemical shift on conformational and stereo-electronic factors. a: correlation plot for  $^{31}\text{P}$  chemical shift of phosphodiester versus the smallest O-P-O bond angle. b: correlation between the constant  $J_{\text{H}3'-\text{P}}$  for scalar coupling between  $^{31}\text{P}$  and  $^1\text{H}_{3'}$  and  $^{31}\text{P}$  chemical shift in oligonucleotides. The solid curve in the figure represents the theoretically derived Karplus relation between  $J_{\text{H}3'-\text{P}}$  and the CO-torsion angle  $\epsilon$ , which in turn, in a large variety of structures is correlated to the PO-torsionangle  $\zeta$ . By variable scaling of the coupled  $\epsilon$  and  $\zeta$  axes, the Karplus curve can be made to fit to the data points. In this way, a correlation between the chemical shift and the two coupled torsionangles is established. c: definition of the various torsionangles (from Gorenstein, 1994).

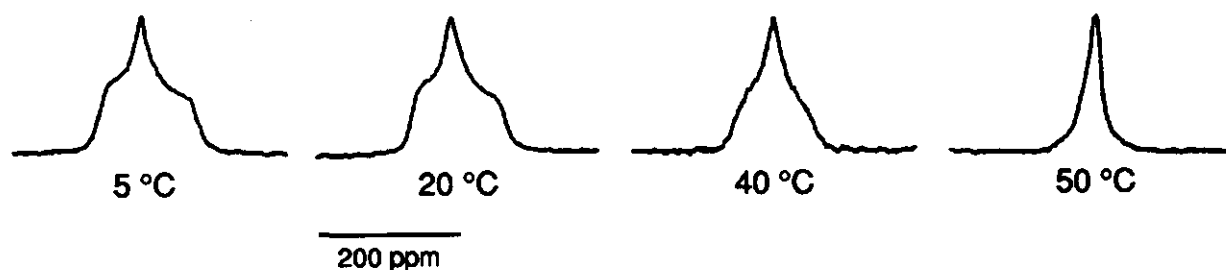


FIGURE 4: 61-MHz  $^{31}\text{P}$  NMR spectra of B-form DNA at various temperatures indicating different mobility (from DiVerdi, and Opella, 1981a.).

This chemical shift anisotropy (CSA) can be described in terms of a shielding tensor with three principal components  $\sigma_{11}$ ,  $\sigma_{22}$  and  $\sigma_{33}$ . In (dilute) solutions, however, fast tumbling of oligonucleotides and segmental motion of larger nucleic acid molecules tend to average the shift, leaving only the isotropic chemical shift  $\sigma_{\text{iso}}$  to be measured. A number of attempts has been made to calculate the  $^{31}\text{P}$  chemical shift tensor and especially  $\sigma_{\text{iso}}$ , for phosphodiester in nucleic acids and model compounds (Prado et al., 1979; Giessner-Prettre et al., 1984). These calculations point out that many factors, including electron negativity, bondangle and  $\pi$ -electron overlap, can affect the  $^{31}\text{P}$  chemical shift, indicating that no single factor can unequivocally explain an observed range or change of  $^{31}\text{P}$  shift. Empirically, a correlation between  $^{31}\text{P}$  chemical shifts and the smallest O-P-O angle has been found for a wide variety of alkylphosphates and oligonucleotides. At increasing bondangle between  $95^\circ$  and  $108^\circ$ ,  $\sigma_{\text{iso}}$  increases by as much as  $\sim 35$  ppm (Fig. 3a) (Gorenstein, 1981). At further increasing bondangle above  $108^\circ$ ,  $\sigma_{\text{iso}}$  decreases again (Gorenstein, 1994). Another correlation is experimentally observed between  $\sigma_{\text{iso}}$  and the scalar coupling constant  $J_{\text{H}3'-\text{P}}$  for the three-bond coupling constant between  $\text{H}_{3'}$  and P (Fig. 3b). Because  $J_{\text{H}3'-\text{P}}$  can be interpreted in terms of the CO torsionangle  $\epsilon$  (Fig. 3c) via a Karplus relationship (Lankhorst et al., 1984), and a linear correlation between  $\epsilon$  and the PO torsionangle  $\zeta$  is found in a variety of duplex structures (Gorenstein, 1994), the correlation between  $\sigma_{\text{iso}}$  and  $J_{\text{H}3'-\text{P}}$  actually reflects the influence of the stereo-electronic factors on the  $^{31}\text{P}$  chemical shift. This semi-empirical correlation between  $\sigma_{\text{iso}}$  and the *coupled* torsionangles  $\epsilon$  and  $\zeta$ , should be distinguished from the *separate* correlations between  $\sigma_{\text{iso}}$  and the P-O torsionangles  $\zeta$  and  $\alpha$ , and between  $\sigma_{\text{iso}}$  and the C-O torsionangles  $\epsilon$  and  $\beta$ , previously suggested on a theoretical basis (Gorenstein, 1981; Giessner-Prettre et al., 1984). Environmental effects on  $^{31}\text{P}$  chemical shifts are generally smaller than the intrinsic structural effects. A shift change of about 3 ppm is observed upon changing the solvent from 100%  $\text{H}_2\text{O}$  to 70% DMSO (Lerner and Kearns, 1980), or the salt concentration from 0 to 5 M (Costello et al., 1976). The bases with their ring-current in the double helical nucleic acids have only small effect on the chemical shift ( $< 0.1$  ppm) (Gorenstein et al., 1988).

Because the range of  $^{31}\text{P}$  chemical shifts for individual phosphates in duplex fragments in solution is typically  $< 0.9$  ppm, resonance lines can generally not be resolved individually in  $^{31}\text{P}$  NMR spectra of nucleic acids longer than 100 basepairs. For this reason, most of the

$^{31}\text{P}$  NMR work on DNA fragments with a length of a few hundred basepairs has concentrated on  $^{31}\text{P}$  relaxation. The measured longitudinal relaxation time ( $T_1$ ), transversal relaxation time ( $T_2$ ), and nuclear overhauser effect (NOE) are usually interpreted in terms of models, which necessarily represent simplifications as compared to the complicated nature of the flexible DNA. A more realistic description of the complex backbone dynamics would require more variables to be fitted, than justified by the amount and quality of the experimental data. Some authors, for instance, assign all relaxation effects to dipolar relaxation between  $^{31}\text{P}$  and the nearest 3', 5' and 5"-protons, assuming the  $^{31}\text{P}$  -  $^1\text{H}$  internuclear distances to be invariant and neglecting the relaxation by the  $^{31}\text{P}$  chemical shift anisotropy (Hogan and Jardetzky, 1980; Bolton and James, 1979). Internal motion of the  $^{31}\text{P}$  -  $^1\text{H}$  internuclear vector has been simplified to two-site exchange (Hogan and Jardetzky, 1980), jumping (Keepers and James, 1982), rotation about a single axis (Bolton and James, 1979) and wobbling (Lipari and Szabo, 1981). Long range bending of the nucleic acids is sometimes approximately described as isotropic motion (Bolton and James, 1979; Opella et al., 1981). Relaxation data are also analyzed by use of a rigid-rod model for the DNA duplex fragment, regarded as a stiff helix (Shindo, 1980). Other authors incorporate collective torsional motion along the DNA duplex into their model (Allison et al., 1982). The large variety of models in the literature, illustrates the lack of unanimity about the details of the motions that mainly cause the observed  $^{31}\text{P}$  NMR relaxation. Several assumptions about the local molecular structure and the predominant relaxation mechanism must usually be made to interpret relaxation in a system of dipolar coupled spins. For  $^{31}\text{P}$  NMR relaxation, CSA-relaxation should also be taken into account. Given the small amount of experimental data, different models, varying in nature between "model-freely" simple and realistically detailed, are equally acceptable. Additional information is necessary to decide between them.

In contrast to the  $^{31}\text{P}$  NMR spectra of DNA duplex fragments in solution,  $^{31}\text{P}$  NMR spectra of dehydrated DNA or large nucleoprotein complexes, such as viruses, potentially offer a wealth of additional mobility information.  $^{31}\text{P}$  NMR spectra of concentrated gels of these large systems generally contain a single broad resonance line reflecting the average  $^{31}\text{P}$  chemical shift anisotropy (CSA) typical for phosphates in DNA or RNA (Fig. 4) (DiVerdi and Opella, 1981a; DiVerdi and Opella, 1981b). In most cases, the observed lineshape also shows signs of motional narrowing and therefore contains information about the underlying motion. It is important to note, that motional distortion of the  $^{31}\text{P}$



lineshapes not merely represents yet another single-valued input for motional analysis, just like  $T_1$  and  $T_2$  values measured for DNA fragments in solution. Partially averaged  $^{31}\text{P}$  NMR lineshapes are typically 200 ppm wide and are therefore defined in the spectrum by a series of data points, each of which carries information about the motions involved. Given the large variety of relaxation models for DNA fragments in solution and the lack of sufficient experimental data to decide between them, it is quite surprising that until this thesis, no studies had been published about quantitatively analyzing or simulating  $^{31}\text{P}$  NMR lineshapes of concentrated nucleic acid or nucleoprotein gels, except in a superficial way (Fig. 5) (Tsang and Opella, 1986). Most authors restrict themselves to qualitative remarks about the motion involved (DiVerdi and Opella, 1981b; Mai et al., 1983). It should be mentioned in this respect, that the literature does contain publications about  $^2\text{H}$  NMR lineshape simulations for  $^2\text{H}$ -labeled nucleic acids (Brandes and Kearns, 1988; Alam and Drobny, 1991) and  $^{31}\text{P}$  NMR lineshape simulations for phospholipids (Dufourc et al., 1992).

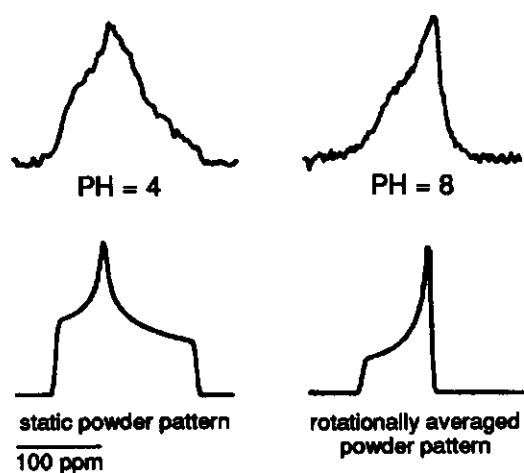


FIGURE 5:  $^{31}\text{P}$  NMR lineshape of bacteriophage Pfl at different pH values. The theoretical lineshapes were calculated, assuming either the complete absence of motion, or complete averaging by fast motion of the rod-shaped virions about their length axis (from Tsang and Opella, 1986).

In large nucleoprotein complexes, such as viruses,  $^{31}\text{P}$  nuclei represent natural NMR labels for studying structural and dynamic properties of the nucleic acid backbone selectively, even when the complex mainly consists of proteins. Indeed, during the last fifteen years  $^{31}\text{P}$  NMR studies of various viruses have appeared in the literature. In one class of studies, rapidly tumbling, mostly spherical viruses, such as the plant viruses alfalfa mosaic virus (AIMV), cowpea mosaic virus (CpMV), tomato bushy stunt virus (TBSV) and the bacteriophages Q $\beta$  and MS2, have been investigated in dilute solution by use of high resolution NMR spectroscopy (Kan et al., 1987; Virudachalam et al., 1985; Munowitz et al., 1980; Bolton et al., 1982). In these studies conclusions about the dynamic behaviour of the nucleic acids inside the virions have been drawn from linewidths and relaxation times. In other studies, solid state NMR techniques have been used to record  $^{31}\text{P}$  spectra of viruses in more

concentrated solutions or viscous gels, such as TBSV, the rod-shaped tobacco mosaic virus (TMV) and the bacteriophages Pfl and fd (Munowitz et al., 1980; Cross et al., 1983a; Tsang and Opella, 1986; DiVerdi and Opella, 1981b; Cross et al., 1983b). From qualitative lineshape analyses, conclusions were drawn about motional frequencies and amplitudes, which agree with the general picture evolved from dilute solution studies: nucleic acids inside virions do not undergo large amplitude motions at frequencies higher than  $10^4$  Hz and motional lineshape effects observed in dilute solutions can be explained by overall motion of the viral particle as a rigid body.

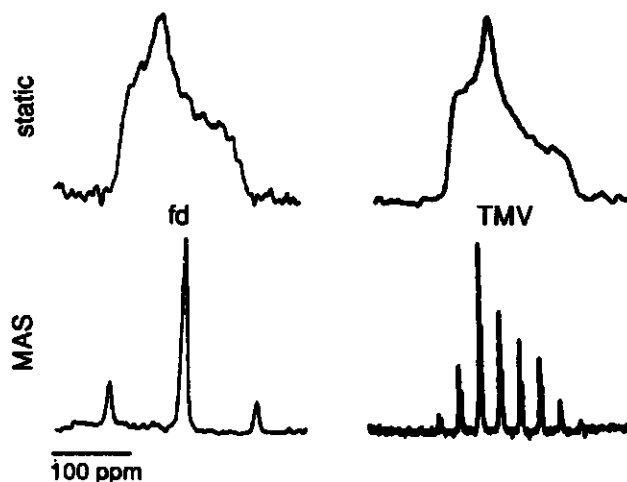


FIGURE 6:  $^{31}\text{P}$  NMR spectra of solid fd (left) and 10% (wt/wt) TMV (right). upper: nonspinning; lower: magic angle spinning (from DiVerdi and Opella, 1981b, and Cross et al., 1983b).

CSA-broadening tends to mask the small differences among the phosphates of the nucleic acid encapsulated in a slowly tumbling virus (Fig. 6). Such phosphodiester inhomogeneity, indicating e.g. inequivalence among binding sites, is best studied using magic angle spinning (MAS) NMR spectroscopy. MAS breaks up the broad  $^{31}\text{P}$  NMR powder lineshape into a sharp centerband at the isotropic chemical shift position flanked by rotational sidebands (Herzfeld and Berger, 1980). Because for phosphodiester compounds, the width of the centerband and the sidebands is typically a few ppm, resonances are more easily resolved and resolved sideband patterns may be assigned to specific phosphates on the basis of their conformation (see above) (Gorenstein, 1994).  $^{31}\text{P}$  MAS NMR spectra of TMV solutions (Cross et al., 1983a) and dried TMV pellets (Hemminga et al., 1987) show two resolved sideband patterns with an overall intensity ratio of approximately 2, which have been assigned by comparing torsion angle values for the three types of phosphodiesters in TMV (Hemminga et al., 1987). MAS NMR spectra of bacteriophage fd, which is closely related to M13, only contain a single, broad centerband flanked by sidebands (DiVerdi and Opella, 1981b), indicating that a continuous distribution of phosphodiester conformations is present in the phage, rather than a distinguishable few (Fig. 6).

## Research history and environment of the project

During the past two decades, the molecular-biophysical aspects of viruses have been studied at the Department of Molecular Physics. A number of workers have participated in this research line. Jan de Wit investigated TMV and its coat protein using  $^1\text{H}$  and  $^{13}\text{C}$  NMR spectroscopy (de Wit, 1978). He concluded that a specific part of the coat protein, which is mobile in dissociated protein subunits and in empty capsids, becomes immobilized by the interaction with RNA. Indeed, transformation of the so-called flexible loop into the V-column seems to be an essential step in the assembly of TMV (see Fig. 3 and remarks about TMV above). Gert Vriend studied the interaction of the coat protein of cowpea chlorotic mottle virus (CCMV) with RNA using  $^1\text{H}$  and  $^{13}\text{C}$  NMR, and ESR spectroscopy (Vriend, 1983). He developed a tentative model for the binding of protein dimers to RNA. In this model, the conformation of the N-terminal protein part changes upon interacting with the RNA from a flexible random-coil conformation into an  $\alpha$ -helical conformation, thereby pulling the coat protein and RNA towards each other. The model was tested by Marinette van der Graaf (van der Graaf, 1992), who investigated the conformation of a synthetic oligopeptide, containing the first 25 amino acids in the N-terminal part, in absence and presence of oligonucleotides and oligophosphates. For this purpose, she used UV/Vis and two-dimensional  $^1\text{H}$  NMR spectroscopy and carried out molecular dynamics calculations. Her conclusions confirmed and refined the "snatch-pull" model.

Klaas Pieter Datema employed various spectroscopic techniques (circular dichroism, time-resolved fluorescence, ESR,  $^{31}\text{P}$  NMR, and  $^2\text{H}$  NMR) to study the interaction of TMV, CCMV, BMV, SBMV and M13, as well as their coat proteins, with membranes (Datema, 1987). He concluded that M13 coat protein readily inserts into lipid bilayers, where it forms aggregates, whereas TMV coat protein only interacts with the negatively charged phospholipid headgroups without actually being inserted into the membrane. Johan Sanders continued this research (Sanders, 1992). He established the conformation of two forms of M13 coat protein in lipid bilayers using several spectroscopic techniques (circular dichroism, raman, fourier transform infra-red, ESR,  $^{31}\text{P}$  NMR, and  $^2\text{H}$  NMR) and molecular dynamics calculations. He concluded that one of the two proteins forms was very similar to the coat protein in M13 virion and was therefore likely to be present in the membrane of infected *E. coli*. His conclusions were supported by the work of Ruud Spruijt and Cor Wolfs (Spruijt et al., 1989).

In 1981, solid-state NMR spectroscopy was introduced to study TMV by Marcus Hemminga and Wiebren Veeman (Hemminga et al., 1981). This line of research was continued in 1985 by Jaap Krüse and Rolf Lamerichs who employed solid-state MAS  $^{13}\text{C}$  and  $^{31}\text{P}$  NMR spectroscopy to study lyophilized or air-dried pellets of intact TMV and CCMV virions (Hemminga et al., 1987). The results of these pilot-experiments gave rise to the project described in this thesis, which started in December 1987.

## Course of the project and outline of the thesis

The objective of the project presented in this thesis was in the first place to obtain information about the protein-nucleic acid interaction in intact virions of M13 and TMV using solid-state  $^{31}\text{P}$  NMR spectroscopy. At the project start, the experience within the Department of Molecular Physics with this type of spectroscopy was still limited. A secondary objective was therefore to find out the practical use of solid-state NMR spectroscopy for studying intact viruses. It was decided to mainly focus on  $^{31}\text{P}$  NMR, because phosphates are probably involved in the protein-nucleic acid interactions and  $^{31}\text{P}$  nuclei are sensitive probes for studying these interactions selectively. Gels of M13 and TMV are difficult samples as compared to polymers or crystalline powders, which are more often studied by use of solid-state NMR spectroscopy. Under "physiological" conditions (0–40 °C, > 50% (w/w) water), the signal-to-noise ratio is low (e.g. 40% M13  $\leftrightarrow$  ~4 mg/ml phage DNA). The high water content in the NMR samples lowers the Q-factor of the probe at the  $^1\text{H}$ -frequency, so that maximal proton power must be used with the risk of probe sparking. In addition,  $^1\text{H}$  -  $^{31}\text{P}$  cross-polarization is relatively ineffective, stable magic angle spinning is difficult to achieve, and the nonspinning  $T_2$  is short (~0.5 ms). For this reason, many of the "fancy" NMR techniques appearing in the literature, could not be successfully applied to the viruses, although some of them were tried. It may be illustrative to briefly present some of these unsuccessful ideas and pilot-experiments.

For instance, to be able to detect the weak dipolar couplings between  $^{31}\text{P}$  and its nearest protons  $\text{H}_3'$ ,  $\text{H}_5'$  and  $\text{H}_5''$  (~2.6 Å in DNA, < 2.5 kHz) and protons in the presumed salt-bridge between phosphates and basic residues (~3 Å in TMV, < 1.5 kHz), we have tried to suppress the much stronger  $^1\text{H}$  homonuclear coupling using off-resonance and multiple-pulse decoupling (Slichter, 1978). However, preliminary results were insufficiently convincing to continue this line of research. An idea to measure the weak  $^{31}\text{P}$  -  $^{15}\text{N}$  dipolar coupling in the presumed salt-bridges between phosphates and  $^{15}\text{N}$ -labeled lysine residues in M13 could not be carried out because isotope-labeling was still in an early stage in our lab (scrambling problems occurred) and the necessary  $^1\text{H}$  -  $^{31}\text{P}$  -  $^{15}\text{N}$  triple-resonance equipment was not available. Besides, the small size of the  $^{31}\text{P}$  -  $^{15}\text{N}$  coupling, presumed to be < 400 Hz on the basis of the 3-Å distance suggested for TMV, was not very motivating. If nonspinning separated local field spectra would be recorded to measure  $^{31}\text{P}$  -  $^{15}\text{N}$  dipolar coupling (DiVerdi and Opella, 1982),  $T_2$  broadening would probably dominate over coupling effects. In one-dimensional rotary resonance recoupling MAS spectra (Levitt et al., 1988), the coupling effect would likely be some minor extra broadening of the centerband and the sidebands already 700–1200 Hz wide at a  $^{31}\text{P}$  resonance frequency of 202.5 MHz.

An attempt was also made to investigate the orientational distribution of phosphodiester within M13 using a rotor-synchronized 2D MAS NMR method introduced for oriented polymers (Harbison, 1986). For

this purpose, we tried to freeze oriented M13 solutions in the (nonspinning) MAS rotor. As carbonyl groups are strongly oriented within M13, the carbonyl resonance lineshape in the  $^{13}\text{C}$  NMR spectrum of M13 is an indicator for the orientation of the virions with respect to the magnetic field. Indeed, a narrow carbonyl lineshape showed up in spectra of dilute M13 solutions, indicating orientation (if not motion) of the virus particles in the 10-T field of the AM500 spectrometer. Unfortunately, upon freezing, the carbonyl lineshape changed into the typical lineshape of an isotropic powder, reflecting the randomizing effect of the ice-formation. Attempts to use MAS 2D-exchange  $^{31}\text{P}$  NMR experiments (Kentgens, 1987) to study slow motion in M13 gels were unsuccessful, because highly concentrated or frozen M13 gels contained too little motion to cause meaningful off-diagonal intensity in the spectra, whereas more dilute gels at room temperature could not spin in a sufficiently stable manner.

Thus, despite much effort, the  $^{31}\text{P}$  NMR results obtained for M13 and TMV during the first three years of the project were little spectacular and rather disappointing: featureless powder lineshapes in nonspinning  $^{31}\text{P}$  NMR spectra, different  $T_2$ -values depending on the sample preparation, no resolution improvement in MAS spectra of 30% TMV as compared to earlier published spectra of air-dried TMV, and featureless lineshapes with various linewidths in MAS spectra of M13. A turning point was reached when a pattern was recognized: the featurelessness of the powder lineshapes and the sample preparation effects were actually highly indicative for the presence of  $^{31}\text{P}$  motion! Various models were developed to simulate the effect of different types of motion on  $^{31}\text{P}$  NMR spectra and transversal relaxation. The quantitative analysis of the experimental data by use of these models, is the main subject of this thesis.

Chapter 2 describes the theoretical background of the three models that will be used in Chapter 3 to simulate the experimental data. An isotropic rotational diffusion model is set up for mobile nucleic acids that are loosely or partially bound to the protein coat. A rigid-rod model is worked out to represent the mobility of rigidly bound phosphates in a rod-shaped virion which rotates about its length axis. In addition, a combined diffusion model is presented, in which fast restricted nucleic acid backbone motions are superimposed on a slow rotation of the virion about its length axis.

Chapter 3 compares the experimental  $^{31}\text{P}$  NMR lineshapes and transversal relaxation decays with the outcome of the simulations by use of the three rotational diffusion models developed in Chapter 2. It is concluded that neither isotropic diffusion, nor (restricted) rigid-rod diffusion offers a consistent explanation for the experimental data. The combined diffusion model is successful for M13. For TMV, the model indicates that one of the three binding sites is more mobile than the other two.

In Chapter 4, the combined diffusion model developed in Chapter 2 and tested in Chapter 3 is extrapolated for MAS experiments. Comparing theoretical and experimental MAS spectra, we conclude that backbone

motions influence the sideband intensities as observed. Backbone motions also seem to cause the decrease of inhomogeneous linewidth in the MAS spectrum and the transversal relaxation measured at spinning rates of 4 kHz or higher. At spinning rates below 2 kHz, transversal relaxation is significantly faster. This effect is assigned to slow, overall rotation of the rod-shaped M13 phage about its length axis.

Chapter 5 finally presents a detailed study of the slow overall motion of M13 and TMV using two-dimensional exchange  $^{31}\text{P}$  NMR spectroscopy. The combined diffusion model of Chapters 2 and 3 is now extended for this type of experiments. It is found that TMV undergoes much slower rotational diffusion than expected on the basis of the analysis in Chapter 3. For M13, the quantitative analysis indicates heterogeneity in the overall motion throughout the gel. The average overall mobility, however, is consistent with the outcome of the analysis in Chapter 3.

## REFERENCES

- Alam, T. M., and G. P. Drobny. 1991. Solid-state NMR studies of DNA structure and dynamics. *Chem. Rev.* 91:1545-1590.
- Allison, S. A., J. H. Shibata, J. Wilcoxon, and J. M. Schurr. 1982. NMR relaxation in DNA. I. The contribution of torsional deformation modes of the elastic filament. *Biopolymers*. 21:729-762.
- Banner, D. W., C. Nave, and D. A. Marvin. 1981. Structure of the protein and DNA in fd filamentous bacterial virus. *Nature*. 289:814-816.
- Bloomer, A. C., J. N. Champness, G. Bricogne, S. R., and A. Klug. 1978. Protein disk of tobacco mosaic virus at 2.8 Å resolution showing the interaction within and between the subunits. *Nature*. 276:362-368.
- Bolton, P. H., G. Clawson, V. J. Basus, and T. L. James. 1982. Comparison of ribonucleic acid-protein interactions in messenger ribonucleoproteins, ribosomes, MS2 virus, and Q $\beta$  virus examined via phosphorus-31 nuclear magnetic resonance relaxation. *Biochemistry*. 21:6073-6081.
- Bolton, P. H., and T. L. James. 1979. Molecular motions in RNA and DNA investigated by phosphorus-31 and carbon-13 NMR relaxation. *J. Phys. Chem.* 83:3359-3366.
- Brandes, R., and D. R. Kearns. 1988.  $^2\text{H}$  NMR of DNA liquid crystals: structural and dynamical aspects. *J. Phys. Chem.* 92:6836-6841.
- Burgess, J., R. Motoyoshi, and E. N. Fleming. 1973a. Effect of poly-L-ornithine on isolated tobacco mesophyll protoplasts: evidence against stimulated pinocytosis. *Planta*. 111:199-208.
- Burgess, J., R. Motoyoshi, and E. N. Fleming. 1973b. The mechanism of infection of plant protoplasts by viruses. *Planta*. 112:323-332.
- Butler, P. J. G. 1979. Assembly of regular viruses. In *Chemistry of Macromolecules IIB*. R. E. Offord, Eds. University Park Press, Baltimore. 205-237.
- Butler, P. J. G. 1984. The current picture of the structure and assembly of tobacco mosaic virus. *J. Gen. Virol.* 65:253-279.
- Butler, P. J. G., and A. Klug. 1978. The assembly of a virus. *Sci. Amer.* 239:62-69.
- Costello, A. J. R., T. Glonek, and J. R. van Wazer. 1976. Phosphorus-31 chemical shift variations with counteraction and ionic strength for the various ethyl phosphates. *J. Inorg. Chem. Soc.* 15:972-974.
- Cross, T. A., S. J. Opella, G. Stubbs, and D. L. D. Caspar. 1983a. Phosphorus-31 nuclear magnetic resonance of the RNA in tobacco mosaic virus. *J. Mol. Biol.* 170:1037-1043.
- Cross, T. A., P. Tsang, and S. J. Opella. 1983b. Comparison of protein and deoxyribonucleic acid backbone structures in fd and Pfl bacteriophages. *Biochemistry*. 22:721-726.
- Datema, K. P. 1987. Virus-membrane interactions. (*Ph.D. Thesis*). Agricultural University Wageningen, The Netherlands.
- Day, L. A. 1973. Circular dichroism and ultraviolet absorption of a deoxyribonucleic acid binding protein of filamentous bacteriophage. *Biochemistry*. 12:5329-5339.
- Day, L. A., C. J. Marzec, S. A. Reisberg, and A. Casadevall. 1988. DNA packing in filamentous bacteriophages. *Ann. Rev. Biophys. Biophys. Chem.* 17:509-539.
- Day, L. A., R. Wiseman L., and C. J. Marzec. 1979. Structure models for DNA in filamentous viruses with phosphates near the center. *Nucleic Acids Res.* 7:1393-1403.
- de Wit, J. L. 1978. NMR of TMV. (*Ph.D. Thesis*). Agricultural University Wageningen, The Netherlands.

- de Wit, J. L., N. C. M. Alma, T. Trienekens, M. A. Hemminga, and T. J. Schaafsma. 1979. Nuclear magnetic resonance of tobacco mosaic virus. In *Magnetic resonance and related phenomena* (20th Ampere Congress). K. E. c. al., Eds. Springer Verlag, Berlin, 560.
- DiVerdi, J. A., and S. J. Opella. 1981a. Dynamics of B-DNA in the solid state. *J. Mol. Biol.* 149:307-311.
- DiVerdi, J. A., and S. J. Opella. 1981b. Phosphorus-31 nuclear magnetic resonance of fd virus. *Biochemistry*. 20:280-284.
- DiVerdi, J. A., and S. J. Opella. 1982. N-H bond lengths in DNA. *J. Am. Chem. Soc.* 104:1761-1762.
- Dufourc, E. J., C. Mayer, J. Stohrer, G. Althoff, and G. Kothe. 1992. Dynamics of phosphate head groups in biomembranes. Comprehensive analysis using phosphorus-31 nuclear magnetic resonance lineshape and relaxation time measurements. *Biophys. J.* 61:42-57.
- Dunker, A. K., R. D. Klausner, D. A. Marvin, and R. L. Wiseman. 1974. Filamentous bacterial viruses X. X-ray diffraction studies of the R4 A-protein mutant. *J. Mol. Biol.* 81:115-117.
- Durham, A. C. H. 1978. The roles of small ions, especially calcium, in virus disassembly, take-over and transformation. *Biomedicine*. 28:307-314.
- Fraenkel-Conrat, H., and R. C. Williams. 1955. Reconstitution of active tobacco mosaic virus from inactive protein and nucleic acid components. *Proc. Natl. Acad. Sci. USA*. 41:690-695.
- Fritzsche, H., T. A. Cross, S. J. Opella, and N. R. Kallenbach. 1981. Structure and architecture of the bacterial virus fd. An infrared linear dichroism study. *Biophys. Chem.* 283-291.
- Giessner-Pretre, C., B. Pullman, F. R. Prado, D. M. Cheng, V. Iuorno, and P. O. P. Ts'o. 1984. Contributions of the PO Ester and CO torsion angles of the phosphate group to  $^{31}\text{P}$ -nuclear magnetic shielding. *Biopolymers*. 23:377-388.
- Gilbert, W., and D. Dressler. 1968. DNA replication: the rolling circle model. In *Cold Spring Harbor Symp. Quant. Biol.* 33 (Replication of DNA in micro organisms):473-484. New York
- Goelet, P., G. P. Lomonosoff, P. J. P. Butler, M. E. Akam, M. J. Gait, and J. Karn. 1982. Nucleotide sequence of tobacco mosaic virus RNA. *Proc. Natl. Acad. Sci. USA*. 79:5818-5822.
- Gorenstein, D. G. 1981. Nucleotide conformational analysis by  $^{31}\text{P}$  nuclear magnetic resonance spectroscopy. *Ann. Rev. Biophys. Bioeng.* 10:355-386.
- Gorenstein, D. G. 1994. Conformation and dynamics of DNA and protein-DNA complexes by  $^{31}\text{P}$  NMR. *Chem. Rev.* 94:1315-1338.
- Gorenstein, D. G., S. A. Schröder, J. M. Fu, J. T. Metz, V. A. Roontga, and C. R. Jones. 1988. Assignments of  $^{31}\text{P}$  NMR resonances in oligodeoxyribonucleotides: origin of sequence-specific variations in the deoxy phosphate backbone conformation and the  $^{31}\text{P}$  chemical shifts of double helical nucleic acids. *Biochemistry*. 27:7223-7237.
- Harbison, G. S. 1986. Two-dimensional magic-angle-spinning NMR of partially ordered systems. *Chem. Phys. Lett.* 124:128-134.
- Hemminga, M. A., P. A. De Jager, J. Krüse, and R. M. J. N. Lamerichs. 1987. Magic-Angle-Spinning NMR on Solid Biological Systems. Analysis of the Origin of the Spectral Linewidths. *J. Magn. Reson.* 71:446-460.
- Hemminga, M. A., W. S. Veeman, H. W. M. Hilhorst, and T. J. Schaafsma. 1981. Magic angle spinning carbon-13 NMR of tobacco mosaic virus. *Biophys. J.* 35:436-470.
- Herzfeld, J., and A. E. Berger. 1980. Sideband intensities in NMR spectra of samples spinning at the magic angle. *J. Chem. Phys.* 73:6021-6030.
- Hogan, M. E., and O. J. Jardetzky. 1980. Internal motions in deoxyribonucleic acid II. *J. Am. Chem. Soc.* 102:3460-3468.
- Hunter, G. J., D. H. Rowitch, and R. N. Perham. 1987. Interaction between DNA and coat protein in the structure and assembly of filamentous bacteriophage fd. *Nature*. 327:252-254.
- Hwang, D.-J., I. M. Roberts, and T. M. A. Wilson. 1994. Assembly of tobacco mosaic virus and TMV-like pseudovirus particles in *Escherichia coli*. *Arch. Virol. Suppl.* 9:543-558.
- Ishikawa, M., T. Meshi, F. Motoyoshi, N. Takamatsu, and Y. Okada. 1986. In vitro mutagenesis of the putative replicase genes of tobacco mosaic virus. *Nucleic Acid Res.* 14:8291-8305.
- Jardetzky, O., K. Akasaka, D. Vogel, S. Morris, and K. C. Holmes. 1978. Unusual segment flexibility in a region of tobacco mosaic virus protein. *Nature*. 273:564-566.
- Kan, J. H., A. F. M. Cremers, C. A. G. Haasnoot, and C. W. Hilbers. 1987. The dynamical structure of the RNA in alfalfa mosaic virus studied by phosphorus-31 nuclear magnetic resonance. *Eur. J. Biochem.* 168:635-639.
- Kassanis, B., R. F. White, T. R. H., and R. D. Woods. 1977. The mechanism of virus entry during infection of tobacco protoplasts with TMV. *Phytopath. Z.* 88:215-228.
- Keepers, J. W., and T. L. James. 1982. Models for DNA backbone motions: an interpretation of NMR relaxation experiments. *J. Am. Chem. Soc.* 104:929-939.
- Kentgens, A. P. M. 1987. Two-dimensional solid state NMR. (Ph.D. Thesis). Catholic University Nijmegen, The Netherlands.
- Kostrikis, L. G., D. I. Liu, and L. Day A. 1994. Ultraviolet absorbance and circular dichroism of Pfl virus: nucleotide/subunit ratio of unity, hyperchromic tyrosines and DNA bases, and high helicity in the subunits. *Biochemistry*. 33:1694-1703.
- Lankhorst, P. P., C. A. G. Haasnoot, C. Erkelenz, and C. J. Altona. 1984. Carbon-13 NMR in conformational analysis of nucleic acid fragments. 2. A reparametrization of the Karplus equation for the vicinal NMR coupling constants in CCOP and HCOP fragments. *Biomol. Struct. Dynam.* 1:1387-1405.
- Lerner, D. B., and D. R. Kearns. 1980. Observation of large solvent effects on the  $^{31}\text{P}$  NMR chemical shifts of nucleotides. *J. Am. Chem. Soc.* 102:7611-7612.
- Levitt, M. H., T. G. Oas, and R. G. Griffin. 1988. Rotary resonance recoupling in heteronuclear spin pair systems. *Isr. J. Chem.* 28:271-282.
- Lipari, G., and A. Szabo. 1981. Nuclear magnetic resonance relaxation in nucleic acid fragments: models for internal motion. *Biochemistry*. 20:6250-6256.
- Liu, D. J., and L. A. Day. 1994. Pfl virus structure: helical coat protein and DNA with paraxial phosphates. *Science*. 265:671-674.
- Mai, M. T., D. E. Wemmer, and O. Jardetzky. 1983. Effects of hydration on the dynamics of deoxyribonucleic acid. *J. Am. Chem. Soc.* 105:7149-7152.
- Marco, R., S. M. Jazwinski, and A. Kornberg. 1974. Binding, eclipse and penetration of the filamentous bacteriophage M13 in intact and disrupted cells. *Virology*. 62:209-223.
- Marvin, D. A. 1989. Dynamics of telescoping Inovirus: a mechanism for assembly at membrane adhesions. *Int. J. Biol. Macromol.* 11:159-164.
- Marvin, D. A. 1990. Model-building studies of Inovirus: genetic variations on a geometric theme. *Int. J. Biol. Macromol.* 12:125-139.
- Marvin, D. A., R. D. Hale, and C. Nave. 1994. Molecular models and structural comparisons of native and mutant class I filamentous bacteriophages. Ff (fd, f1, M13), If1, Ike. *J. Mol. Biol.* 235:260-286.
- Marvin, D. A., R. L. Wiseman, and E. J. Wachtel. 1974. Filamentous bacterial viruses XI. Molecular architecture of the class II (Pfl, Xf) virion. *J. Mol. Biol.* 82:121-138.
- Munowitz, M. G., C. M. Dobson, R. G. Griffin, and S. C. Harrison. 1980. On the rigidity of RNA in tomato bushy stunt virus. *J. Mol. Biol.* 141:327-333.
- Ohno, T., M. Aoyagi, Y. Yamanashi, H. Saito, S. Ikawa, T. Meshi, and Y. Okada. 1984. Nucleotide sequence of the tobacco mosaic virus (tomato strain) genome and comparison with the common strain genome. *J. Biochem.* 96:1915-1923.
- Opella, S. J., W. B. Wise, and J. A. DiVerdi. 1981. Deoxyribonucleic acid dynamics from phosphorus-31 nuclear magnetic resonance. *Biochemistry*. 20:284-290.
- Prado, F. R., C. Giessner-Pretre, B. Pullman, and J.-P. Daudley. 1979. Ab initio quantum mechanical calculations of the magnetic shielding tensor of phosphorus-31 of the phosphate group. *J. Am. Chem. Soc.* 101:1737-1742.
- Rasched, I., and E. Oberer. 1986. Ff Coliphages: Structural and Functional Relationships. *Microbiol. Rev.* 50:401-427.
- Reinero, A., and R. N. Beachy. 1989. Reduced photosystem II activity and accumulation of viral coat protein in chloroplasts of leaves infected with tobacco mosaic virus. *Plant. Physiol.* 89:111-116.
- Russel, M. 1991. Filamentous phage assembly. *Mol. Microbiol.* 5:1607-1613.
- Saito, T., K. Yamanaka, and Y. Okada. 1990. Long-distance movement and viral assembly of tobacco mosaic virus mutants. *Virology*. 176:329-336.
- Sanders, J. C. 1992. The interaction of M13 coat protein with lipid bilayers: a spectroscopic study (Ph.D. Thesis). Agricultural University Wageningen, The Netherlands.
- Scheck, R. M. 1994. The best approach to functional protein dynamics. (Meeting of the department of molecular and cellular biophysics of the association for biophysics and the foundation for biosciences):Lunteren
- Schröder, S. A., J. M. Fu, C. R. Jones, and D. G. Gorenstein. 1987. Assignment of phosphorus-31 and nonexchangeable proton resonances in a symmetrical 14 base pair *lac* pseudooperator DNA fragment. *Biochemistry*. 26:3812-3821.
- Shindo, H. 1980. NMR relaxation processes of phosphorus-31 in macromolecules. *Biopolymers*. 19:509-522.
- Slichter, C. P. 1978. Principles of Magnetic Resonance. Springer-Verlag, Berlin. 397 pp.
- Spuij, R. B., C. J. A. M. Wolfs, and M. A. Hemminga. 1989. Aggregation-related conformational change of the membrane-associated coat protein of bacteriophage M13. *Biochemistry*. 28:9158-9165.
- Stubbs, G., and C. Stauffacher. 1981. Structure of the RNA in tobacco mosaic virus. *J. Mol. Biol.* 152:387-396.

- Stubbs, G., S. Warren, and K. Holmes. 1977. Structure of RNA and RNA binding site in tobacco mosaic virus from 4-Å map calculated from x-ray fiber diagrams. *Nature*. 267:216-221.
- Thomas, G. J., Jr., B. Prescott, S. J. Opella, and L. A. Day. 1988. Sugar pucker and phosphodiester conformations in viral genomes of filamentous bacteriophages: fd, If1, IKE, Pf1, Xf, and Pf3. *Biochemistry*. 27:4350-4357.
- Tomenius, K., D. Clapham, and T. Meshi. 1987. Localization by immunogold cytochemistry of the virus-coded 30K protein in plasmodesmata of leaves infected with tobacco mosaic virus. *Virology*. 160:363-371.
- Tsang, P., and S. J. Opella. 1986. Pf1 virus particle dynamics. *Biopolymers*. 25:1859-1864.
- van de Ven, F. J. M., and C. W. Hilbers. 1988. Nucleic acids and nuclear magnetic resonance. *Eur. J. Biochem.* 178:1-38.
- van der Graaf, M. 1992. Conformation of the RNA-binding N-terminus of the coat protein of cowpea chlorotic mottle virus. (*Ph.D. Thesis*). Agricultural University Wageningen, The Netherlands.
- Virudachalam, R., M. Harrington, J. E. Johnson, and J. L. Markley. 1985. Proton, carbon-13, and phosphorus-31 nuclear magnetic resonance studies of cowpea mosaic virus: detection and exchange of polyamines and dynamics of the RNA. *Virology*. 141:43-50.
- Vriend, G. 1983. Molecular interactions during the assembly of cowpea chlorotic mottle virus (*Ph.D. Thesis*). Agricultural University Wageningen, The Netherlands.
- Wilson, T. M. A. 1985. Nucleocapsid disassembly and early gene expression by positive-strand RNA viruses. *J. Gen. Virol.* 66:1201-1207.

## **CHAPTER 2**

### **A theoretical study of rotational diffusion models for rod-shaped viruses.**

**The influence of motion on  $^{31}\text{P}$  nuclear magnetic resonance  
lineshapes and transversal relaxation.**

**(published in 1993, Biophys. J. 64 , 1851-1860)**

## A theoretical study of rotational diffusion models for rod-shaped viruses

### The influence of motion on $^{31}\text{P}$ nuclear magnetic resonance lineshapes and transversal relaxation

Pieter C. M. M. Magusin and Marcus A. Hemminga

Department of Molecular Physics, Agricultural University, Dreijenlaan 3, 6703 HA Wageningen, The Netherlands

**ABSTRACT** Information about the interaction between nucleic acids and coat proteins in intact virus particles may be obtained by studying the restricted backbone dynamics of the encapsulated nucleic acids using  $^{31}\text{P}$  nuclear magnetic resonance (NMR) spectroscopy. In this article, simulations are carried out to investigate how reorientation of a rod-shaped virus particle as a whole and isolated nucleic acid motions within the virion influence the  $^{31}\text{P}$  NMR lineshape and transversal relaxation dominated by the phosphorus chemical shift anisotropy. Two opposite cases are considered on a theoretical level. First, isotropic rotational diffusion is used as a model for mobile nucleic acids that are loosely or partially bound to the protein coat. The effect of this type of diffusion on lineshape and transversal relaxation is calculated by solving the stochastic Liouville equation by an expansion in spherical functions. Next, uniaxial rotational diffusion is assumed to represent the mobility of phosphorus in a virion that rotates as a rigid rod about its length axis. This type of diffusion is approximated by an exchange process among discrete sites. As turns out from these simulations, the amplitude and the frequency of the motion can only be unequivocally determined from experimental data by a combined analysis of the lineshape and the transversal relaxation. In the fast motional region both the isotropic and the uniaxial diffusion model predict the same transversal relaxation as the Redfield theory. For very slow motion, transversal relaxation resembles the nonexponential relaxation as observed for water molecules undergoing translational diffusion in a magnetic field gradient. In this frequency region  $T_{2e}$  is inversely proportional to the cube root of the diffusion coefficient. In addition to the isotropic and uniaxial diffusion models, a third model is presented, in which fast restricted nucleic acid backbone motions dominating the lineshape are superimposed on a slow rotation of the virion about its length axis, dominating transversal relaxation. In an accompanying article the models are applied to the  $^{31}\text{P}$  NMR results obtained for bacteriophage M13 and tobacco mosaic virus.

## INTRODUCTION

Phosphorus nuclear magnetic resonance (NMR) spectroscopy is a powerful technique for obtaining information about structure and dynamics of the nucleic acid backbone in intact bacteriophages and plant viruses. As all phosphorus nuclei belong to the viral genome, information about the nucleic acid backbone can be obtained selectively, even though the virus particles largely consist of proteins. Indeed, during the last 15 years  $^{31}\text{P}$  NMR studies of various viruses have appeared in the literature. In one class of studies, rapidly tumbling, mostly spherical viruses, such as the plant viruses alfalfa mosaic virus, cowpea mosaic virus, tomato bushy stunt virus, and the bacteriophages Q $\beta$  and MS2, have been investigated in dilute solution by use of high resolution NMR spectroscopy (1-4). In these studies conclusions about the dynamic behavior of the nucleic acids inside the virions have been drawn from linewidths and relaxation times. In other studies, solid-state NMR techniques have been used to record  $^{31}\text{P}$  spectra of viruses in more concentrated solutions or viscous gels, such as tomato bushy stunt virus and the rod-shaped tobacco mosaic virus (TMV) and the bacteriophages Pfl and fd (3, 5-8). From qualitative lineshape analyses conclusions were drawn about motional frequencies and amplitudes, which agree with the general picture evolved from dilute

solution studies: nucleic acids inside virions do not undergo large amplitude motions at frequencies higher than  $10^4$  Hz and motional lineshape effects observed in dilute solutions can be explained by overall motion of the viral particle as a rigid body.

To interpret our  $^{31}\text{P}$  NMR results for bacteriophage M13 and plant virus TMV in more detail, we have carried out simulations of the  $^{31}\text{P}$  lineshape and transversal relaxation for various types of diffusion with intermediate motional frequencies and amplitudes. As for phosphorus nuclei in biomolecular systems such simulations have been carried out for phospholipid membrane systems (9, 10), but not for nucleic acids encapsulated in viruses. Several diffusion models can be constructed to explain the motional effects observed by NMR spectroscopy. On the one hand, as in general a virion is a complex structure of a nucleic acid molecule situated within a protein coat, the observed  $^{31}\text{P}$  lineshape and transversal relaxation may actually reflect a superposition of many types of motion, such as overall rotation of the virus particle as a whole and isolated backbone motions of the nucleic acid inside. All these motions together may influence the lineshape and relaxation decay in a way roughly comparable with random rotational diffusion in a viscous solution. Similar assumptions were made in  $^{31}\text{P}$  NMR studies of DNA in solution (11, 12). In this article, an isotropic diffusion model is set up and the effects of this type of diffusion on the lineshape and transversal relaxation will be presented. On the other hand, one may

Address correspondence to M. A. Hemminga, Department of Molecular Physics, Agricultural University, P.O. Box 8128, 6700 ET Wageningen, The Netherlands.

try to interpret the motional effects observed in  $^{31}\text{P}$  NMR spectra and transversal relaxation in terms of rigid body motion. For rod-shaped viruses of the size of filamentous phages ( $\sim 1\ \mu\text{m}$  length and  $9\ \text{nm}$  diameter) in water, diffusion coefficients in the order of  $10^4$  and  $10^1$  Hz can be calculated for diffusion about the length axis and of the length axis itself (13). Rigid body rotation of these rod-shaped viruses is thus well approximated by uniaxial diffusion about the length axis. To show the effect of this type of diffusion, we construct a uniaxial diffusion model. In addition, we use alternative simulation methods to check the limiting behavior of the isotropic and the uniaxial diffusion model for fast and very slow diffusion. In both diffusion models one single type of motion is assumed to influence both the lineshape and transversal relaxation. In general, the observed lineshape and transversal relaxation may be dominated by different motions. To study such a case we will test a simple model, which combines slow motion of the virion as a whole with fast motion of the phosphodiester inside. The application of these simulation models to the experimental data will be treated in an accompanying article (14). In this article we present the theory of the simulations and discuss the outcome and trends therein in a general manner.

## THEORY

In the presence of only Zeeman interaction, anisotropic chemical shift, and rotational diffusion,  $^{31}\text{P}$  lineshapes and transversal relaxation can be described by the positive and negative-helicity components  $\mu_{\pm}(\Omega, t)$  of the spin density operator  $\rho(\Omega, t)$ , where  $\Omega$  denotes the orientation of the principal axis system of the chemical shift tensor in a laboratory frame with the z-axis parallel to the magnetic field,  $t$  represents the time, and  $I_+$  and  $I_-$  are the raising and lowering operators for a spin- $1/2$  nucleus. By assumption, the detected NMR signal is proportional to the positive-helicity component integrated over all shift tensor orientations

$$\mu_+(t) = \int d\Omega \mu_+(\Omega, t). \quad (1)$$

The positive and negative-helicity components obey part of the stochastic Liouville equation (10, 15)

$$\frac{d\mu_{\pm}(\Omega, t)}{dt} = (\pm i\omega(\Omega) + \Gamma_0)\mu_{\pm}(\Omega, t), \quad (2)$$

where  $\omega(\Omega)$  denotes the combined Zeeman and orientation-dependent chemical shift interaction and  $\Gamma_0$  is the stochastic operator representing a specific type of rotational diffusion. Combining Eq. 1 with the formal solution of Eq. 2 and assuming isotropic spin density at  $t = 0$ ,  $\mu_{\pm}(\Omega, 0) = \mu_0$  (e.g., after a nonselective pulse), it follows that the normalized free induction decay (FID)  $S(t)$  is given by

$$S(t) = \frac{\mu_+(t)}{\mu_+(0)} = \frac{\int d\Omega e^{(i\omega(\Omega) + \Gamma_0)t} \mu_0}{\int \mu_0 d\Omega}. \quad (3)$$

As a  $\pi$  pulse interchanges the positive and negative-helicity component, an echo produced by a  $\pi$  pulse at time  $\tau$  is given at a time  $2\tau + t$  by

$$E(2\tau, t) = \frac{\mu_+(2\tau + t)}{\mu_+(0)} = \frac{\int d\Omega e^{(i\omega(\Omega) + \Gamma_0)(\tau+t)} e^{(-i\omega(\Omega) + \Gamma_0)\tau} \mu_0}{\int \mu_0 d\Omega}, \quad (4)$$

(16). A "powder average" relaxation decay, i.e., the spatial average relaxation curve of all orientations, is defined for a series of  $\tau$  values by setting  $t = 0$  in Eq. 4. Although Eqs. 3 and 4 are formally correct, an appropriate method for dealing with the exponential operators therein should be used to actually calculate free induction and relaxation decays. However, already from these formal solutions it can be derived for many types of motion, including the ones discussed in this article, that motion does not change the second moment of the lineshape and causes nonexponential transversal relaxation, which contradicts what is often assumed (17–19). This contradiction becomes clear when Eqs. 3 and 4 are expanded as Taylor series in  $t$  and  $\tau$ , respectively.

For types of diffusion which are nonorienting, i.e., lead to an isotropic distribution of spin density, and which cannot create or annihilate net spin density, although they can, of course, change "local" spin density, the diffusion operator  $\Gamma_0$  satisfies the mathematical conditions  $\Gamma_0 1 = 0$ , where  $1$  denotes the isotropic distribution, and  $\langle \Gamma_0 f(\Omega) \rangle = 0$  for any distribution function  $f(\Omega)$ . For example, for restricted diffusion, the latter condition ensures that no loss of spin density occurs at the boundaries. Any type of motion that fulfils both conditions may be shown to change only third and higher order terms in the Taylor series of the calculated free induction decays and relaxation decays, as derived from Eqs. 3 and 4

$$S(t) = S_0(t) + 2Bt^3 + \dots, \quad (5a)$$

and

$$E(2\tau, 0) = 1 - B(2\tau)^3 + \dots, \quad (5b)$$

with

$$B = - \frac{\int d\Omega \omega(\Omega) \Gamma_0 \omega(\Omega)}{12 \int d\Omega}, \quad (5c)$$

where  $S_0(t)$  denotes the FID in the absence of diffusion. The constant  $B$  in Eqs. 5a, 5b, and 5c is positive, so that



relaxation curves actually decay (sufficiently close to  $t = 0$ ) and lineshapes are narrowed by motion. Eqs. 5a and 5b further indicate that diffusion does not change the second moment of the lineshape and transversal relaxation is nonexponential. Obviously, this does not agree with the common, experimentally confirmed assumption that fast motion modulates the second moment of a lineshape and causes exponential relaxation. However, higher order terms in the Taylor series become dominant at larger values of  $t$  or  $\tau$ , especially for fast motions, which may mask this disagreement and reduce it to a purely theoretical detail. Although Taylor series provide some information about lineshape moments and relaxation decays close to  $t = 0$ , they are not easily applicable to simulate motional effects completely. Instead, we have used different approaches, which will be explained in more detail below.

### Isotropic diffusion

The effect of isotropic diffusion on  $^{31}\text{P}$  lineshapes and relaxation decays can be calculated by introducing the spin density operator  $\rho(\Omega, t)$  as a function of the chemical shift tensor orientation  $\Omega = (\alpha, \beta, \gamma)$  relative to the laboratory frame and calculating this density as a function of orientation and time. The specific form of Eq. 2 for isotropic diffusion is

$$\frac{d\mu_{\pm}(\Omega, t)}{dt} = (\pm i\omega(\Omega) - D\nabla_{\Omega}^2)\mu_{\pm}(\Omega, t), \quad (6)$$

with the combined Zeeman and orientation dependent chemical shift interaction expressed in terms of the Wigner functions  $D_{m'm}^2(\alpha\beta\gamma) = \exp(im'\gamma)d_{m'm}^2(\beta) \times \exp(im\alpha)$  (20, 21) as

$$\omega(\Omega) = \omega_0 + \omega_0\sigma_0 + \omega_0F_0D_{00}^2(\Omega) + \omega_0F_2(D_{20}^2(\Omega) + D_{-20}^2(\Omega)), \quad (7)$$

where  $\omega_0 = \gamma B_0$  is the Zeeman angular frequency,  $\sigma_0 = (\sigma_{11} + \sigma_{22} + \sigma_{33})/3$  is the isotropic shift,  $F_0 = (\sigma_{33} - \sigma_0)$  is the anisotropy parameter, and  $F_2 = (\sigma_{22} - \sigma_{11})/\sqrt{6}$  characterizes the asymmetry of the chemical shift tensor with Cartesian components  $\sigma_{11}$ ,  $\sigma_{22}$ , and  $\sigma_{33}$ . Isotropic diffusion is represented in Eq. 3 by the differential operator

$$D\nabla_{\Omega}^2 = \frac{D\partial}{\sin\beta\partial\beta} \left( \sin\beta \frac{\partial}{\partial\beta} \right) + \frac{D}{\sin^2\beta} \frac{\partial^2}{\partial\gamma^2}, \quad (8)$$

where  $D$  denotes the diffusion coefficient. Utilizing the method of Freed (9, 15) Eq. 6 is solved by making an expansion of the two transversal spin density components in Wigner functions  $D_{m'm}^1(\Omega)$  being eigenfunctions of the diffusion operator. In contrast with the usual procedure, however, we carry out our simulations in the time domain, because the calculation of free induction decays can be more easily extended to the calculation of echoes and transversal relaxation decays.

As follows from Eqs. 7 and 8, the chemical shift and the diffusion operator are independent of  $\alpha$  and invari-

ant under the rotations  $\gamma \rightarrow \pi \pm \gamma$  and  $\beta \rightarrow \pi - \beta$ . Therefore, if initial spin density is homogeneously distributed over all tensor orientations,  $\mu_{\pm}(\Omega, 0) = \mu_0 D_{00}^0(\Omega)$ , spin density bears the same symmetry at all times and may thus be expanded more compactly in terms of the normalized eigenfunctions  $\sqrt{(4l+1)/8\pi^2}(D_{-2m'0}^{2l}(\Omega) + D_{2m'0}^{2l}(\Omega))$ . Neglecting terms with  $l$  larger than a specific value  $L$  and substituting the expansion in Eq. 6, this equation reduces to a matrix equation of the order  $N = (L+1)(L+2)/2$ , the formal solution of which is

$$\mu_+(t) = e^{\mathbf{M}t}\mu_+(0) \quad (9a)$$

and

$$\mu_-(t) = e^{\mathbf{M}^*t}\mu_-(0), \quad (9b)$$

where  $\mu_+(t)$  and  $\mu_-(t)$  have been redefined as vectors containing the  $N$  expansion components of the positive and negative-helicity component, respectively, the matrix  $\mathbf{M}$  contains the couplings among the coefficients in  $\mu_+(t)$ , and  $\mathbf{M}^*$  is the complex conjugate of  $\mathbf{M}$ . To calculate the FID the positive-helicity component must be integrated over all tensor orientations (Eq. 1). All expansion terms vanish under this integration, except for the first, isotropic term. If initial spin density is homogeneously distributed over all tensor orientations, as assumed earlier, the normalized FID  $S(t)$  is proportional to the "upper-left" element of the exponential matrix

$$S(t) = (e^{\mathbf{M}t})_{11}, \quad (10)$$

(see Eq. 3) where the exponential matrix is calculated by diagonalizing  $\mathbf{M}$ . It follows from Eqs. 9a and 9b that a  $\pi$  pulse, which interchanges the positive and negative-helicity component at time  $\tau$ , produces an echo given at time  $2\tau + t$  by

$$E(2\tau, t) = (e^{\mathbf{M}(\tau+t)}e^{\mathbf{M}^*\tau})_{11}, \quad (11)$$

(see Eq. 4). Fourier transformation of a calculated FID or echo produces the corresponding lineshape. A powder average decay can be calculated for a series of  $\tau$  values using Eq. 11 by setting  $t = 0$ . Note that in this case the product matrix of the two exponential matrices is hermitian, so that its diagonal elements are real and the transversal decay is purely absorptive.

### Uniaxial diffusion

In the uniaxial diffusion model the orientation of the principal axis system of the chemical shift tensor is specified by the Euler angles  $\Omega' = (\alpha, \beta, \gamma)$  in a coordinate system fixed in a rotor, representing the virion. The orientation of this rotor axis system in the laboratory frame, in turn, is given by  $\Omega'' = (\phi, \theta, \psi)$ . In an isotropic powder, the rotors are randomly oriented with respect to the magnetic field. The number of relative chemical shift tensor orientations within the virion may vary from a single one

in Pfl or three in TMV to a large value representing a nucleic acid backbone without structural correlation to the viral coat geometry, like bacteriophage fd (5, 8). In this model it is assumed that there is an isotropic distribution of relative chemical shift tensor orientations inside the virion. By introducing the spin density operator  $\rho(\Omega'', \Omega', t)$ , the specific form of Eq. 2 for rotor diffusion is

$$\frac{d\mu_{\pm}(\Omega'', \Omega', t)}{dt} = (\pm i\omega(\Omega'', \Omega') + \Gamma_{\psi})\mu_{\pm}(\Omega'', \Omega', t), \quad (12)$$

with the combined Zeeman and chemical shift interaction

$$\begin{aligned} \omega(\Omega'', \Omega') &= \omega_0 + \omega_0\sigma_0 + \omega_0 \\ &\times \sum_{m'=-2}^2 D_{m'0}^2(\Omega'') [F_0 D_{0m'}^2(\Omega') \\ &+ F_2 (D_{2m'}^2(\Omega') + D_{-2m'}^2(\Omega'))] \\ &= \omega_0 + \omega_0\sigma_0 + \omega_0 \\ &\times \sum_{m'=-2}^2 d_{m'0}^2(\theta) [F_0 d_{0m'}^2(\beta) + F_2 (d_{2m'}^2(\beta)e^{2i\gamma} \\ &+ d_{-2m'}^2(\beta)e^{-2i\gamma})] e^{im'(\psi+\alpha)}, \end{aligned} \quad (13)$$

where the parameters are explained in Eq. 7. For uniaxial diffusion restricted to angles  $\psi \in [\psi_0 - \lambda, \psi_0 + \lambda]$ , the diffusion operator  $\Gamma_{\psi}$  in Eq. 12 is defined on this interval as

$$\Gamma_{\psi} = D \frac{\partial^2}{\partial \psi^2} + D B_{\psi}(\psi_0, \lambda), \quad (14)$$

where  $D(\partial^2/\partial \psi^2)$  denotes the free uniaxial diffusion operator (10) and  $B_{\psi}(\psi_0, \lambda)$  is a boundary operator, which vanishes everywhere except at the edges and ensures that  $\Gamma_{\psi}$  fulfils the conditions  $\Gamma_{\psi}1 = 0$  and  $\langle \Gamma_{\psi}f(\Omega) \rangle = 0$  (see above). It follows from the symmetry properties of Eqs. 12, 13, and 14 that, if spin density is homogeneously distributed over all rotor orientations and the relative tensor orientations at time  $t = 0$ ,  $\mu_{\pm}(\Omega'', \Omega', t)$  are independent of  $\phi$  at any time. Furthermore, as  $\alpha$  and  $\psi$  are rotation angles about the same axis, there is no way to distinguish between  $\alpha$ -diffusion,  $\psi$ -diffusion, or a combination of both and  $\mu_{\pm}(\Omega'', \Omega', t)$  should be a function of  $\psi + \alpha$  rather than of  $\psi$  and  $\alpha$  separately. By redefining the average angle  $\psi_0$  as  $\langle \psi + \alpha \rangle$  and the fluctuating angle  $\psi$  as  $\psi + \alpha - \psi_0$  and collecting the nonfluctuating angles in  $\Theta = (\theta, \psi_0, \beta, \gamma)$  the notation for the spin density components can be changed to  $\mu_{\pm}(\Theta, \psi, t)$ .

Following the procedure of Dufourc et al. (10), we solve Eq. 12 by using a finite-difference approximation of the diffusion operator. To simulate the effect of uniaxial diffusion restricted by  $\pm\lambda$  on the positive-helicity component,  $N$  discrete values  $\psi_n$  are taken from the interval  $[-\lambda, +\lambda]$  with a constant difference  $\delta$  between subsequent values. Exchange among these  $N$  orientations is calculated from the coupled equations for  $2 < n < N-1$

$$\begin{aligned} \frac{d\mu_{+}(\Theta, \psi_n, t)}{dt} &= \frac{D}{\delta^2} \mu_{+}(\Theta, \psi_{n-1}, t) \\ &+ \left( i\omega(\Theta, \psi_n) - \frac{2D}{\delta^2} \right) \mu_{+}(\Theta, \psi_n, t) \\ &+ \frac{D}{\delta^2} \mu_{+}(\Theta, \psi_{n+1}, t), \end{aligned} \quad (15a)$$

combined with the equations for the boundaries

$$\begin{aligned} \frac{d\mu_{+}(\Theta, \psi_1, t)}{dt} &= \left( i\omega(\Theta, \psi_1) - \frac{D}{\delta^2} \right) \mu_{+}(\Theta, \psi_1, t) \\ &+ \frac{D}{\delta^2} \mu_{+}(\Theta, \psi_2, t) \end{aligned} \quad (15b)$$

$$\begin{aligned} \frac{d\mu_{+}(\Theta, \psi_N, t)}{dt} &= \frac{D}{\delta^2} \mu_{+}(\Theta, \psi_{N-1}, t) \\ &+ \left( i\omega(\Theta, \psi_N) - \frac{D}{\delta^2} \right) \mu_{+}(\Theta, \psi_N, t). \end{aligned} \quad (15c)$$

For free rotor diffusion we take  $\lambda = \pi$  and connect the boundaries by defining exchange between  $\psi_N$  and  $\psi_1$ . By combination of the  $N$  components in the vector  $\mu_{+}(\Theta, \Psi, t)$  and the shift and the diffusion factors in the symmetric matrix  $\mathbf{M}$  Eq. 12 may be rewritten as a matrix equation, the formal solution of which is

$$\mu_{+}(\Theta, t) = e^{\mathbf{M}t} \mu_{+}(\Theta, 0). \quad (16a)$$

Also here the analogous solution for the negative-helicity component is simply

$$\mu_{-}(\Theta, t) = e^{\mathbf{M}^*t} \mu_{-}(\Theta, 0). \quad (16b)$$

Because the FID is proportional to the positive-helicity component, Eq. 16a must be summed over all orientations (Eq. 1). If at  $t = 0$  all orientations have the same spin density, i.e.,  $\mu_{+}(\Theta, 0) = \mu_0(1, 1, \dots, 1, 1)$ , the normalized contribution  $S(\Theta, t)$  to the FID by  $N$  diffusion-coupled orientations for a specific combination of static angles  $\Theta$  is

$$S(\Theta, t) = \frac{1}{N} \sum_{i,j} (e^{\mathbf{M}t})_{ij}, \quad (17)$$

where the exponential matrix is calculated by diagonalizing  $\mathbf{M}$  (see Appendix). A  $\pi$  pulse at time  $\tau$  produces an echo given at time  $2\tau + t$  by

$$E(\Theta, 2\tau, t) = \frac{1}{N} \sum_{i,j} (e^{\mathbf{M}(\tau+t)} e^{\mathbf{M}^*\tau})_{ij}. \quad (18)$$

A way to calculate Eq. 18 efficiently is discussed in the Appendix. To simulate a FID, an echo or an average transversal decay curve of a powder of randomly oriented rotors, Eqs. 17 and 18 should be integrated for all rotor orientations  $(\theta, \psi_0)$  and summed over all internal chemical shift tensor orientations  $(\beta, \gamma)$ . Fourier transformation of a simulated FID or echo produces the corresponding lineshape. Like for isotropic diffusion the

decay of transversal coherence is purely absorptive due to the hermitian character of the product matrix of the two exponential matrices in Eq. 18.

### Ultra-slow and fast diffusion

For very slow and fast diffusion matrix calculations as discussed above are not necessary and faster simulation procedures can be used instead. Here we discuss such alternative procedures, because they provide independent checks for the limiting behavior of the isotropic and uniaxial diffusion models. For very slow diffusion with a diffusion coefficient  $D$  much smaller than the inhomogeneous linewidth  $|\omega_0(\sigma_{33} - \sigma_{11})|$ , the lineshape is hardly influenced by motion and can well be calculated following one of the standard procedures for simulating static lineshapes (21). If the diffusion coefficient is even smaller than the average motion-induced homogeneous linewidth, transversal relaxation may also be calculated in an alternative way. In this case it may be assumed that within a time that the echo intensity decays to typically  $e^{-1}$  of its initial value, spin density mainly spreads out to orientations close to its initial orientation. As a consequence the variation of chemical shift as a function of orientation is well approximated by a "local" linear or bilinear field gradient. It has been derived earlier that the Hahn echo in a linear field gradient  $G$  decays in a nonexponential way as  $\exp(-DG^2t^3/12)$  (19, 22). Similarly we find for ultra-slow uniaxial diffusion (neglecting boundary effects in the case of restricted diffusion)

$$E(t, 0) = \frac{\int d\Omega \int d\Omega' \exp(-D(\partial\omega/\partial\psi)^2 t^3/12)}{\int d\Omega \int d\Omega'}, \quad (19a)$$

and for ultra-slow isotropic diffusion

$$E(t, 0) = \frac{\int d\Omega \exp(-D\{(\partial\omega/\partial\beta)^2 + (\sin\beta)^{-2}(\partial\omega/\partial\gamma)^2\} t^3/12)}{\int d\Omega} \quad (19b)$$

Eqs. 19a and 19b show that the transversal decay  $E(t, 0)$  can generally be described as  $F(Dt^3)$ , where  $F(x)$  is some nonexponential, decaying function independent of  $D$ . For this decay of the echo produced by a single  $\pi$  pulse, a transversal relaxation time  $T_{2e}$  may be empirically defined by fitting a single exponential to the curve. If  $F(x)$  reaches the value  $e^{-1}$  for a specific value of  $x$ , defined as  $x_0$ ,  $T_{2e}$  should be approximately  $(x_0/D)^{1/3}$ . Obviously, in the ultra-slow motion region  $T_{2e}$  is inversely proportional to the cube root of  $D$ .

For fast diffusion the lineshape may be calculated from the time-averaged expression  $\langle\omega\rangle$  for  $\omega$ . Under fast isotropic diffusion chemical shift anisotropy is averaged to  $\langle\omega\rangle = \omega_0 + \omega_0\sigma_0$  and the lineshape becomes lorentzian

with a linewidth  $1/(\pi T_2)$ . In contrast, fast uniaxial diffusion does not completely average the chemical shift anisotropy. Replacing the complex exponentials in Eq. 13 by their average value  $\exp\{im'(\psi + \alpha)\} \text{sinc}(m'\lambda)$  on the interval  $\langle\psi + \alpha - \lambda, \psi + \alpha + \lambda\rangle$ , where  $\text{sinc}(m'\lambda)$  denotes  $\sin(m'\lambda)/(m'\lambda)$ , one obtains the average chemical shift expression for fast rotor diffusion with restriction half-angle  $\lambda$  as

$$\begin{aligned} \langle\omega(\Omega'', \Omega')\rangle = & \omega_0 + \omega_0\sigma_0 + \omega_0 \sum_{m'=-2}^2 d_{m'0}^2(\theta) [F_0 d_{0m'}^2(\beta) \\ & + F_2(d_{2m'}^2(\beta)e^{2i\gamma} + d_{-2m'}^2(\beta)e^{-2i\gamma}) \\ & e^{im'(\psi+\alpha)} \text{sinc}(m'\lambda). \end{aligned} \quad (20)$$

From Eq. 20 the lineshape may be simulated numerically by calculating  $\langle\omega\rangle$  for a large number of combinations  $(\cos\theta, \psi + \alpha, \cos\beta, \gamma)$ .

In the limit of short correlation times,  $T_{2e}$  may be calculated using the Redfield approximation, which relates  $T_{2e}$  to the spectral density. The general equation for the transversal relaxation for a chemical shift tensor undergoing axially symmetric diffusion is

$$1/T_{2e} = (1/40)(\omega_0 F_0)^2 \sum_{i=0}^2 c_i(\Omega) \{3J_1(\omega_0) + 4J_i(0)\}, \quad (21)$$

where  $c_i(\Omega)$  are geometric parameters relating the principle axis systems of the diffusion and the chemical shift tensors, and  $J_i(\omega)$  are the spectral density functions  $2\tau_i/(1 + \omega^2\tau_i^2)$ , with correlation times  $\tau_i$  depending on the diffusion model (23). In the case of isotropic diffusion  $\tau_0 = \tau_1 = \tau_2 = 1/(6D)$  and  $\langle c_0(\Omega) + c_1(\Omega) + c_2(\Omega) \rangle = (1 + \eta^2/3)$ , so that for correlation times shorter than  $T_{2e}$  but larger than  $1/\omega_0$ , the general equation simply reduces to

$$T_{2e} = \frac{6D}{M_2}, \quad (22a)$$

where  $M_2$  is the second moment of the static lineshape:  $(1/5)(\omega_0 F_0)^2(1 + \eta^2/3)$ . For uniaxial diffusion of a rotor containing many randomly oriented shift tensors inside,  $J_0(\omega) = 0$ ,  $\tau_1 = 1/D$ ,  $\tau_2 = 1/(4D)$ , and  $\langle c_1(\Omega) \rangle = \langle c_2(\Omega) \rangle = (2/5)(1 + \eta^2/3)$ . This may be substituted into Eq. 21 to show that for  $D \ll \omega_0$

$$T_{2e} = \frac{2D}{M_2}. \quad (22b)$$

To use Eq. 21 for restricted diffusion the spectral density functions should be modified in a rather complicated way (24). Instead,  $T_{2e}$  may be approximately calculated from a more simple equation, which for short correlation times relates  $T_{2e}$  to the portion  $\Delta M_2$  of the second lineshape moment  $M_2$  that is modulated by the motion

$$\frac{1}{T_{2e}} = \Delta M_2 \tau, \quad (23)$$

(17, 18). Theoretically Eq. 23 disagrees with Eq. 5, because, as discussed above, the latter implicates that diffu-

sion does not change the second moment. From Eq. 20, however, which we derived neglecting the time-dependent part of  $\omega$ , a second moment can be calculated for fast uniaxial diffusion, which does vary as a function of the restriction angle

$$M_2(\lambda) = M_2(0)\left\{\left(\frac{1}{5}\right) + \left(\frac{2}{5}\right)\text{sinc}^2(2\lambda) + \left(\frac{2}{5}\right)\text{sinc}^2(2\lambda)\right\}, \quad (24)$$

where  $M_2(0)$  is the second moment of the static lineshape (see Eq. 22a). From Eq. 24,  $\Delta M_2$  may be calculated as  $M_2(0) - M_2(\lambda)$ . The occurrence of only one correlation time in Eq. 23 provides another inconsistency: two correlation times are necessary for unrestricted uniaxial diffusion and for the restricted case the correlation function is multiexponential. Often, however,  $\tau = 1/(6D)$  is used as "the" correlation time of unrestricted uniaxial diffusion (10). Substitution of  $\Delta M_2$  and  $\tau$  into Eq. 23 then yields

$$T_{2e} = \frac{6D}{(2/5)M_2(0)\{2 - \text{sinc}^2(\lambda) - \text{sinc}^2(2\lambda)\}}. \quad (25)$$

For free uniaxial diffusion, i.e., for  $\lambda \rightarrow \infty$ , Eq. 25 predicts a higher value for  $T_{2e}$  than Eq. 22b. Interestingly, the two equations would match if the average of the two correlation times used in the derivation of Eq. 22b,  $(\tau_1 + \tau_2)/2 = 5/(8D)$ , were taken for  $\tau$ . Both variants will be compared with the outcome of simulations using the uniaxial diffusion model (see below).

### Combined diffusion

In the combined diffusion model nucleic acid backbone motion, represented by very fast, restricted  $\psi$  or  $\alpha$ -diffusion, is superimposed on top of slow, free  $\psi$ -diffusion, representing overall rotation of the virion as a whole. The approach is the same as for the uniaxial diffusion model (see above), except that Eq. 20 is used instead of Eq. 13. The effect of the superimposed diffusion is thus merely a pseudostatic reduction of the chemical shift anisotropy. In principle, both the fast restricted and the slow free diffusion influence the lineshape and transversal relaxation. It is assumed in this model, however, that the overall diffusion is too slow to effect the lineshape, whereas the superimposed, restricted diffusion is so fast, that it only has an indirect effect on transversal relaxation by scaling the chemical shift anisotropy in a pseudostatic way. Under these conditions the lineshape is dominated by the fast, restricted motion and transversal relaxation by the slow overall diffusion.

### METHODS

All simulations were carried out on a  $\mu\text{VAX}$  and a VAX workstation VS2000 (Digital Equipment Corp., Maynard, MA) using self-made Fortran programs as described in Theory. The double-precision complex IMSL routine EIGCC (IMSL Inc., Houston, Texas) was employed for matrix diagonalization. Lineshapes and powder average transversal

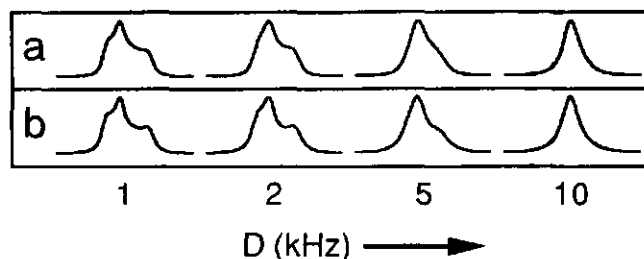


FIGURE 1 Fourier transformed free induction decays (a) and echoes at  $2\tau = 60 \mu\text{s}$  (b) for isotropic diffusion with a diffusion coefficient of 1, 2, 5, and 10 kHz.

relaxation decays presented here were simulated for  $^{31}\text{P}$  at 121.5 MHz with relative chemical shift tensor values  $\sigma_{11} - \sigma_0 = 77$  ppm,  $\sigma_{22} - \sigma_0 = 18$  ppm, and  $\sigma_{33} - \sigma_0 = -95$  ppm. For simulations of isotropic diffusion, the number of expansion terms was taken as high as necessary for lineshapes and relaxation curves not to change any more upon a further increase. The exact number depended on the diffusion coefficient  $D$  put into the calculation, but for  $D = 5$  kHz as a typical example, the expansion was truncated after 45 terms. For the other diffusion models a random distribution of rotor orientations with respect to the magnetic field and a random distribution of relative chemical shift tensor orientations within the virion were assumed. The number of angles  $\theta$ ,  $\beta$ ,  $\gamma$  between 0 and  $\pi/2$ ,  $\psi_0$  between 0 and  $2\pi$  and  $\psi$  between  $-\lambda$  and  $\lambda$  (see Theory and Appendix) was taken high enough to observe no change upon a further increase and depended on the diffusion coefficient  $D$  and the restriction halfangle  $\lambda$ . Typically for a simulation using the uniaxial diffusion model with  $D = 50$  kHz and  $\lambda = 1.25$  rad 10 values each for  $\cos \theta$  and  $\psi_0$ , 5 values each for  $\cos \beta$  and  $\gamma$ , and 12  $\psi$  values were taken into account. Except for the simulations of the fast diffusion lineshapes, all simulations were carried out in the time domain. Lineshapes were obtained by Fourier transformation after multiplication with an exponential function corresponding to 1 kHz line-broadening, in analogy with the processing of experimental data. For the nonexponential powder average decays, a  $T_{2e}$  value was defined by fitting a single exponential to the calculated decay (11), which differs from the  $e^{-1}$  definition by Woessner et al. (25), but is closer to the analysis of experimental decays in practice.

### DISCUSSION

#### Isotropic diffusion

Fig. 1 shows the lineshape effect of isotropic diffusion with a diffusion coefficient increasing from 1 to 10 kHz: discontinuities get increasingly less pronounced and the resonance line narrows more and more. Discontinuities tend to be more pronounced in echo spectra than in FID spectra caused by  $T_{2e}$  anisotropy or, in particular, the first derivatives of the chemical shift to  $\beta$  and  $\gamma$  being zero at these positions (Eq. 19b). For fast diffusion,  $D \geq 10$  kHz, powder average decays of transversal coherence are practically indistinguishable from single exponentials (not shown), which agrees with Redfield's relaxation theory for fast motions. Below 10 kHz, however, the simulated relaxation decays are significantly nonexponential, as expected from Eq. 5b, and  $T_{2e}$  values defined by least-square fitting a single exponential to the simulated decay depend on the time domain sampled

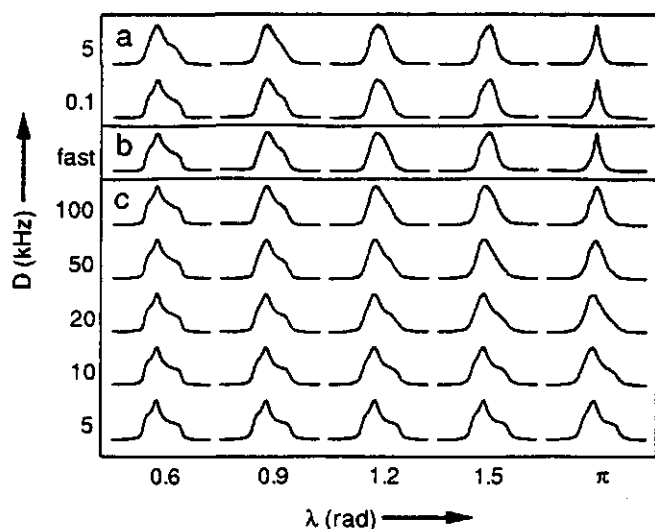


FIGURE 2 Fourier transformed echoes at  $2\tau = 60 \mu\text{s}$  for the three types of uniaxial diffusion with various coefficients and restriction angles: (a) combined diffusion, (b) fast diffusion, and (c) intermediate diffusion.

(see Fig. 3 a). In general, for fast motions Redfield theory predicts  $T_2$  to become longer at increasing mobility and the opposite trend is proposed for slow motions (19). Indeed, our calculations show that for an increasing diffusion coefficient  $D$ ,  $T_{2e}$  first decreases as a linear function of the cube root of  $D$ , and then passes through a minimum for  $D = 5 \text{ kHz}$  and finally becomes proportional to  $D$ . A similar trend has been calculated by Woessner et al. (25). Instead of the cube root dependence in the slow motion region, Pauls et al. (17) have suggested that for a process of large rotational jumps among discrete sites  $T_{2e}$  would be inversely proportional to the jumping rate ( $\approx D$ ). However, in their jumping model only spin density leaving the sites is taken into account and the contribution of spin density arriving at the sites is neglected, so that the corresponding jumping operator  $\Gamma$  does not fulfill the condition  $\Gamma 1 = 0$  (Eqs. 5a and 5b). In an attempt to find an empirical formula for  $T_{2e}$  as a function of  $D$ , it was found that the curves in Fig. 3 a fit well to  $T_{2e} = \{ (aD^{-1/3})^c + (bD)^c \}^{1/c}$ , where parameters  $a$  and  $b$  determine the limiting behavior for slow and fast motion, respectively, and parameter  $c$  defines the "sharpness" of the transition between the two limits. As a consequence of this hyperbolic correlation, an experimentally observed  $T_{2e}$  above the minimum value can be interpreted in two ways and a lineshape analysis is necessary to decide between the two. For slow diffusion up to  $1 \text{ kHz}$  plots of echo decays  $E(t, 0)$  versus  $Dt^3$  are independent of  $D$ , as expected from the linear field gradient approximation (Eq. 19b). This also explains the cube root dependence of  $T_{2e}$  on  $D$  in the slow-motion region. In the fast-motion region chemical shift anisotropy relaxation can be calculated alternatively from  $T_2 = 6D/M_2$  (Eq. 22a). As shown in Fig. 3 a this agrees

well with the simulation results for fast diffusion, which proves that the isotropic diffusion model is consistent with Redfield theory.

### Uniaxial diffusion

The influence of uniaxial diffusion on  $^{31}\text{P}$  lineshapes and relaxation curves has been calculated for various restriction half-angles and diffusion coefficients (Figs. 2 c and 3 d). Hardly any lineshape effect is observed for rotor diffusion with coefficients below  $10^4 \text{ Hz}$  or restriction half-angles below  $0.5 \text{ rad}$ . For diffusion coefficients larger than  $10^5 \text{ Hz}$ , the lineshape does not change upon a further increase and above a half-angle of  $\pi \text{ rad}$ ; the lineshapes are indistinguishable from free rotor diffusion lineshapes at the same diffusion coefficients. In contrast with the simulated lineshape for isotropic diffusion, the lineshapes of Fourier transformed free induction decays differ only slightly from the corresponding echoes at  $60 \mu\text{s}$ , probably as a consequence of the random orientation of shift tensors with respect to the rotor axis in this model.

Powder average  $T_{2e}$  values have been obtained by fitting the simulated echo decays to a single exponential. In Fig. 3 b these  $T_2$  values are plotted versus the diffusion

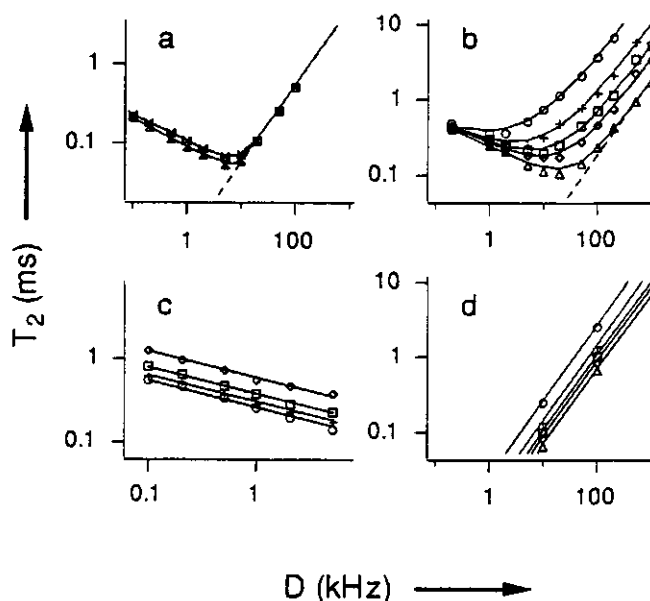


FIGURE 3  $T_{2e}$  values as a function of the diffusion coefficients for (a) isotropic diffusion, (b) uniaxial diffusion, (c) combined diffusion and (d) fast diffusion. For isotropic diffusion (a)  $T_{2e}$  values obtained by fitting a single exponential to the powder average decay up to a time of  $0.8 \text{ ms}$  ( $\times$ ) and  $1.6 \text{ ms}$  ( $\times$ ) are shown in the same plot for comparison. For the uniaxial and combined diffusion model the presented  $T_{2e}$  values are obtained by fitting up to  $0.8$  and  $1.6 \text{ ms}$ , respectively, for various restriction half-angles:  $0.6 \text{ rad}$  ( $\circ$ ),  $0.9 \text{ rad}$  ( $+$ ),  $1.2 \text{ rad}$  ( $\square$ ),  $1.5 \text{ rad}$  ( $\diamond$ ), and  $\pi \text{ rad}$  ( $\triangle$ ). For the fast diffusion model  $T_{2e}$  was calculated from Eq. 25. The broken lines in a and b represent the  $T_{2e}$  values calculated using the Redfield approximation for isotropic diffusion (Eq. 22a) and free uniaxial diffusion (Eq. 22b), respectively.

coefficients for a number of restriction angles. Similarly as for isotropic diffusion, the curves fit well to  $T_{2e} = \{(aD^{-1/3})^c + (bD)^c\}^{1/c}$ . Thus, for slow motion  $T_{2e}$  is inversely proportional to the cube root of  $D$ , reaches a minimum value in the intermediate region, and is proportional to  $D$  for fast motions. Again we find for slow diffusion that plots of echo decays  $E(t, 0)$  versus  $Dt^3$  are independent of  $D$  and that Eq. 19a provides a good approximation, which explains the cube root dependence of  $T_{2e}$  on  $D$  in the slow-motion region. For fast, unrestricted diffusion about a single axis,  $T_{2e}$  may be calculated alternatively from  $T_{2e} = 2D/M_2$  (Eq. 22b). This agrees well with the outcome of the simulations for fast diffusion with restriction half-angle  $\pi$  (Fig. 3 b).

Fig. 3 b also shows the effects of motional amplitude on  $T_{2e}$ . For a given diffusion coefficient,  $T_{2e}$  decreases as the restriction angle becomes larger, but for coefficients below 1 kHz the curves in Fig. 3 b start to coincide. Apparently, for ultraslow diffusion the fraction of spin density that actually reaches the boundaries within a time comparable to  $T_{2e}$  is neglectable. In contrast, for fast motion the curves are well resolved. Relaxation curves simulated for a restriction half-angle of  $\pi$  are indistinguishable from free rotor relaxation curves.

The presence of the restriction half-angle  $\lambda$  as another fitting parameter beside the diffusion coefficient  $D$  complicates the interpretation of experimental data. A continuous set of parameter pairs  $(D, \lambda)$  share the same  $T_{2e}$  value (Fig. 3 b), so that the observed transversal relaxation can be interpreted in many ways, especially when noise hides detailed features of the relaxation curve. Likewise, a continuous set of  $(D, \lambda)$  lineshapes can be simulated that fit to the experimental line equally well. Even the theoretical lineshape simulated for free diffusion at 20 kHz is hard to distinguish from the one simulated for  $D = 50$  kHz and  $\lambda = 1.5$  rad (Fig. 2 c). Obviously, only a combined analysis of lineshape and transversal relaxation must be used to unequivocally interpret the data.

### Fast uniaxial diffusion

Fast diffusion lineshapes, calculated from Eq. 20, correspond well to the lineshapes simulated for fast diffusion using the uniaxial diffusion model (Fig. 2 b). Clearly, the neglect of the time dependent part of  $\omega$  from which Eq. 20 was derived is allowed in the fast frequency region. In contrast,  $T_{2e}$  values calculated from Eq. 25 do not match the values simulated for uniaxial diffusion. The order of magnitude, however, is the same and the tendency of increasing  $T_{2e}$  with decreasing  $\lambda$  is comparable. Given the earlier discussed inconsistency between Eqs. 5a and 23 on a theoretical basis, the similarity between the outcome of the two methods is striking. The alternative variant of Eq. 25, derived by taking  $\tau = 5/(8D)$ , does not provide a better approximation, except for  $\lambda > 1$  rad. In the analysis of experimental data the fast diffusion

model can be useful to make a quick estimation of the motional amplitude and frequency.

### Combined diffusion

Utilizing the combined diffusion model, lineshapes and relaxation decays have been simulated for several combinations of internal restriction half-angles  $\lambda$  and overall diffusion coefficients  $D$ . For coefficients below 5 kHz lineshapes are hardly influenced by slow overall diffusion, but only depend on the internal restriction angles (Fig. 2 a). Slow overall diffusion does, however, influence transversal relaxation (Fig. 3 d). In the frequency region up to 5 kHz investigated,  $T_{2e}$  is inversely proportional to the cube root of  $D$ , as expected for ultraslow diffusion. In contrast to the  $T_{2e}$  trend observed in the uniaxial diffusion simulations, where  $T_{2e}$  shortens as the restriction half-angle  $\lambda$  increases, the combined diffusion model predicts that  $T_{2e}$  becomes larger at increasing  $\lambda$ , because internal motions with larger amplitudes average the shift anisotropy to a larger extent and thereby reduce the chemical shift fluctuations caused by overall diffusion more. The curves for  $\lambda = 0.6$  and  $0.9$  rad in Fig. 3 c almost coincide, indicating that very fast, internal motion with amplitudes below 1 rad hardly influence  $T_{2e}$ . Clearly, under these circumstances transversal relaxation is dominated by the overall diffusion alone.

In the strategy for interpreting experimental results in terms of combined diffusion, the first step is the determination of the internal restriction angle from the lineshape using the fast diffusion model. Then, for this restriction angle the overall diffusion coefficient can be obtained from an analysis of the relaxation curve using the combined diffusion model. This procedure of extracting  $\lambda$  from the experimental lineshape first and then  $D$  from the observed relaxation curve is much less time consuming than a "two-dimensional" searching procedure necessary to unequivocally determine  $\lambda$  and  $D$  using the uniaxial diffusion model discussed above.

### CONCLUSION

In summarizing the simulation results discussed above, it is convenient to divide motional amplitudes into three ranges. Small amplitude motions do not cause detectable lineshape effects; e.g., uniaxial diffusion with a restriction half-angle  $< 0.5$  rad ( $30^\circ$ ) hardly influences the lineshape. Obviously, one should be careful to conclude the absence of motion from the absence of motional narrowing alone. In this range motional information can best be obtained from relaxation studies. Motions with larger amplitudes can significantly alter the lineshape. An intermediate amplitude range may be distinguished between 0.5 and 1.5 rad, where lineshape and transversal relaxation are sensitive to small changes in the amplitude. The third range consists of still larger amplitudes.

In this region lineshapes and transversal relaxation are insensitive to amplitude changes and restricted motion hardly can be distinguished from unrestricted motion.

A similar division can be made for motional frequencies as well. The slow-motion range contains low frequencies as compared with static linewidth and correlation times in the order of the transversal relaxation time  $T_{2c}$  or longer. In this region diffusion does not alter the lineshape in a detectable way and causes nonexponential relaxation. Typically the powder average decay of the echo  $E(t, 0)$  is a function of  $Dt^3$  and  $T_{2c}$  is inversely proportional to the cube root of the diffusion coefficient. In contrast, in the fast-motion region lineshapes are generally strongly narrowed and transversal relaxation is exponential. Within this frequency region the lineshape is dominated by the time-independent part of the chemical shift interaction and transversal relaxation is well described by the Redfield theory. In the intermediate region the time-dependent part of the chemical shift interaction cannot be neglected in lineshape calculations and the Redfield theory is not applicable. Other methods are necessary to simulate lineshapes and transversal relaxation.

The diffusion models discussed in this article serve to interpret the  $^{31}\text{P}$  lineshapes and powder average decays measured for large virions in viscous gels. The application of these models on our NMR results obtained for M13 and TMV will be treated in a following article.

## APPENDIX

### Speeding up uniaxial diffusion simulations

An echo or free induction decay can be calculated from Eq. 18 for a series of  $t$  or  $\tau$  values, respectively. After diagonalizing  $M = DAD^{-1}$  the calculation may proceed in a straightforward way

$$\sum_{i,j} (e^{M(\tau+t)} e^{M^* \tau})_{ij} = \sum_{i=1}^N \sum_{j=1}^N \sum_{k=1}^N \sum_{l=1}^N D_{ik} e^{A_{kk}(\tau+t)} D_{kl}^{-1} D_{lm}^* e^{A_{mm}^* \tau} (D_{ji}^{-1})^*. \quad (\text{A1})$$

Due to the symmetry properties of matrix  $M$ , matrix  $D$  can be orthogonalized by normalizing its columns, so that the inverse matrix  $D^{-1}$  can quickly be obtained by simple transposition. Still, however, the multiple sum in Eq. A1 for every  $t$  or  $\tau$  value separately takes much computer time, which increases as the fifth power of the number of sites. Furthermore Eq. A1 also should be summed over many rotor orientations  $(\theta, \psi_0)$  and internal chemical shift tensor orientations  $(\beta, \gamma)$ . Therefore, speeding up the simulation is therefore essential for a practical use. A more efficient way is to calculate in a first step

$$A_{km} = D_{mk} \sum_{i=1}^N D_{ik}, \quad (\text{A2})$$

and in the second step

$$B_m(\tau, t) = \sum_{k=1}^N A_{km} e^{A_{kk}(\tau+t)}. \quad (\text{A3})$$

To simulate an echo,  $B_m(\tau, t)$  is calculated for a specific value of  $\tau$  and a series of  $t$  values and the echo is obtained from

$$\sum_{i,j} (e^{M(\tau+t)} e^{M^* \tau})_{ij} = \sum_{m=1}^N B_m(\tau, t) B_m^*(\tau, 0) \quad (\text{A4})$$

To simulate a decay,  $B_m(\tau, 0)$  is calculated for a series of  $\tau$  values and the decay follows from

$$\sum_{i,j} (e^{M\tau} e^{M^* \tau})_{ij} = \sum_{m=1}^N |B_m(\tau, 0)|^2. \quad (\text{A5})$$

Assuming that the rotors are randomly oriented in an isotropic powder and that the chemical shift tensors are also randomly oriented within every rotor separately (as may be the case for M13), Eqs. A4 and A5 still have to be summed over a large variety of rotor orientations  $(\theta, \psi_0)$  and internal chemical shift tensor orientations  $(\beta, \gamma)$ . It is well known that, for simulating static powder lineshapes, only part of the orientations within an isotropic powder has to be taken into account due to the symmetry of the chemical shift anisotropy (21). Likewise, symmetric properties of Eq. 13 reduce the number of rotor and tensor orientations that are actually needed in rotor diffusion simulations. Using the properties  $d_{mm'}^2(\beta) = (-1)^{m-m'} d_{-m-m'}^2(\beta)$  and  $d_{mm'}^2(\beta) = (-1)^{m'} \times d_{mm'}^2(\pi - \beta)$  and combining the terms  $\pm m'$ , the anisotropic part of Eq. 13 may be rewritten as

$$\begin{aligned} & \omega_0 d_{00}^2(\theta) [F_0 d_{00}^2(\beta) + 2F_2 d_{20}^2(\beta) \cos(2\gamma)] \\ & + 2\omega_0 d_{10}^2(\theta) [F_0 d_{01}^2(\beta) \cos(\varphi) \\ & + F_2 (d_{21}^2(\beta) \cos(\varphi + 2\gamma) \\ & - d_{21}^2(\pi - \beta) \cos(\varphi - 2\gamma))] \\ & + 2\omega_0 d_{20}^2(\theta) [F_0 d_{02}^2(\beta) \cos(2\varphi) \\ & + F_2 (d_{22}^2(\beta) \cos(2\varphi + 2\gamma) \\ & + d_{22}^2(\pi - \beta) \cos(2\varphi - 2\gamma))], \end{aligned} \quad (\text{A6})$$

where  $\varphi = \psi + \alpha$ . Eq. A6 shows that the chemical shift is invariant under the rotations  $(\theta, \varphi) \rightarrow (\pi - \theta, \pi + \varphi)$ ,  $(\beta, \varphi) \rightarrow (\pi - \beta, \pi + \varphi)$ ,  $\gamma \rightarrow \pi + \gamma$ , and  $(\gamma, \varphi) \rightarrow (\pi - \gamma, 2\pi - \varphi)$ . The diffusion operator (Eq. 14) is invariant under these rotations as well. Thus, if for rotor diffusion simulations  $\varphi$  is sampled from the whole interval  $\langle 0, 2\pi \rangle$ , the lineshape is sufficiently defined by  $\theta$ ,  $\beta$ , and  $\gamma$  taken from  $\langle 0, \pi/2 \rangle$ , which only represent one-sixteenth of all possible orientations.

This research was supported by the Netherlands Foundation of Biophysics with financial aid of the Netherlands Organization for Scientific Research (NWO).

Received for publication 30 November 1992 and in final form 23 February 1993.

## REFERENCES

1. Kan, J. H., A. F. M. Cremers, C. A. G. Haasnoot, and C. W. Hilbers. 1987. The dynamical structure of the RNA in alfalfa mosaic virus studied by phosphorus-31 nuclear magnetic resonance. *Eur. J. Biochem.* 168:635-639.
2. Virudachalam, R., M. Harrington, J. E. Johnson, and J. L. Markley. 1985. Proton, carbon-13, and phosphorus-31 nuclear magnetic resonance studies of cowpea mosaic virus: detection and exchange of polyamines and dynamics of the RNA. *Virology* 141:43-50.
3. Munowitz, M. G., C. M. Dobson, R. G. Griffin, and S. C. Harrison. 1980. On the rigidity of RNA in tomato bushy stunt virus. *J. Mol. Biol.* 141:327-333.

4. Bolton, P. H., G. Clawson, V. J. Basus, and T. L. James. 1982. Comparison of ribonucleic acid-protein interactions in messenger ribonucleoproteins, ribosomes, MS2 virus, and Q $\beta$  virus examined via phosphorus-31 nuclear magnetic resonance relaxation. *Biochemistry*. 21:6073-6081.
5. Cross, T. A., S. J. Opella, G. Stubbs, and D. L. D. Caspar. 1983. Phosphorus-31 nuclear magnetic resonance of the RNA in tobacco mosaic virus. *J. Mol. Biol.* 170:1037-1043.
6. Tsang, P., and S. J. Opella. 1986. Pfl virus particle dynamics. *Biopolymers*. 25:1859-1864.
7. DiVerdi, J. A., and S. J. Opella. 1981. Phosphorus-31 nuclear magnetic resonance of fd virus. *Biochemistry*. 20:280-284.
8. Cross, T. A., P. Tsang, and S. J. Opella. 1983. Comparison of protein and deoxyribonucleic acid backbone structures in fd and Pfl bacteriophages. *Biochemistry*. 22:721-726.
9. Campbell, R. F., E. Meirovitch, and J. H. Freed. 1979. Slow-motional NMR line shapes for very anisotropic rotational diffusion. Phosphorus-31 NMR of phospholipids. *J. Phys. Chem.* 83:525-533.
10. Dufourc, E. J., C. Mayer, J. Stohrer, G. Althoff, and G. Kothe. 1992. Dynamics of phosphate head groups in biomembranes. Comprehensive analysis using phosphorus-31 nuclear magnetic resonance lineshape and relaxation time measurements. *Biophys. J.* 61:42-57.
11. Bolton, P. H., and T. L. James. 1979. Molecular motions in RNA and DNA investigated by phosphorus-31 and carbon-13 NMR relaxation. *J. Phys. Chem.* 83:3359-3366.
12. Opella, S. J., W. B. Wise, and J. A. DiVerdi. 1981. Deoxyribonucleic acid dynamics from phosphorus-31 nuclear magnetic resonance. *Biochemistry*. 20:284-290.
13. Edsall, J. T. 1953. Size, shape and hydration of protein molecules. In *The Proteins*. H. Neurath and K. Bailey, editors. Academic Press Inc., New York. 549-686.
14. Magusin, P. C. M. M., and M. A. Hemminga. 1993. Analysis of  $^{31}\text{P}$  NMR lineshapes and transversal relaxation of bacteriophage M13 and Tobacco Mosaic Virus. *Biophys. J.* 64:1861-1868.
15. Freed, J. H., G. V. Bruno, and C. F. Polnaszek. 1971. Electron spin resonance line shapes and saturation in the slow motional region. *J. Phys. Chem.* 75:3385-3399.
16. Spiess, H. W., and H. Sillescu. 1981. Solid echoes in the slow-motion region. *J. Magn. Reson.* 42:381-389.
17. Pauls, K. P., A. L. MacKay, O. Soederman, M. Bloom, A. K. Tanjea, and R. S. Hodges. 1985. Dynamic properties of the backbone of an integral membrane polypeptide measured by deuterium NMR. *Eur. Biophys. J.* 12:1-11.
18. Alam, T. M., and G. P. Drobny. 1991. Solid-state NMR studies of DNA structure and dynamics. *Chem. Rev.* 91:1545-1590.
19. Abragam, A. 1961. *The Principles of Nuclear Magnetism*. Oxford University Press, London. 599 pp.
20. Edmonds, A. R. 1960. *Angular Momentum in Quantum Mechanics*. Princeton University Press, Princeton, NJ. 146 pp.
21. Haeberlen, U. 1976. *High Resolution NMR in Solids: Selective Averaging. Adv. Magn. Reson. Suppl. 1* (J. S. Waugh, editor). Academic Press, New York. 208 pp.
22. Slichter, C. P. 1978. *Principles of Magnetic Resonance*. Springer-Verlag, Berlin. 397 pp.
23. Hull, W. E., and B. D. Sykes. 1975. Fluorotyrosine alkaline phosphatase: internal mobility of individual tyrosines and the role of chemical shift anisotropy as a  $^{19}\text{F}$  nuclear spin relaxation mechanism in proteins. *J. Mol. Biol.* 98:121-153.
24. Wittebort, R. J., and A. J. Szabo. 1978. Theory of NMR relaxation in macromolecules: restricted diffusion and jump models for multiple internal rotations in amino acid side chains. *J. Chem. Phys.* 69:1722-1736.
25. Woessner, D. E., B. S. Snowden, Jr., and G. H. Meyer. 1969. Calculation of N.M.R. free induction signals for nuclei of molecules in a highly viscous medium or a solid-liquid system. *J. Chem. Phys.* 51:2968-2976.



## **CHAPTER 3**

### **Analysis of $^{31}\text{P}$ nuclear magnetic resonance lineshapes and transversal relaxation of bacteriophage M13 and tobacco mosaic virus**

(published in 1993, Biophys. J. 64 , 1861-1868)

## Analysis of $^{31}\text{P}$ nuclear magnetic resonance lineshapes and transversal relaxation of bacteriophage M13 and tobacco mosaic virus

Pieter C. M. M. Magusin and Marcus A. Hemminga

Department of Molecular Physics, Agricultural University, Dreijenlaan 3, 6703 HA Wageningen, The Netherlands

**ABSTRACT** The experimentally observed  $^{31}\text{P}$  lineshapes and transversal relaxation of 15% (wt/wt) M13, 30% M13, and 30% tobacco mosaic virus (TMV) are compared with lineshapes and relaxation curves that are simulated for various types of rotational diffusion using the models discussed previously (Magusin, P. C. M. M., and M. A. Hemminga. 1993. *Biophys. J.* 64:1851-1860). It is found that isotropic diffusion cannot explain the observed lineshape effects. A rigid rod diffusion model is only successful in describing the experimental data obtained for 15% M13. For 30% M13 the experimental lineshape and relaxation curve cannot be interpreted consistently and the TMV lineshape cannot even be simulated alone, indicating that the rigid rod diffusion model does not generally apply. A combined diffusion model with fast isolated motions of the encapsulated nucleic acid dominating the lineshape and a slow overall rotation of the virion as a whole, which mainly is reflected in the transversal relaxation, is able to provide a consistent picture for the 15 and 30% M13 samples, but not for TMV. Strongly improved lineshape fits for TMV are obtained assuming that there are three binding sites with different mobilities. The presence of three binding sites is consistent with previous models of TMV. The best lineshapes are simulated for a combination of one mobile and two static sites. Although less markedly, the assumption that two fractions of DNA with different mobilities exist within M13 also improves the simulated lineshapes. The possible existence of two  $^{31}\text{P}$  fractions in M13 sheds new light on the nonintegral ratio 2.4:1 between the number of nucleotides and protein coat subunits in the phage: 83% of the viral DNA is less mobile, suggesting that the binding of the DNA molecule to the protein coat actually occurs at the integral ratio of two nucleotides per protein subunit.

### INTRODUCTION

Bacteriophage M13 has a cylindrical shape with a length of  $\sim 900$  nm and a varying outer diameter between 6 and 10 nm depending on the relative humidity (1, 2). The molecular mass of the phage is  $\sim 16$  MD. Its genome is a circular single-stranded DNA molecule of 6,407 nucleotides (3) protected by a protein coat mainly consisting of  $\sim 2,700$  copies of the gene-8 protein. The DNA molecule is situated along the virion in a core of  $<2.5$  nm wide. Studies by x-ray fiber diffraction applied to bacteriophage fd, which is closely related to M13, indicate that the symmetry of the protein coat involves a five-fold axial rotation axis combined with a two-fold axial screw axis of pitch  $32 \text{ \AA}$  (4). Much less is known about the geometry of the encapsulated DNA molecule. The absence of DNA reflections in earlier reported x-ray patterns has led to the conclusion that the molecule is mobile or disordered (5), but later results show that some regular DNA structured with a pitch of  $27 \text{ \AA}$  may exist and that many of the bases are stacked axially  $\sim 3.4 \text{ \AA}$  apart (4). Substantial base stacking is detected by ultraviolet (UV) spectroscopy as well (6), but the distance of  $3.4 \text{ \AA}$  is difficult to reconcile with the mean axial rise of  $2.7 \text{ \AA}$  expected for homogeneous distribution of DNA along the inside of the protein coat, as commonly assumed (4, 7). Raman spectra of fd contain the characteristics of nucleoside sugar pucker and glycosyl torsion typical for A-DNA. However, only 20% of the viral DNA at most seems to have the regular phosphodiester back-

bone found in A-DNA (8). In fact, infrared linear dichroism results indicate that the DNA backbone mainly has a B-type conformation (9). Phosphorus solid state nuclear magnetic resonance (NMR) studies applied to bacteriophage fd have indicated that the DNA within the virion is relatively immobile (10), probably as a consequence of the electrostatic interaction between the negatively charged phosphodiester in the DNA to the positively charged lysine residues located on the inside of the tubular protein coat. There are no signs for any regularity in the DNA structure present in the spectra of oriented fd gels (11). The motional narrowing of the phosphorus lineshape observed for unoriented and oriented fd gels has been interpreted qualitatively in terms of both rotational diffusion of the virion as a whole around its length axis (10) and limited motions present in the DNA backbone (11).

Tobacco mosaic virus (TMV) is a rod-shaped single-stranded RNA virus with a length of  $3,000 \text{ \AA}$  and an outer diameter of  $180 \text{ \AA}$ . The protein coat is formed by 2,200 subunits ( $M_r = 17,500$ ) arranged in a helix with 49 subunits per three turns. In contrast to the DNA molecule in fd, the structure of the RNA molecule, which consists of 6,600 nucleotides, has been well determined. It is buried within the coat between layers of subunits, following the protein helix with three nucleotides per protein subunit at a radius of  $\sim 40 \text{ \AA}$  (12). Three sorts of binding between RNA and protein subunits inside TMV have been suggested: electrostatic interactions between phosphodiester and arginine residues, hydrophobic interactions between the nucleotide bases and the left radial  $\alpha$ -helix of the subunits, and hydrogen bridges (13).

Address correspondence to M. A. Hemminga, Department of Molecular Physics, Agricultural University, P. O. Box 8128, 6700 ET Wageningen, The Netherlands.

As a consequence of the regular RNA geometry, three types of phosphorus nuclei can be distinguished in NMR spectra of oriented TMV samples and in magic angle spinning (MAS) NMR spectra of TMV. The three phosphorus resonances in the spectrum of oriented TMV samples have different linewidths that have been assigned to varying degrees of disorder in the orientation of the phosphates in the various binding sites of the coat protein (14). In MAS spectra of TMV, two lines strongly overlap indicating similar electronic environments for two of three binding sites (14, 15).

To gain information about the dynamic behavior of the nucleic acid backbone in M13 and TMV, we used  $^{31}\text{P}$  solid state NMR spectroscopy. In a previous report we demonstrated how isotropic diffusion and various types of uniaxial diffusion influence  $^{31}\text{P}$  NMR lineshapes and transversal relaxation theoretically (16). Here we will compare the experimental NMR results with the outcome of these simulations.

## MATERIALS AND METHODS

### Preparation and purification of M13 and TMV

M13 bacteriophage was grown and purified as described by Spruijt et al. (17) except for 10 mM Tris, 0.2 mM EDTA being used as the final dialyzing and storage buffer. TMV was prepared as described previously (15). Gels containing 30% (wt/wt) TMV or up to 20% M13 were directly obtained from the storage suspensions by centrifugating for 4 h in a Ti-75 rotor (model Ti-75; Beckman Instruments, Inc., Palo Alto, CA) at 55,000 rpm. To prepare gels containing more M13, wet M13 pellets were concentrated further by drying. Finally, the wet pellets were spread out on the inside of the centrifuge tube and the material was dried under a flow of air during 2–8 h at slightly below room temperature. For maximal homogeneity of humidity within the pellets, the material was repelleted at low speed and spread out again on the inside of the centrifuge tube several times during the drying procedure. The change of water content in the drying pellets was roughly followed by weighing and finally determined by measuring the phage concentration spectrophotometrically using  $A_{260} = 3.80$  (0.1% wt/vol, 1-cm path length) for M13 and  $A_{260} = 3.00$  for TMV. Samples were prepared  $\geq 12$  h before the NMR experiments and were stored at 4°C.

### NMR methods

NMR spectra were recorded on a spectrometer (model CXP300; Bruker Instruments, Inc., Billerica, MA) operating at a  $^{31}\text{P}$  NMR frequency of 121.5 MHz. Because of the dielectric properties of wet M13 and TMV gels, the  $\pi/2$  pulse was carefully set to 5  $\mu\text{s}$  on the weak  $^{31}\text{P}$  signal of the sample itself. For cross-polarization experiments, the Hartmann–Hahn condition was found by measuring the  $^1\text{H}$   $\pi/2$  pulse length directly on the water signal and setting it equal to the  $^{31}\text{P}$   $\pi/2$  pulse length. In all experiments a CYCLOPS phase alternation was used to remove the effects of pulse imperfections and high power proton decoupling was on during refocussing delays and acquisition time.

Sample tubes were sealed with glue to keep the water content in the gel constant. This was checked by comparing the sample weight before and after the experiments. Temperature was controlled by a temperature unit (Bruker Instruments, Inc.) connected to a thermocouple positioned at a 3-cm distance from the sample coil. This system was calibrated using an 1010 fluoroptic thermometer (model 1010; ASEA, Västerås, Sweden). The glass fiber detection probe of this instrument does not contain electronic parts and therefore functions correctly in

strong electromagnetic fields, so that the temperature can be measured inside the sample during the actual pulse experiment. The fluoroptic thermometer could only be used for calibration, because sample tubes could not be sealed completely with the temperature fiber penetrating through the tube cap. Substantial differences were observed between the indication of the fluoroptic thermometer and the Bruker unit, especially below room temperature, because a temperature gradient existed within the probehead between the sample directly cooled by a flow of nitrogen and the probewall heated by the surrounding shim coils. The fluoroptic thermometer also showed that the immediate heating effect by high power decoupling was much stronger than estimated from the steady state indication of the temperature unit (Bruker Instruments, Inc.).

Spectra were recorded using cross-polarization and a Hahn echo pulse sequence to remove the effect of probe ringing on the weak signal. For recording standard spectra the echo was made to occur 60  $\mu\text{s}$  after excitation. Transversal relaxation was studied by acquiring the Hahn echoes for a series of refocussing delays and analyzing them in a powder average way by fitting an exponential curve to the echo decay directly. Longitudinal relaxation was determined using the direct inverse recovery pulse sequence, followed by curve fitting applied to the spectra after Fourier transformation. Because in M13 gels  $^{31}\text{P}$  longitudinal relaxation is much slower than transversal relaxation, it was possible to develop a  $T_1$ -filtered  $T_2$  experiment by combining the Carr–Purcell–Meiboom–Gill (CPMG) experiment for the  $T_2$  measurement (18) and the progressive saturation method for the  $T_1$  measurement. This enabled us to investigate a possible correlation between longitudinal and transversal relaxation in M13 gels (19, 20). The pulse spacing in the CPMG sequence was set to 650  $\mu\text{s}$ , because spinlocking effects occurred at smaller pulse interspacing. At the end of the acquisition time of 20 ms an additional  $\pi/2$  pulse was given to reduce longitudinal magnetization effects due to pulse imperfections. The repetition time was varied from 2 to 24 s.

### Simulation procedures

Phosphorus NMR lineshapes and powder average transversal relaxation decays at 121.5 MHz have been simulated for isotropic, uniaxial, and combined diffusion using self-made Fortran programs as described previously (16). For  $^{31}\text{P}$  NMR in M13, relative chemical shift tensor values  $\sigma_{xx} - \sigma_o = 77$  ppm,  $\sigma_{yy} - \sigma_o = 18$  ppm, and  $\sigma_{zz} - \sigma_o = -95$  ppm were taken (where  $\sigma_o$  is the isotropic shift), as obtained from analysis of sideband intensities in several MAS spectra of dehydrated and frozen samples recorded at 202.5 MHz. These values correspond within experimental error to the values reported for bacteriophage fd, which is closely related to M13 (10). For TMV the values 83, 25, and  $-108$  ppm were taken from the literature (14). In simulations for M13 it was assumed that a random distribution of shift tensor orientations exists within the phage, much like the random orientations of microcrystallites within a MAS spinner. For TMV the orientation of  $^{31}\text{P}$  shift tensor for the three different binding sites with respect to the rod-shaped TMV was approximately derived from the  $^{31}\text{P}$  atomic coordinates (13), assuming that in phosphodiester the  $\sigma_{yy}$  lies in the direction of the bisector of the O–P–O angle (as opposed to the RO–P–OR' angle) and that  $\sigma_{zz}$  lies in the O–P–O plane, as well (21). From these approximate tensor orientations ( $\beta_i, \gamma_i$ ) the chemical shift values of the three  $^{31}\text{P}$  NMR lines in the spectrum of an oriented sample of TMV were calculated. By comparing these shift values with the ones calculated earlier (14), we found that sites 1, 2, and 3 as labeled by Stubbs and Stauffer (13) probably correspond to the lines A, C, and B, respectively, according to the labeling by Cross et al. (14). Because the calculated shift values differ from the experimentally observed ones (14), we slightly modified the angles  $\beta_i$  such that the three  $^{31}\text{P}$  lines shifted to the observed positions in the spectrum of oriented TMV without changing their frequency order. These modified angles  $\beta_i$  and the unchanged angles  $\gamma_i$  were used to define the orientation of  $^{31}\text{P}$  tensors within TMV (Table 1). The best fits to the experimental lineshapes of M13 and TMV were found by a least-square fitting, allowing height, baseline, and isotropic

TABLE 1 Labeling of the three binding sites in TMV in different papers and the orientation of the three shift tensors with respect to the axis of TMV as calculated from model coordinates\* and refined from the shift in the oriented spectrum†

Label			Calculated $\beta$	Calculated $\gamma$	Calculated $\sigma$	Observed $\sigma^\ddagger$	Refined $\beta$
Ref. 13	Ref. 12	Ref. 14					
			rad		ppm		rad
1	2	A	0.85	1.21	-29.2	+27	1.03
2	1	C	0.63	0.81	-51.9	0	0.93
3	3	B	0.48	1.02	-76.6	-25	0.75

\* Reference 13.

† Reference 14.

shift of simulated lineshapes to vary. Simulated transversal relaxation curves were fitted to the experimental relaxation decays with only height as a variable.

## RESULTS

The <sup>1</sup>H decoupled <sup>31</sup>P NMR spectra of samples of 15 and 30% (wt/wt) M13 and 30% (wt/wt) TMV at 121.5 (Fig. 1 a) and at 202.5 MHz (not shown) show the characteristic lineshape caused by chemical shift anisotropy (CSA). From these spectra the difference between the largest and the smallest CSA tensorvalue  $|\sigma_{zz} - \sigma_{xx}|$  can be directly estimated as 170 ppm for M13 and 190 ppm for TMV. Lineshape discontinuities are only partially defined in the spectra of M13 and TMV gels. The powder average decays of <sup>31</sup>P NMR Hahn echoes fit well to single exponentials for the two M13 samples and reasonably for TMV (Fig. 2 a). In this way, transversal re-

laxation times  $T_{2e}$  of 0.39, 0.79, and 1.5 ms are found for <sup>31</sup>P in 15, and 30% M13 and 30% TMV gels, respectively. The results above have been obtained using cross-polarization, but no significant differences in lineshapes or relaxation rates are observed when direct excitation is used.

To gain more information about the mechanism causing transversal relaxation, M13 gels have been studied at various frequencies, concentrations, and temperatures.

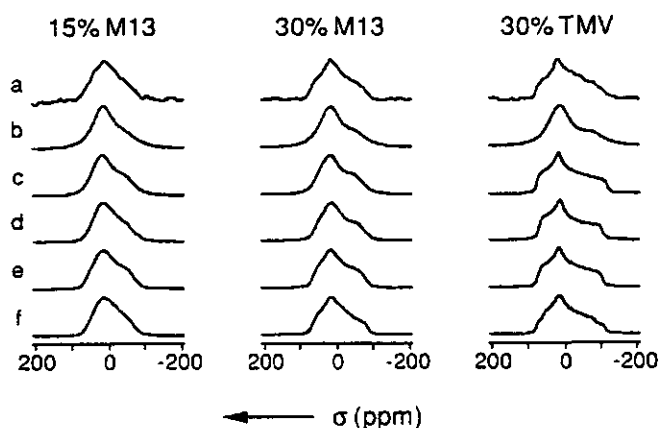


FIGURE 1 Experimental and simulated <sup>31</sup>P lineshapes obtained for 15% (wt/wt) M13 (left; 2,560 scans), 30% M13 (middle; 768 scans), and 30% TMV (right; 512 scans). Experimental spectra (a) are obtained by Fourier transformation of the echo at 60  $\mu$ s created by a  $\pi$  pulse of 10  $\mu$ s centered at 30  $\mu$ s; best-fitting lineshapes by Fourier transformation of echoes (b) and free induction decays (c) simulated for isotropic diffusion; best echo simulated for rigid rod diffusion (d); best echo simulated for combined diffusion (e); best echo simulated for combined diffusion with two (left and central columns) or three (right column) internal components; for diffusion coefficients and restriction halfangles see text.

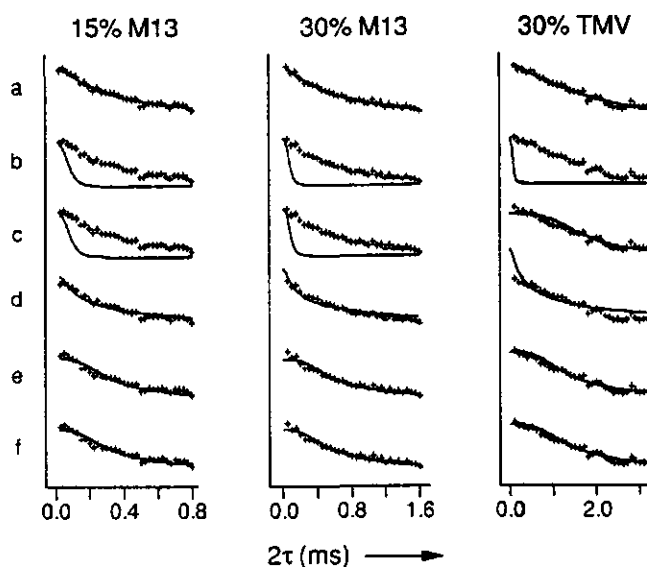


FIGURE 2 Experimental (a) and simulated (b-f) <sup>31</sup>P transversal relaxation decays for 15% M13 (left) 30% M13 (middle), and 30% TMV (right); for 15% M13 32 echoes were measured at subsequent multiples of 25  $\mu$ s starting at 25  $\mu$ s, including the finite pulse length of 10  $\mu$ s (left, a); for 30% M13 32 echoes were measured at subsequent multiples of 50  $\mu$ s starting at 50  $\mu$ s (center, a); for 30% TMV 32 echoes were measured at subsequent multiples of 100  $\mu$ s starting at 200  $\mu$ s (right, a); decay for best Fourier-transformed echo (b) and FID (c) simulated for isotropic diffusion; best decay simulated for rigid rod diffusion (d), best decay simulated for combined diffusion (e), best decay simulated for combined diffusion with two (left and middle, f) or three (right, f) internal components; for diffusion coefficients and restriction halfangles see text.

In these studies it was generally observed that  $T_{2e}$  times, obtained by single-exponential fitting, decrease with magnetic field strength and increase with decreasing temperature and hydration, i.e., with increasing sample viscosity. Proton-decoupled  $T_{2e}$  values measured for gels of M13 in  $\text{D}_2\text{O}$ , are shorter than the corresponding values measured for equally concentrated gels in  $\text{H}_2\text{O}$ . This is presumably due to static  $^2\text{H}$ - $^{31}\text{P}$  dipolar interactions, which could not be eliminated in our experiments. In contrast to  $T_{2e}$ , the longitudinal relaxation time  $T_1$  does not vary significantly for M13 concentrations between 10 and 40% (wt/wt) and temperatures between 10 and  $40^\circ\text{C}$ . In this range of concentrations and temperatures, an average  $T_1$  value of  $4.0 \pm 0.4$  s is measured at 121.5 MHz. Only at low hydration  $T_1$  becomes larger, e.g., 8 s for 80% M13. The large difference between  $T_1$  and  $T_2$  makes it possible to carry out hybrid relaxation experiments. It is found in these experiments that the transversal relaxation time  $T_2^{\text{CP}}$ , measured from the decay of CPMG echoes, is roughly independent of the repetition rate and that the longitudinal relaxation time is approximately the same for all the CPMG echoes. Thus, no  $T_1$  filtering effect on  $T_2^{\text{CP}}$ , nor  $T_2^{\text{CP}}$  filtering effect on  $T_1$  is detectable. Transversal relaxation rates as obtained from the decay of CPMG echoes in our hybrid experiments do not differ significantly from the rates observed in the Hahn echo decay for the pulse interspacing ( $650 \mu\text{s}$ ) used. If the pulse interspacing is decreased, however,  $T_2^{\text{CP}}$  becomes longer.

## DISCUSSION

The width of the observed  $^{31}\text{P}$  NMR line and its proportionality to the magnetic field provide strong evidence for CSA being the dominant line-broadening factor in  $^{31}\text{P}$  spectra of M13 and TMV gels. Because line discontinuities characteristic for static CSA are only partially defined in the experimental spectra, other influences on the lineshape should be considered as well. As no protons are directly bound to  $^{31}\text{P}$  in the nucleic acid backbone, the high power proton decoupling used is sufficient to remove heteronuclear dipolar broadening from the spectra completely. The large distance between subsequent phosphorus nuclei of about 6–7 Å in TMV and presumably in M13 as well (13, 22) and the low gyromagnetic ratio of phosphorus nuclei, rule out the possibility that homonuclear dipolar coupling has a strong effect on the  $^{31}\text{P}$  resonance line. This finally leaves motional narrowing as the most likely explanation for the absence of sharp line discontinuities. Indeed, in M13 spectra the narrowing effect appears more pronounced at high hydration (Fig. 1).

In contrast to their effect on the lineshape, hydration and temperature strongly influence transversal relaxation of phosphorus nuclei in M13. For example, as hydration decreases from 85 to 70%,  $T_{2e}$  doubles from 0.39 to 0.79 ms. Because at higher hydration and temperature

more motion is probably present in M13 gels,  $T_{2e}$  ap-trend expected from Redfield theory. The value of  $T_{2e}$  of 1.5 ms found for TMV suggests that  $^{31}\text{P}$  mobility in 30% TMV gels is less than in M13 gels at a comparable hydration percentage. Several transversal relaxation mechanisms can be considered to explain this effect. High power decoupling, as used in our experiments, is sufficient to remove static  $^1\text{H}$ - $^{31}\text{P}$  dipolar coupling effects from the transversal relaxation decay, as was tested by varying the decoupling power. It does not, however, eliminate the relaxing influence of highly mobile water protons in the vicinity of  $^{31}\text{P}$ .  $T_2$  experiments in  $\text{D}_2\text{O}$  to evaluate this solvent effect suffer from the difficulty that deuterons exchange with protons in the virion and thereby cause static  $^2\text{H}$ - $^{31}\text{P}$  dipolar effects, which cannot be removed unless deuterons are decoupled at a third frequency. In principle, the observed  $T_{2e}$  increase at decreasing hydration could indeed result from the removal of mobile water protons close to  $^{31}\text{P}$ . For motions with such short correlation times, however,  $T_2$  should increase with increasing mobility, which is inconsistent with the observed decrease of  $T_{2e}$  at increasing temperature. This indicates that the relaxing influence of water close to  $^{31}\text{P}$  is relatively unimportant. Neither can  $^{31}\text{P}$ - $^{31}\text{P}$  dipolar coupling account for the observed relaxation, because for bacteriophage fd this type of coupling seems to cause the echo intensity to drop to  $e^{-1}$  of its initial value after 2.6 ms (22), which is long compared with the  $T_{2e}$  values found in our experiments. However, chemical shift fluctuations caused by motions can also spoil the refocussing of transversal coherence by  $\pi$  pulses and thereby shorten  $T_{2e}$  (23). For very slow motions such a mechanism would explain the observed  $T_{2e}$  trend (16). In the fast motion region, where  $T_{2e}$  increases as the motional frequency increases, the observed  $T_{2e}$  trend can only be the consequence of an increase of both motional amplitude and frequency together.

As the dynamic behavior of "naked" nucleic acids is already complex with a variety of internal motions taking place in a wide frequency range (24), the assumption of one single type of motion explaining all experimental  $^{31}\text{P}$  data obtained for M13 and TMV is probably too simple. In fact, the absence of correlation between longitudinal and transversal relaxation as observed for M13 in our hybrid relaxation experiments and their different dependence on hydration suggest that  $T_1$  and  $T_{2e}$  are governed by different types of independent motions. The relative similarity between spectra of 15 and 30% M13 gels in contrast with their large  $T_{2e}$  difference also indicates that lineshapes and transversal relaxation could well be dominated by different motions. A fact that further complicates the analysis of experimental results is that motional variations probably occur because of local viscosity variations within the gel and differences in local  $^{31}\text{P}$  environments within the virion. Nevertheless, we have used the simple diffusion models for phosphorus mobility in M13 and TMV described in the pre-

vious paper (16) to interpret the experimental lineshapes and transversal relaxation decays in a more quantitative manner.

### Isotropic diffusion

The combined effect of uncorrelated internal backbone motions and overall virion motions on  $^{31}\text{P}$  NMR lineshapes and relaxation decays can be assumed to be roughly comparable to the effect of random  $^{31}\text{P}$  diffusion in a viscous solution. This hypothesis was tested using the isotropic diffusion model discussed previously (16). For this type of diffusion, however, no echo lineshapes can be simulated that fit well to the experimental lineshapes of M13 and TMV. The relatively best, least-square fits for 15 and 30% M13 and 30% TMV are found for a diffusion coefficient of 6, 5, and 5 kHz, respectively (Fig. 1*b*), but for these diffusion constants the simulated transversal relaxation is much too fast (Fig. 2*b*). Clearly, the observed motional effects cannot be described by unrestricted, isotropic diffusion.

In the case of restricted motion, boundary effects become more significant as time increases. As a consequence, the isotropic diffusion model may provide a better description for the lineshape, defined by the quickly decaying free-induction decay, than for the relatively slow transversal relaxation. Therefore, neglecting  $T_{2c}$  anisotropy, we have also compared Fourier-transformed free-induction decays with the observed  $^{31}\text{P}$  lines. Again, no lineshapes can be calculated that fit well to the experimental lineshapes. For TMV the simulated lineshape that relatively fits the best is the static lineshape (Fig. 1*c*). Using the equation for ultraslow isotropic diffusion discussed previously (16), the observed relaxation curve can be reasonably simulated for a diffusion constant as small as 0.25 Hz (Fig. 2*c*). For 15 and 30% M13 the relatively best fit is found for 3 and 4 kHz (Fig. 1*c*). Once more, for these diffusion constants the simulated transversal relaxation is too fast (Fig. 2*c*). Obviously, the isotropic diffusion model does not agree with the experimental data.

### Rigid rod diffusion

By use of a uniaxial diffusion model, the hypothesis is tested that free or restricted rotation of the virions as rigid rods about their length axis explains both the observed motional lineshape narrowing and transversal relaxation. For several pairs of the diffusion coefficients  $D$  and restriction halfangles  $\lambda$ , lineshapes can be simulated that fit to the experimental lineshape of 15% M13 equally well. A good fit is produced by, for example, free rotor diffusion with a coefficient of 20 kHz, which seems to confirm an earlier suggestion (10), but the simulated  $T_{2c}$  (0.10 ms) for this case is lower than the experimental one (0.39 ms). The best fit to both the lineshape and the relaxation curve is found for a diffusion coefficient of 50 kHz and a restriction halfangle of 1.25 rad. For 30% M13

the experimental lineshape and transversal relaxation can hardly be interpreted consistently: the lineshape calculated for 0.75 rad and 200 kHz fits the best, but in this case the simulated  $T_{2c}$  value, 3 ms, is much too high. A reasonable fit to both the lineshape and the relaxation curve is produced by a diffusion coefficient of 40 kHz combined with a restriction halfangle of 1.0 rad. For TMV even the experimental lineshape alone cannot be simulated by use of the uniaxial diffusion model because of the sharp top in combination with the large linewidth in the lower part of the line. The most reasonable fit to both the lineshape and the relaxation curve is found for  $D = 25$  kHz and  $\lambda = 0.7$  rad.

Although in the highly viscous gels that we studied, the magnetic field is probably unable to orient the rod-shaped virus particles, we have also added partial orientation to the rigid rod model in an attempt to account for the inconsistency between lineshape effects and transversal relaxation. Indeed, as rotation about the magnetic field axis does not change the chemical shift, the net relaxation becomes slower for given  $D$  and  $\lambda$ , if the weight of parallel rod orientations is increased compared with an isotropic gel. For the same reason, however, motional narrowing also becomes less pronounced in the simulated spectrum. As a consequence, the experimental lineshapes and transversal relaxation decays still cannot be interpreted consistently in terms of rigid rod motion.

For rigid cylinders of the same dimensions as M13 and TMV, constants of 55 and 20 kHz can be calculated for unrestricted diffusion about the cylinder axis in pure water (25). These values almost equal the diffusion constants 50 and 25 kHz found above for 15% M13 and 30% TMV. This finding puzzled us, because gels of M13 and especially TMV are highly viscous: are translational and rotational diffusion in these concentrated gels governed by different viscosity parameters or do the high values of the simulated constants indicate collective motions of segments of the virus rather than rotation of the virus as a whole? The latter interpretation, however, is difficult to reconcile with the outcome of curvature studies, which show that M13 behaves as a rigid rod and not as a string of beads (26). Thus, although more successful than the isotropic diffusion model, the rigid rotor model fails to provide an unambiguous fit for 30% M13 and TMV, and the best diffusion constants that follow from the simulations are much higher than expected for viscous gels.

### Combined diffusion

Instead of regarding M13 and TMV as rigid rods without internal mobility, we also considered the possibility that the nucleic acid backbone within the viruses undergoes restricted motion, superimposed on rotation of the virus particles as a whole. Such a picture is supported by the observation that motional narrowing is still prominently present in spectra of oriented solutions of bacteriophage fd, which is closely related to M13 (11). In the combined diffusion model used here, the internal motion is simpli-

fied to fast, restricted rotation about the length axis of the virus and the overall rotation is assumed to be unrestricted and very slow. Under these conditions the lineshape is dominated by the amplitude of the internal motion only, whereas transversal relaxation also reflects the influence of the overall diffusion (16). A good fit to the lineshape of 30% M13 is calculated for internal rotation with a restriction halfangle  $\lambda$  of 0.75 rad (Fig. 1 *e*). For  $\lambda$  kept at this value, the best fit to the experimental relaxation curve is calculated for an overall diffusion coefficient of  $D = 50$  Hz (Fig. 2 *e*). Assuming first that hydration only influences the overall rotation of the virion, an attempt has been made to simulate the 15% M13 lineshape for  $\lambda = 0.75$  rad as well. A good fit to the lineshape is obtained for  $D = 5$  kHz, but the corresponding  $T_{2e}$  (0.16 ms) is too small. When  $\lambda$  is left free to vary, the best fit to both the lineshape and the relaxation curve of 15% M13 is obtained for  $\lambda = 0.9$  rad and  $D = 400$  Hz. For TMV the observed lineshape cannot be simulated well by use of the combined diffusion model. The relatively best fit to both the lineshape and the relaxation curve is found for  $\lambda = 0.6$  rad and  $D = 3$  Hz.

Despite this success in the simulation of M13 lineshapes, the treatment of the complicated backbone dynamics as simple uniaxial rotation is bound to be too simple. Diffusion models involving more angle fluctuations would probably result in smaller restriction angles per fluctuating angle than the  $\lambda$  values found above. This should be borne in mind when comparing the halfangles between 0.6 and 0.9 rad with, for example, backbone fluctuations of  $\pm 27^\circ$  in the GHz range reported earlier for DNA (27). Interestingly, unoriented fd solutions show more motional narrowing than oriented ones at the same or even lower concentration (10, 11), which suggests that rotation about the length axis of fd does contribute a significant part to internal motion. That hydration influences both motional frequencies and amplitudes, as observed for M13, has been reported for DNA as well (24) and could be related somehow to the swelling of M13 upon hydration (2).

The low coefficients for overall diffusion as interpreted from the observed transversal relaxation better reflect the macroscopic viscosity of the virus gels than the values that followed from the rigid rod analysis above. Although the simulated decays fit well (Fig. 2 *e*), the observed decays still fit better to single exponentials (Fig. 2 *a*). This may be a consequence of the fact that the combined diffusion model neglects the exponential contribution of fast internal motions to transversal relaxation. In the  $T_{2e}$  region of interest such a contribution could only be significant for internal motions with frequencies  $< 10^5$  Hz. Alternatively, the observed exponential deviation from the theoretical decays could be explained by local viscosity variations within the virus gels because of local hydration differences: contributions of more rapidly rotating virus particles would mask the

nonexponential character of transversal relaxation close to  $t = 0$ .

### Internal mobility variations

The impossibility to produce lineshapes that fit well the observed TMV line by use of the isotropic, rotor, or combined diffusion model has led us to include possible mobility differences among the three binding sites in TMV in our simulations. Using the fast diffusion model (16), a set of 10 lineshapes has been calculated for restriction halfangles  $\lambda$  being multiples of 0.15 rad up to 1.5 rad for every of the three sites separately. From the three sets 1,000 spectra were generated by making triple combinations. Comparing these combined spectra with the observed TMV spectrum, we generally found that a combination of two static sites and one mobile site greatly improved the lineshape fit. The best fit was produced by a  $\lambda$  value of 0.15 rad for site 1, 1.5 rad for site 2, and 0.3 rad for site 3 (as labeled by Stubbs and Stauffacher [13]; Fig. 1 *e*). Keeping this optimal combination of three halfangles  $\lambda$  fixed, the best fitting  $T_2$  decay was calculated for overall diffusion with a coefficient of 3 Hz (Fig. 2 *e*). The model that sites 1 and 3 undergo only small amplitude motion, whereas site 2 is relatively mobile, is confirmed by NMR spectra of oriented TMV samples, in which the central resonance line is much broader than the other two (11) and by an early TMV model, on the basis of x-ray results, in which site 1 and 3 (labeled there as 2 and 3) are in close contact with arginine residues (12). A recently refined model with two arginines binding site 1 and site 2 (28) would favor a combination of halfangles 0.15, 0.15, and 0.9 rad for sites 1, 2, and 3, respectively, which fits to the observed lineshape almost equally well within experimental error.

Because of a slight, but systematic mismatch at the top between the experimental lineshape of 30% M13 and the best-fitting simulated lineshapes, we have tried to improve the lineshape fit for M13 assuming two  $^{31}\text{P}$  fractions with different mobilities. Using the fast diffusion model, we calculated 10 spectra for  $\lambda$  values being multiples of 0.15 rad up to 1.5 rad and combined them in hundred pairs. For every pair the best bilinear fit to the experimental lineshape was calculated and the statistical variance was compared with the other bilinear fits. The best bilinear fit of all pairs to the lineshape of 30% M13, produced by a combination of 83%  $\lambda = 0.6$  rad and 17%  $\lambda = 1.5$  rad, reproduces the experimental lineshape very well indeed (Fig. 1 *e*). Keeping the fraction ratio fixed, we also find for 15% M13 that the lineshape is better described by a combination of 83%  $\lambda = 0.9$  rad and 17%  $\lambda = 1.5$  rad than by 100% 0.9 rad (Fig. 1 *e* and *d*, respectively). For these combinations of halfangles the best fits to the decays of 30 and 15% M13 are obtained for overall diffusion coefficients of 70 and 550 Hz, respectively (Fig. 2 *e*), which are slightly larger than the coefficients found for the single component model above.

When, in analogy with TMV, the immobile phosphorus fraction in M13 is associated with the phosphodiester that interact most strongly with coat proteins, the percentage of 83% would indicate that per 10 monomers forming a unit cell of the protein coat, 20 out of 24 phosphodiester are actually rigidly bound at a ratio of two nucleotides per monomer. The same stoichiometry is suggested by the observation that during the extrusion of a completed virion out of the host cell every gene-5 protein molecule, which binds four nucleotides, is replaced by two gene-8 protein molecules (29). Interestingly, viral DNA that is twisted into a form resembling a double-stranded B-DNA helix with a pitch of 34 Å, a diameter of ~20 Å and 10 nucleotides per strand per turn, would fit in the hollow tube formed by the coat proteins with approximately the same protein/nucleotide ratio 1:2 and with the axial rise of about 3.4 Å per nucleotide observed in x-ray studies (4). Such a model seems to be confirmed by infrared linear dichroism results indicating a B-type backbone conformation as well (9). Perhaps the indications for maximal 20% A-DNA backbone in Raman spectra (8) and some regular DNA structure with a pitch of 27 Å in diffraction patterns (4) are related to the mobile fraction of 17% DNA found in our experiments.

Obviously, details of the tentative model of 83% viral DNA twisted into a sort of double-stranded B-helix should be specified in agreement with the experimental data reported until now. Raman spectroscopy has shown the sugar pucker to be C3'-endo, a feature of double-stranded A-DNA, rather than C2'-endo, typical for double-stranded B-DNA (8), but the absence of basepairing in the viral DNA could possibly allow such an A-type sugar puckering in combination with a B-type backbone. The different symmetries of the DNA helix and the protein coat would cause binding to distort the DNA backbone and destroy the equivalence among the phosphodiester, which could offer a possible explanation for the absence of B-DNA backbone characteristics in diffraction patterns, Raman spectra, and NMR spectra. This would also explain the characteristics of a disordered DNA backbone found in  $^{31}\text{P}$  NMR spectra of oriented and MAS samples in contrast to the case of, for example, TMV, where the RNA molecule and the protein share the same symmetry and as a consequence the  $^{31}\text{P}$  NMR resonances of the three binding sites can be resolved. Backbone motions could further strengthen these features of disorder, especially under the high hydration conditions used for sample orientation, when the motional amplitudes tend to be large (see above).

## CONCLUSION

In this paper we have shown by simulations that motional effects on  $^{31}\text{P}$  NMR lineshapes and transversal re-

laxation of M13 and TMV cannot be described in terms of simple isotropic diffusion. The model for M13 diffusing as a rigid rod about its length axis is more successful for interpreting the NMR results obtained for 15% M13, although the diffusion coefficient, determined from the simulations, seems much higher than expected from the high viscosity of the gel. For 30% M13, however, the lineshape and transversal relaxation cannot be interpreted consistently and for 30% TMV the observed lineshape cannot even be simulated, indicating that the rigid rod model does not actually apply. Using a combined diffusion model, which assumes the lineshape to be dominated by fast internal DNA motions and transversal relaxation to reflect slow rotation of the virus as a whole, we can interpret the NMR results obtained for M13 in a consistent way. The diffusion coefficients for the slow overall diffusion are found to be low, as expected from the high sample viscosity. The restriction halfangle found for internal DNA motion indicates that the encapsulated DNA has substantial motional freedom. In contrast to simulations for M13, combined diffusion simulations fail to produce the experimental TMV lineshape. However, significantly improved lineshape fits are obtained for TMV under the assumption that the three binding sites have different mobilities. The finding that the best lineshape fits consist of one mobile and two static phosphodiester seems to be confirmed by TMV models deduced from x-ray studies. Combined diffusion simulations with two components also improve the calculated lineshapes for M13. About 83% of the viral DNA appears to be rigidly bound at a protein/nucleotide ratio of 1:2. Together with the structural parameters of the protein coat this ratio suggests that despite the sugar pucker typical for A-DNA found by Raman spectroscopy, the backbone structure of 83% of the encapsulated DNA molecule may be roughly comparable to the backbone structure of double-stranded B-DNA, although binding to the protein coat probably induces significant distortions.

In this paper, parameters for  $^{31}\text{P}$  mobility in M13 and TMV have been estimated by assuming motion and chemical shift anisotropy to be the only factors influencing the lineshape and transversal relaxation. Especially in the case of TMV, however, homonuclear dipolar coupling cannot be excluded as a significant contributor to the observed transversal relaxation (22). If this relaxation mechanism would be included in our simulation models, the resulting diffusion coefficients would be lower, but our limited experimental data do not allow such a refinement. Therefore, values of the diffusion coefficients presented in paper are safest when regarded as upper limits. As for the method of extracting motional parameters from experimental data by comparison with simulated data, our experience is that it is risky to analyze a NMR lineshape or a transversal relaxation decay alone. Both the lineshape and transversal relaxation



should be used to check motional models and obtain better estimations for the motional parameters.

We are grateful to Ruud Spruijt for isolation and purification of M13 and TMV, to Willem Stolp for lending us the fluoroptic thermometer, to Adrie de Jager and Lucie van de Steeg for experimental assistance, and to Ben Harmsen and Ruud Konings for helpful discussions.

This research was supported by the Netherlands Foundation of Biophysics with financial aid of the Netherlands Organization for Scientific Research (NWO).

Received for publication 30 November 1992 and in final form 11 February 1993.

## REFERENCES

1. Rasched, I., and E. Oberer. 1986. Ff coliphages: structural and functional relationships. *Microbiol. Rev.* 50:401-427.
2. Dunker, A. K., R. D. Klausner, D. A. Marvin, and R. L. Wiseman. 1974. Filamentous bacterial viruses X. X-ray diffraction studies of the R4 A-protein mutant. *J. Mol. Biol.* 81:115-117.
3. Van Weezenbeeck, P. M. G. F., T. J. M. Hulsebos, and J. G. G. Schoenmakers. 1980. Nucleotide sequence of the filamentous bacteriophage M13 DNA genome: comparison with phage fd. *Gene* 11:129-148.
4. Banner, D. W., C. Nave, and D. A. Marvin. 1981. Structure of the protein and DNA in fd filamentous bacterial virus. *Nature (Lond.)* 289:814-816.
5. Marvin, D. A., R. L. Wiseman, and E. J. Wachtel. 1974. Filamentous bacterial viruses XI. Molecular architecture of the class II (Pfl, Xf) virion. *J. Mol. Biol.* 82:121-138.
6. Day, L. A. 1973. Circular dichroism and ultraviolet absorption of a deoxyribonucleic acid binding protein of filamentous bacteriophage. *Biochemistry* 12:5329-5339.
7. Day, L. A., R. Wiseman L., and C. J. Marzec. 1979. Structure models for DNA in filamentous viruses with phosphates near the center. *Nucleic Acids Res.* 7:1393-1403.
8. Thomas, G. J., Jr., B. Prescott, S. J. Opella, and L. A. Day. 1988. Sugar pucker and phosphodiester conformations in viral genomes of filamentous bacteriophages: fd, Ifl, IKe, Pfl, Xf, and Pf3. *Biochemistry* 27:4350-4357.
9. Fritzsche, H., T. A. Cross, S. J. Opella, and N. R. Kallenbach. 1981. Structure and architecture of the bacterial virus fd. An infrared linear dichroism study. *Biophys. Chem.* 283-291.
10. DiVerdi, J. A., and S. J. Opella. 1981. Phosphorus-31 nuclear magnetic resonance of fd virus. *Biochemistry* 20:280-284.
11. Cross, T. A., P. Tsang, and S. J. Opella. 1983. Comparison of protein and deoxyribonucleic acid backbone structures in fd and Pfl bacteriophages. *Biochemistry* 22:721-726.
12. Stubbs, G., S. Warren, and K. Holmes. 1977. Structure of RNA and RNA binding site in tobacco mosaic virus from 4 Å map calculated from x-ray fiber diagrams. *Nature (Lond.)* 267:216-221.
13. Stubbs, G., and C. Stauffacher. 1981. Structure of the RNA in tobacco mosaic virus. *J. Mol. Biol.* 152:387-396.
14. Cross, T. A., S. J. Opella, G. Stubbs, and D. L. D. Caspar. 1983. Phosphorus-31 nuclear magnetic resonance of the RNA in tobacco mosaic virus. *J. Mol. Biol.* 170:1037-1043.
15. Hemminga, M. A., P. A. De Jager, J. Krüse, and R. M. J. N. Lamerichs. 1987. Magic-angle-spinning NMR on solid biological systems. Analysis of the origin of the spectral linewidths. *J. Magn. Reson.* 71:446-460.
16. Magusin, P. C. M. M., and M. A. Hemminga. 1993. A theoretical study of rotational diffusion models for rod-shaped viruses: the influence of motion on <sup>31</sup>P NMR lineshapes and transversal relaxation. *Biophys. J.* 64:1851-1860.
17. Spruijt, R. B., C. J. A. M. Wolfs, and M. A. Hemminga. 1989. Aggregation-related conformational change of the membrane-associated coat protein of bacteriophage M13. *Biochemistry* 28:9158-9165.
18. Slichter, C. P. 1978. Principles of Magnetic Resonance. Springer-Verlag, Berlin. 397 pp.
19. Eisenstadt, M. 1980. NMR hybrid relaxation methods of studying chemical, physical, and spin exchange. I. General theory and experimental methods. *J. Magn. Reson.* 38:507-527.
20. Snaar, J. E. M., and H. E. Van As. 1990. Discrimination of different types of motion by modified stimulated-echo NMR. *J. Magn. Reson.* 87:132-140.
21. Herzfeld, J., R. G. Griffin, and R. A. Haberkorn. 1978. Phosphorus-31 chemical-shift tensors in barium diethyl phosphate and urea-phosphoric acid: model compounds for phospholipid head-group studies. *J. Am. Chem. Soc.* 100:2711-2718.
22. Opella, S. J., and J. A. DiVerdi. 1982. Properties of the phosphodiester backbone of duplex DNA and filamentous bacteriophage DNA. In *Biochemical Structure Determination by NMR*. A. A. Bothner-By, J. Glickson, and B. D. Sykes, editors. Marcel Dekker, New York. 149-168.
23. Abragam, A. 1961. The Principles of Nuclear Magnetism. Oxford University Press, London. 599 pp.
24. Alam, T. M., and G. P. Drobny. 1991. Solid-state NMR studies of DNA structure and dynamics. *Chem. Rev.* 91:1545-1590.
25. Edsall, J. T. 1953. Size, shape and hydration of protein molecules. In *The Proteins*. H. Neurath, and K. Bailey, editors. Academic Press, Inc., New York. 549-686.
26. Song, L., U.-S. Kim, J. Wilcoxon, and J. M. Schurr. 1991. Dynamic light scattering from weakly bending rods: estimation of the dynamic bending rigidity of the M13 virus. *Biopolymers* 31:547-569.
27. Hogan, M. E., and O. J. Jardetzky. 1980. Internal motions in deoxyribonucleic acid II. *J. Am. Chem. Soc.* 102:3460-3468.
28. Namba, K., R. Pattanayek, and G. Stubbs. 1989. Visualization of protein-nucleic acid interactions in a virus. Refined structure of intact tobacco mosaic virus at 2.9 Å resolution by x-ray fiber diffraction. *J. Mol. Biol.* 208:307-325.
29. Marvin, D. A., W. J. Pigram, R. L. Wiseman, E. J. Wachtel, and F. J. Marvin. 1974. Filamentous bacterial viruses XII. Molecular architecture of the class I (fd, Ifl, IKe) Virion. *J. Mol. Biol.* 88:581-600.

## **CHAPTER 4**

### **Analysis of $^{31}\text{P}$ MAS NMR spectra and transversal relaxation of bacteriophage M13 and tobacco mosaic virus**

(published in 1994, Biophys. J. 66 , 1197-1208)

## Analysis of $^{31}\text{P}$ MAS NMR Spectra and Transversal Relaxation of Bacteriophage M13 and Tobacco Mosaic Virus

Pieter C. M. M. Magusin and Marcus A. Hemminga

From the Department of Molecular Physics, Agricultural University, Dreijenlaan 3, 6703 HA Wageningen, The Netherlands

**ABSTRACT** Phosphorus magic angle spinning nuclear magnetic resonance (NMR) spectra and transversal relaxation of M13 and TMV are analyzed by use of a model, which includes both local backbone motions of the encapsulated nucleic acid molecules and overall rotational diffusion of the rod-shaped virions about their length axis. Backbone motions influence the sideband intensities by causing a fast restricted reorientation of the phosphodiester. To evaluate their influence on the observed sideband patterns, we extend the model that we used previously to analyze nonspinning  $^{31}\text{P}$  NMR lineshapes (Magusin, P.C.M.M., and M. A. Hemminga, 1993a, *Biophys. J.* 64:1861-1868) to magic angle spinning NMR experiments. Backbone motions also influence the conformation of the phosphodiester, causing conformational averaging of the isotropic chemical shift, which offers a possible explanation for the various linewidths of the centerband and the sidebands observed for M13 gels under various conditions. The change of the experimental lineshape of M13 as a function of temperature and hydration is interpreted in terms of fast restricted fluctuation of the dihedral angles between the POC and the OCH planes on both sides of the  $^{31}\text{P}$  nucleus in the nucleic acid backbone. Backbone motions also seem to be the main cause of transversal relaxation measured at spinning rates of 4 kHz or higher. At spinning rates less than 2 kHz, transversal relaxation is significantly faster. This effect is assigned to slow, overall rotation of the rod-shaped M13 phage about its length axis. Equations are derived to simulate the observed dependence of  $T_{2e}$  on the spinning rate.

### INTRODUCTION

Although the protein coats of both bacteriophage M13 and tobacco mosaic virus (TMV) are highly regular cylindrical arrays of rigidly fixed protein monomers, the packing of the viral genome within the virions is completely different. From x-ray studies, much information is obtained about the structure and the interactions of the single-stranded RNA molecule in TMV, which is buried within the coat between layers of subunits, following the protein helix with three nucleotides per protein subunit at a radius of about 40 Å (Stubbs et al., 1977). In contrast, much less is known about the geometry of the circular, single-stranded DNA molecule in M13, which is probably located along the inside of the tubular protein coat. Phosphorus nuclear magnetic resonance (NMR) studies have indicated that the DNA molecule is immobilized (DiVerdi and Opella, 1981), presumably due to electrostatic interaction between the negatively charged phosphodiester of the nucleic acid backbone and positively charged lysine residues of the protein coat. The interaction with the highly regular protein coat, however, does not seem to force the DNA backbone into some regular structure, because a large variety of crystallographic and spectroscopic techniques have been unable to reveal such regularity (Marvin et al., 1974; Banner et al., 1981; Thomas et al., 1988; Cross et al., 1983b). Because phosphorus nuclei in M13 and TMV are only present in the phosphodiester of the encapsulated nucleic acid molecules,  $^{31}\text{P}$  NMR spectroscopy can be used

to study structure and dynamics of the nucleic acid backbone selectively. Motional lineshape narrowing and transversal relaxation observed in  $^{31}\text{P}$  NMR studies of virus gels can neither be explained by (restricted) overall rotation of the virus particles as rigid rods about their length axis, nor by isotropic motion of the phosphodiester inside (Magusin and Hemminga, 1993a). Instead, a combined diffusion model with fast restricted motions of the encapsulated nucleic acid dominating the spectrum superimposed on slow overall rotation of the virions affecting transversal relaxation provides a consistent picture. Simulation of the nonspinning  $^{31}\text{P}$  NMR lineshape of TMV is greatly improved by the assumption that one of the three binding sites is more mobile than the other two. However, unambiguous assignment of motional amplitudes to specific binding sites is not possible, because their powder lineshapes strongly overlap.

The problem of overlapping resonances may be solved by employing magic angle spinning (MAS), which breaks up a broad  $^{31}\text{P}$  NMR powder lineshape into a sharp centerband at the isotropic chemical shift position flanked by rotational sidebands. The relative intensities of these sidebands have been calculated for the "ideal" case that the orientations of the chemical shift tensors in the sample are rigidly fixed with respect to the rotor (Herzfeld and Berger, 1980). Motions, however, may cause "anomalous" MAS behavior and, in fact, motional information may be extracted from anomalous features (Schmidt et al., 1986; Schmidt and Vega, 1987). Resonances are more easily resolved and specific sideband patterns, including their motional information, may be assigned to specific isotropic chemical shifts, because for phosphodiester compounds, the width of the centerband and the sidebands is typically a few parts per million. Assignment of isotropic chemical shifts, in turn, is facilitated by the strong

Received for publication 13 April 1993 and in final form 25 January 1994.

Address reprint requests to Dr. Hemminga, the Department of Molecular Physics, Agricultural University, P.O. Box 8128, 6700 ET Wageningen, The Netherlands.

© 1994 by the Biophysical Society

0006-3495/94/04/1197/12 \$2.00

dependence of the isotropic chemical shift on the conformation of the phosphodiester group (Gorenstein, 1981; Giessner-Prettre et al., 1984). Resonances of inequivalent phosphodiesters in a nucleic acid molecule packed within a virion may therefore be resolved in MAS NMR spectra, if their conformations are sufficiently different. Indeed, <sup>31</sup>P MAS NMR spectra of TMV solutions (Cross et al., 1983a) and dried TMV pellets (Hemminga et al., 1987) show two resolved sideband patterns with an overall intensity ratio of approximately 2, which have been assigned by comparing torsion angle values for the three types of phosphodiesters in TMV (Hemminga et al., 1987). MAS NMR spectra of bacteriophage fd, which is closely related to M13, only contain a single, broad centerband flanked by sidebands (DiVerdi and Opella, 1981), indicating that a continuous distribution of phosphodiester conformations is present in the phage, rather than a distinguishable few.

In this paper, we will present the results of <sup>31</sup>P MAS NMR experiments applied to M13 and TMV. Anomalous sideband patterns of M13 and TMV will be analyzed in terms of restricted reorientation of the phosphodiester groups which is caused presumably by fast nucleic acid backbone motions. It will be demonstrated that the same type of restricted phosphodiester reorientation can also explain transversal <sup>31</sup>P relaxation measured at a spinning rate of 4 kHz or more. Especially for M13, a model is developed to interpret the lineshape of the centerband and the sidebands in terms of a continuous distribution of phosphodiester conformations and to calculate the narrowing effect of specific conformational fluctuations on the lineshape of the centerband and sidebands. The spinning rate dependence of the  $T_{2e}$  values measured for M13 at low spinning rates will be explained by slow, overall rotation of the rod-shaped virions about their length axis.

## THEORY

### Sideband intensities

To calculate the combined effect of both MAS and rotational diffusion on NMR spectra and transversal relaxation of <sup>31</sup>P in virions, the orientation of a <sup>31</sup>P chemical shift tensor is specified most conveniently by a sequence of three rotation steps, which relates the laboratory frame via subsequent axis systems fixed to the rotor and the virus particle to the principle axis system of the chemical shift tensor given by the Euler angles  $\Omega = (\chi, \zeta, \xi)$ ,  $\Omega' = (\phi, \theta, \psi)$ , and  $\Omega'' = (\alpha, \beta, \gamma)$ , respectively. Consequently, the precession frequency  $\omega$  caused by the combined Zeeman and orientation-dependent chemical shift interaction may be expressed in terms of the Wigner functions  $D_{m'm}^2(\alpha\beta\gamma) = \exp(im'\gamma)d_{m'm}^2(\beta)\exp(im\alpha)$  (Edmonds, 1960; Haeberlen, 1976) as

$$\omega(\Omega, \Omega', \Omega'') = \omega_0 + \omega_0\sigma_0 + \omega_0 \sum_{m,m'=-2}^2 D_{m'm}^2(\Omega)D_{m'm}^2(\Omega') \times [F_0 D_{0m}^2(\Omega'') + F_2(D_{2m}^2(\Omega'') + D_{-2m}^2(\Omega''))] \quad (1)$$

where  $\omega_0 = \gamma B_0$  is the Zeeman angular frequency,  $\sigma_0 = (\sigma_{11} + \sigma_{22} + \sigma_{33})/3$ ,  $F_0 = (\sigma_{33} - \sigma_0)$  and  $F_2 = (\sigma_{22} - \sigma_{11})/\sqrt{6}$  for a chemical shift tensor with principle values  $\sigma_{11}$ ,  $\sigma_{22}$ , and  $\sigma_{33}$ . It is assumed that, although conformational motions may cause  $\sigma_0$  to fluctuate,  $F_0$  and  $F_2$  are constant in time. This is a reasonable assumption, because the  $F_0$  and  $F_2$  values measured for

<sup>31</sup>P in various nucleic acids, generally occur within the ranges  $-105 \pm 10$  ppm and  $-25 \pm 2$  ppm, respectively (Magusin and Hemminga, 1993a; Hemminga et al., 1987), indicating that conformationally induced changes of  $F_0$  and  $F_2$  are relatively small. For MAS at an angular frequency  $\omega_r$ , the angles  $\zeta$  and  $\xi$  in Eq. 1 are set to  $\arccos(1/\sqrt{3})$  and  $\omega_r t$ , respectively. All virion orientations  $\Omega'$  with respect to the MAS rotor equally occur in an isotropic powder and the number of relative chemical shift tensor orientations  $\Omega''$  within the virion may vary from a single one in Pf1 (Cross et al., 1983b), for example, or three in TMV (Cross et al., 1983a), for instance, to a large value representing a nucleic acid backbone without structural correlation to the viral coat geometry, such as bacteriophage fd (Cross et al., 1983b), so that the number of angles actually involved in the calculation can become quite large. Due to the symmetry properties of Eq. 1, however, only  $\theta$ ,  $\beta$ , and  $\gamma$  values between 0 and  $\pi/2$  need to be taken into account, as long as  $\phi$  and  $\psi$  vary between 0 and  $2\pi$ , and  $\alpha$  may be chosen 0 without loss of generality.

In our previous analysis of static <sup>31</sup>P NMR lineshapes of both viruses at 121.5 MHz, we characterized the net effect of the probably complex dynamics of the encapsulated nucleic acid molecule by a single "cumulative motional amplitude" using a simple model, in which the phosphodiesters undergo fast restricted rotation about the length axis of the virions. Extending this model to MAS NMR, we assume that the phosphodiesters undergo uniaxial diffusion restricted to angles  $\alpha$  [ $\alpha_0 - \lambda$ ,  $\alpha_0 + \lambda$ ], fast enough to allow us to replace  $D_{m'm}^2(\Omega'')$  in Eq. 1 by the average value  $D_{m'm}^2(\Omega'') \text{sinc}(m'\lambda)$ , where  $\Omega''$  is redefined as  $(\alpha_0, \beta, \gamma)$  and  $\text{sinc}(m'\lambda)$  denotes the function  $\sin(m'\lambda)/m'\lambda$ . After this substitution, the relative sideband intensities in the MAS NMR spectrum may be calculated by Fourier transformation of the free induction decay

$$S(t) = (8\pi^2)^{-2} \int d\Omega' \int d\Omega'' \exp \left[ i \int_0^t \omega(\zeta, \omega_r, t', \Omega', \lambda, \Omega'') dt' \right] \quad (2)$$

with

$$\begin{aligned} & \int_0^t \omega(\zeta, \omega_r, t', \Omega', \lambda, \Omega'') dt' \\ &= \omega_0(1 + \sigma_0)t + \omega_0 \sum_{m \neq 0} d_{m0}^2(\zeta) \frac{e^{im\omega_r t} - 1}{m\omega_r} \\ & \times \sum_{m'=-2}^2 D_{m'm}^2(\Omega') \frac{\sin(m'\lambda)}{m'\lambda} [F_0 D_{0m}^2(\Omega'') + F_2(D_{2m}^2(\Omega'') + D_{-2m}^2(\Omega''))] \end{aligned}$$

As Eq. 2 shows, a fast restricted motion reduces the apparent chemical shift anisotropy and thereby influences the sideband pattern produced by MAS.

### Transversal relaxation

Slow, unrestricted rotational diffusion of the rod-shaped virions about their length axes superimposed on the fast restricted nucleic acid motions inside is incorporated in our model by adding a diffusion term  $D(\partial^2/\partial\psi^2)$  to the so-called stochastic Liouville equation (SLE) (Dufourc et al., 1992). For the positive and negative-helicity components  $\mu_{\pm}(\Omega', \Omega'', t)$  of the spin density operator  $\rho(\Omega', \Omega'', t)$ , where  $I_+$  and  $I_-$  are the raising and lowering operators for a spin-1/2 nucleus, the relevant part of the SLE becomes

$$\frac{d\mu_{\pm}(\Omega', \Omega'', t)}{dt} = \left( \pm i\omega(\Omega', \Omega'', t) + D \frac{\partial^2}{\partial\psi^2} \right) \mu_{\pm}(\Omega', \Omega'', t) \quad (3)$$

where the notation of  $\omega(\zeta, \omega_r, t, \Omega', \lambda, \Omega'')$  in Eq. 2 has been simplified to  $\omega(\Omega', \Omega'', t)$ . Unfortunately, Eq. 3 cannot be solved analytically and some approximation must be made. Theoretical investigation of the influence of rotational diffusion on transversal relaxation under nonspinning conditions, has shown that for very slow diffusion the relaxation rate may be much larger than the diffusion coefficient (Magusin and Hemminga, 1993b). In such cases, most spin density stays close to its initial orientation within times comparable with the transversal relaxation time. This allows local, linear approximations to be made for the chemical shift as a function of the ori-

entation, which greatly facilitates the calculation of transversal relaxation. We have employed the same method to approximately solve Eq. 3 for very slow diffusion. For every orientation  $\Omega'_0 = (\phi, \theta, \psi_0)$ ,  $\omega(\Omega', \Omega'', t)$  is locally approximated as  $\omega(\Omega'_0, \Omega'', t) + \omega'(\Omega'_0, \Omega'', t)(\psi - \psi_0)$ , where  $\omega'(\Omega'_0, \Omega'', t)$  denotes the derivative  $\partial\omega/\partial\psi$  for  $\psi = \psi_0$ . With this linear approximation, the two spin density components can be obtained analytically from Eq. 3. Similar to the derivation of transversal relaxation for spins diffusing in a static field gradient (Slichter, 1978), it follows that a  $\pi$  pulse at  $t = \tau$  produces an echo at  $t = 2\tau$  given by

$$E(2\tau) = (8\pi^2)^{-2} \int d\Omega' \quad (4)$$

$$\int d\Omega'' \exp \left[ -2D \int_0^\tau \left\{ \int_0^t \omega'(\Omega', \Omega'', t') dt' \right\}^2 dt \right]$$

where  $\Omega'$  has been redefined as  $\Omega'_0$ . When the refocussing  $\pi$  pulse is given at  $t = nT_r$ , i.e., after an integral number of spinner rotations, the oscillating terms in the argument of the exponential function in Eq. 4 vanish and only terms linear in  $t$  remain

$$E(2nT_r) = (8\pi^2)^{-2} \int d\Omega' \int d\Omega'' \exp \left[ -D \frac{\omega_0^2}{\omega_i^2} 2nT_r a(\Omega', \Omega'') \right] \quad (5)$$

where

$$a(\Omega', \Omega'') = \left\{ \left[ \sum_{m \neq 0} d_{m0}^2(\xi) \frac{1}{m} \sum_{m' \neq 0} D_{m'm}^2(\Omega'_0) \frac{\sin(m'\lambda)}{\lambda} \right. \right. \\ \times [F_0 D_{0m}^2(\Omega'') + F_2(D_{2m}^2(\Omega'') + D_{-2m}^2(\Omega''))] \Bigg]^2 \\ - \sum_{m \neq 0} d_{m0}^2(\xi) d_{-m0}^2(\xi) \frac{1}{m^2} \sum_{m' \neq 0} D_{m'm}^2(\Omega'_0) \frac{\sin(m'\lambda)}{\lambda} \\ \times [F_0 D_{0m}^2(\Omega'') + F_2(D_{2m}^2(\Omega'') + D_{-2m}^2(\Omega''))] \\ \times \sum_{m' \neq 0} D_{m'-m}^2(\Omega'_0) \frac{\sin(m'\lambda)}{\lambda} \\ \times [F_0 D_{0m}^2(\Omega'') + F_2(D_{2m}^2(\Omega'') + D_{-2m}^2(\Omega''))] \Bigg\}$$

Eq. 5 can be used to calculate the decay of echoes numerically. In practice, however, this multiexponential relaxation is hard to distinguish from a single exponential. An apparent relaxation time  $T_{2e}^{\text{SOR}}$  due to the slow overall rotation (SOR) of the virions, may be defined from the apparent derivative of Eq. 5 at  $nT_r = 0$ , which can be derived by use of the orthogonal properties of the second rank Wigner functions as

$$\frac{1}{T_{2e}^{\text{SOR}}} = D \frac{M_2}{\omega_i^2} \left\{ \frac{1}{5} \text{sinc}^2(\lambda) + \frac{4}{5} \text{sinc}^2(2\lambda) \right\} \quad (6)$$

where  $M_2$  denotes the second moment of the nonspinning lineshape in the absence of backbone motions, given by  $\omega_0^2(F_0^2 + 2F_2^2)/5$ . For extremely slow motion, a similar equation may be derived for  $T_2$  effects caused by homonuclear dipolar fluctuations in MAS experiments (Mehring, 1983). As follows from Eq. 6, on the one hand,  $T_{2e}^{\text{SOR}}$  decreases as the slow overall rotation becomes faster and as  $M_2$  becomes larger at increasing magnetic field strength. On the other hand,  $T_{2e}^{\text{SOR}}$  increases at increasing amplitude  $\lambda$  of the backbone motions and at increasing spinning rate  $\omega_i$ . At high spinning rates, therefore, other relaxation mechanisms, which are independent of the spinning rate, become more important. The same fast backbone motions that modify the sideband intensities (Eq. 2) and suppress the relaxation effect caused by slow overall rotation (Eq. 6), also induce transversal relaxation by causing local field fluctuations due to the chemical shift anisotropy (CSA) of the  $^{31}\text{P}$  nuclei. From the general formula  $1/T_{2e} \approx \Delta M_2 \tau$ , which relates  $T_{2e}$  to the portion of the second moment  $\Delta M_2$  modulated by motion

with a short correlation time  $\tau$  (Pauls et al., 1985), we previously derived for fast restricted uniaxial diffusion about the length axis of the virus particle an approximate contribution  $1/T_{2e}^{\text{CSA}}$  to the transversal relaxation rate under nonspinning conditions as (Magusin and Hemminga, 1993b)

$$\frac{1}{T_{2e}^{\text{CSA}}} = \frac{M_2 \{2 - \text{sinc}^2(\lambda) - \text{sinc}^2(2\lambda)\}}{15D'} \quad (7)$$

where the diffusion coefficient  $D'$  may be regarded as an effective measure of the rate of backbone motions. If the backbone motions are much faster than the spinning rate ( $10^3$  Hz), their influence on transversal relaxation is hardly modified by MAS, and Eq. 7 is still approximately valid under spinning conditions. In contrast to  $T_{2e}^{\text{SOR}}$ ,  $T_{2e}^{\text{CSA}}$  increases as the motion becomes faster and decreases as the amplitude  $\lambda$  becomes larger. This is a consequence of the fact that the backbone motions are assumed to be fast, as compared with the nonspinning linewidth in the absence of backbone motion, and that the portion of the second moment that is modulated by the backbone motion increases as the motional amplitudes become larger. Similar to  $T_{2e}^{\text{SOR}}$ ,  $T_{2e}^{\text{CSA}}$  is inversely proportional to the square of the resonance frequency  $\omega_0$ . In our previous analysis of transversal  $^{31}\text{P}$  relaxation of nonspinning samples (Magusin and Hemminga, 1993a), we have assumed that  $T_{2e}^{\text{CSA}} \gg T_{2e}^{\text{SOR}}$  so that it may be neglected. In contrast, it will be shown in this paper that  $T_{2e}^{\text{SOR}}$  is negligible at spinning rates of 4 kHz or higher. At intermediate spinning rates, the total transversal relaxation time  $T_{2e}$  is given by

$$\frac{1}{T_{2e}} = \frac{1}{T_{2e}^{\text{SOR}}} + \frac{1}{T_{2e}^{\text{CSA}}} \quad (8)$$

## Lineshape of the centerband and the sidebands

To simulate a finite linewidth for the centerband and the sidebands, Eq. 2 must still be multiplied by some slowly decaying function representing the effect of inhomogeneous and homogeneous line broadening. For this purpose, one could use a simple gaussian or exponential decay, selected by fitting calculated spectra to the experimental spectrum. Such a procedure, however, does not explain the observed lineshape of the centerband and the sidebands, and changes thereof under various conditions. Therefore, a model is set up here, especially for M13, which relates the lineshape to a continuous distribution of phosphodiester conformations and transversal relaxation. It further demonstrates how conformational fluctuations may influence the linewidth.

A strong correlation has been found between the isotropic chemical shift  $\sigma_0$  and the RO-P-OR' bond angle  $\Phi$ , which typically varies in the range  $102^\circ \pm 3^\circ$  for different nucleic acid molecules (Giessner-Prettre et al., 1984). Because the backbone of M13 DNA is probably disordered, values of  $\Phi$  in our model are distributed in a range around some central value  $\Phi_0$ , which could be, e.g.,  $102^\circ$ , according to the density function  $P_\omega(\Phi - \Phi_0) = \exp[-\{(\Phi - \Phi_0)/w\}^2]$ , where  $w$  determines the distribution width. In this range  $\sigma_0$  is a linear function of  $\Phi$ ,  $\sigma_0(\Phi) = G(\Phi - \Phi_0)$  with  $G \approx -2$  ppm per degree (Gorenstein, 1981). Ab initio calculations have indicated that the isotropic chemical shift  $\sigma_0$  of the  $^{31}\text{P}$  nucleus in the dimethyl phosphate anion also strongly depends on the two smallest dihedral angles  $\theta_1$  and  $\theta_2$  on both sides of the  $^{31}\text{P}$  nucleus between the respective POC and OCH planes (Giessner-Prettre et al., 1984). Effects on  $\sigma_0$  caused by simultaneous variation of both angles are simply additive. The graphic representation of  $\sigma_0$  versus  $\theta_1$  or  $\theta_2$  shows a  $120^\circ$ -periodic, roughly sinusoidal dependence on each angle, whereby  $\sigma_0$  shifts approximately 3.5 ppm upfield as  $\theta_1$  or  $\theta_2$  increases from  $0^\circ$  to  $60^\circ$ . We therefore assume in our model for the phosphodiester in the DNA molecule encapsulated in M13, that the static contribution of the two dihedral angles to the isotropic  $^{31}\text{P}$  shift is  $b \sin\{3(\theta_k - \theta_0)\}$  each, where  $\theta_0 = 30^\circ$  and  $b$  is a fitting parameter roughly equal to  $-1.75$  ppm. In addition, because the absolute values of  $\theta_1$  and  $\theta_2$  typically vary in a range  $35^\circ \pm 20^\circ$  for different nucleic acid helices (Giessner-Prettre et al., 1984) and the geometry of the M13 DNA backbone seems to be irregular, we take values for  $\theta_1$  and  $\theta_2$  symmetrically distributed according to the density function  $P_\nu(\theta_k - \theta_0) = \exp[-\{(\theta_k - \theta_0)/\nu\}^2]$ , where  $\theta_0 = 30^\circ$  (causing symmetric lineshapes) and  $\nu = 20^\circ$  (as a realistic

distribution width). To include the effect of conformational fluctuations into the model as well, we further assume that the dihedral angles  $\theta_\alpha$  are not rigidly fixed, but fluctuate very rapidly between a lower value  $\langle\theta_\alpha\rangle - \mu$  and an upper value  $\langle\theta_\alpha\rangle + \mu$ , so that the contribution to  $\sigma_o$  is scaled to the time-average  $b \sin\{3(\langle\theta_\alpha\rangle - \theta_o)\} \text{sinc}(3\mu)$ , where the sinc function is as defined before Eq. 2. Taking both bond angle and dihedral angle effects into account and adding to this the transversal relaxation caused by slow overall motion and fast backbone motion (Eq. 8), we calculate the lineshape of the centerband and the sidebands by Fourier transformation of the free induction decay defined at integer multiples of the spinner rotation time by

$$S(nT_r) = \exp\left[-\frac{nT_r}{T_2}\right] \int P_w(\Phi) \exp[iGw\Phi nT_r] d\Phi \\ \times \int P_1(\theta_1) \exp[ib \sin(3\theta_1) \text{sinc}(3\mu) nT_r] d\theta_1 \\ \times \int P_2(\theta_2) \exp[ib \sin(3\theta_2) \text{sinc}(3\mu) nT_r] d\theta_2 \quad (9)$$

where  $\Phi$ ,  $\theta_1$ , and  $\theta_2$  have been redefined as  $\Phi - \Phi_o$ ,  $\langle\theta_1\rangle - \theta_o$ , and  $\langle\theta_2\rangle - \theta_o$ , respectively. As Eq. 9 indicates, there is dual effect of nucleic acid backbone motions on the lineshape. On the one hand, the fluctuation of the dihedral angles caused by them tends to narrow the centerband and the sidebands in <sup>31</sup>P MAS NMR spectra. On the other hand, backbone motions also cause transversal relaxation (Eq. 7), which broadens the lineshape. In principle, the isotropic chemical shift fluctuations caused by conformational changes also contribute to transversal relaxation. This contribution, however, is presumably small as compared with relaxation by phosphodiester reorientation, because the width of the isotropic chemical shift range of a few parts per million associated with conformational inhomogeneity is much smaller than the "size"  $\sigma_{33} - \sigma_{11}$  of the chemical shift anisotropy being 180 ppm for <sup>31</sup>P nuclei in phosphodiesters. The relaxation effect caused by isotropic chemical shift fluctuations is therefore assumed to be negligible.

## MATERIAL AND METHODS

M13 and TMV were grown, purified, and concentrated as described previously (Magusin and Hemminga, 1993a). NMR spectra were recorded on a Bruker AM500 and a CXP300 spectrometer operating at a <sup>31</sup>P frequency of 202.5 and 121.5 MHz, respectively. The MAS experiments were conducted in standard 7-mm Bruker VT MAS-DAB probes. For M13 and TMV gels at room temperature special care had to be taken to let the samples spin. The following spinner preparation was the most successful. Zirconia spinners were carefully filled with the sticky viral material, packed by use of an Eppendorf lab centrifuge to remove air bubbles from the samples. Tightly fitting Kel-F caps were used to close the spinners, and an ink marker was used for sealing. Leakage of material or evaporation of water from the samples was checked by comparing the spinner weights before and after every experiment. It was important to clean the outside of the spinner thoroughly with alcohol to remove all traces of material. After this preparation spinners could sometimes attain spinning speeds up to 5 kHz. Stable spinning of dilute viral gels was almost impossible at concentrations less than 200 mg/ml or at temperatures more than 40°C, probably due to the high fluidity of the sample under these conditions.

Because the tuning properties of the wet virus gels were quite different as compared with the solid reference compounds commonly used to set the experimental conditions, the rf pulses were adjusted on the sample itself. In experiments at 121.5 MHz the <sup>31</sup>P  $\pi/2$  pulse length was set to 5  $\mu$ s and at 202.5 MHz to 8  $\mu$ s. The <sup>1</sup>H decoupler field strength was measured on the sample itself by varying the length of the proton excitation pulse in a cross-polarization pulse sequence. Spectra were recorded using a Hahn echo pulse sequence to remove the effect of probe ringing on the weak signal. For recording standard MAS NMR spectra, a refocusing pulse was given after one spinner rotation. In all experiments a CYCLOPS phase alternation was used to remove the effects of pulse imperfections, and high-power proton decoupling was on during refocussing delays and acquisition time. Trans-

versal relaxation was studied by acquiring the Hahn echoes at even multiples of the spinner rotation time. To suppress noise, the echoes were Fourier transformed, and only the relevant parts of the spectrum were integrated.

Sideband patterns, lineshapes, and transversal relaxation at high and low spinning rates were simulated utilizing Fortran and Igor programs based on the equations described under Theory. For <sup>31</sup>P NMR in M13 relative chemical shift tensor values  $\sigma_{11} - \sigma_o = 77$  ppm,  $\sigma_{22} - \sigma_o = 18$  ppm, and  $\sigma_{33} - \sigma_o = -95$  ppm were taken (where  $\sigma_o$  is the isotropic shift). For TMV the values 83, 25, and -108 ppm were taken from the literature (Cross et al., 1983a). In simulations for M13 it was assumed that a random distribution of chemical shift tensor orientations exists within the phage. For TMV the orientation of <sup>31</sup>P chemical shift tensor for the three different binding sites with respect to the rod-shaped TMV was approximately derived from the <sup>31</sup>P atomic coordinates as described earlier (Magusin and Hemminga, 1993a). The best fits to the experimental sideband patterns and lineshapes of M13 and TMV were found by least square fitting, allowing height, baseline, and isotropic shift of simulated sideband patterns and lineshapes to vary. Simulated transversal relaxation curves were fitted to the experimental relaxation decays with only height as a variable.

## RESULTS

MAS NMR spectra of 40% and 70% (w/w) M13 consist of a gaussian-shaped centerband surrounded by several similar sidebands (Fig. 1), in agreement with results reported for bacteriophage fd (DiVerdi and Opella, 1981). The linewidth  $\Delta\nu_{1/2}$  of the centerband and the sidebands, defined as the full width at half-height, depends on the hydration of the gel and the temperature: at a <sup>31</sup>P NMR frequency of 202.5 MHz linewidths of 3.9, 3.2,  $3.9 \pm 0.2$  ppm are found for 25%, 40%, and 70% M13 at 25°C and 4.0, 5.1, and 5.5 ppm for 18% M13 frozen at -40, -100, and -140°C, respectively (Fig. 2). For 40% M13, a linewidth of  $2.7 \pm 0.5$  ppm is measured in the MAS NMR spectrum recorded at 121.5 MHz. The linewidth is independent of the spinning rate. By use of Herzfeld and Berger's sideband intensity tables (Herzfeld and Berger, 1980), MAS NMR spectra of 70% M13 at 25°C (Fig. 1) and 18% M13 frozen at -40°C (not shown) at various spinning rates can well be fitted by sideband patterns of a chemical shift tensor with relative tensor values  $\sigma_{11} - \sigma_o = 77$ ,

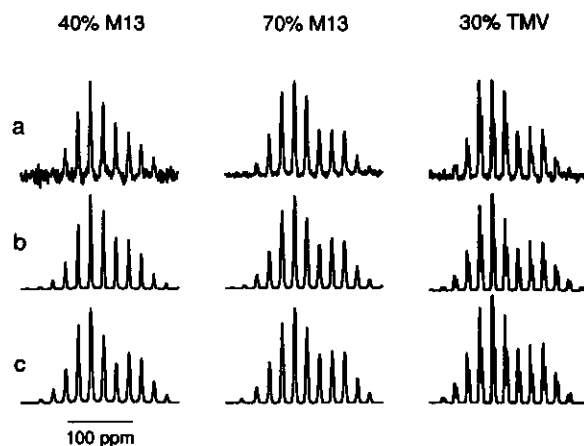


FIGURE 1 Experimental MAS NMR spectra of 40% M13 (128 scans) and 70% M13 (256 scans) and 30% TMV (20,000 scans) at 25°C (row a), simulated sideband patterns influenced by backbone motion (row b), and best "ideal" sideband fits (row c).

FIGURE 2 Experimental lineshape of the left first-order sideband (column 1), average lineshape obtained by resampling the experimental MAS-free induction decay at multiples of the spinner rotation time after artificially increasing the time resolution by zero, filling in the spectral domain (column 2) and simulated lineshapes (column 3) consisting of a  $\Phi$  contribution (column 4), a  $\theta_x$  contribution (column 5), and a contribution by homogeneous line broadening (column 6), for 30% TMV (row a; 20,000 scans), 18% M13 at  $-140^\circ\text{C}$  (row b; 10,000 scans),  $-100^\circ\text{C}$  (row c; 10,000 scans) and  $-40^\circ\text{C}$  (row d; 1,000 scans), 70% M13 (row e; 256 scans), 40% M13 (row f; 128 scans), 40% M13 at 121.5 MHz (row g; 1,000 scans) and 25% M13 (row h; 1,800 scans). Unless stated otherwise, experiments were conducted at  $25^\circ\text{C}$  and 202.5 MHz. The  $\Phi$  contribution for TMV (row a; column 5) also includes the effect of arginine binding (see text).

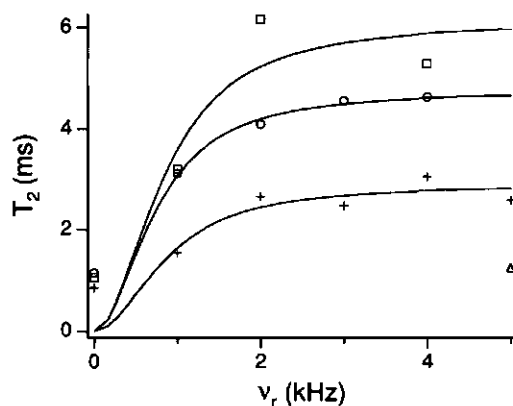
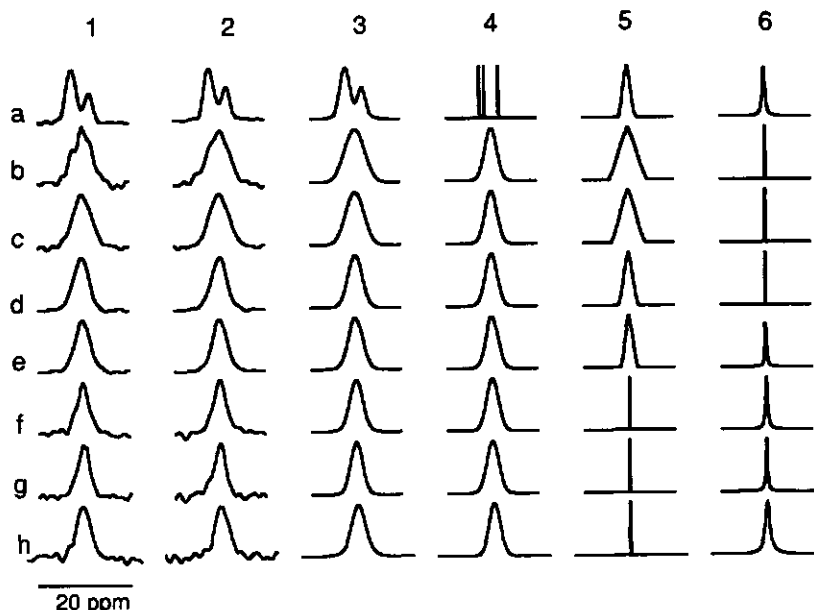


FIGURE 3  $T_{2e}$  values obtained at various spinning rates for 70% M13 at 202.5 MHz ( $\circ$ ), 40% M13 at 202.5 MHz ( $+$ ), and 121.5 MHz ( $\square$ ) and 25% M13 at 202.5 MHz ( $\triangle$ ).

$\sigma_{22} - \sigma_o = 18$ , and  $\sigma_{33} - \sigma_o = -95 \pm 2$  ppm (Fig. 1 c). This agrees well with the values that have been estimated from the static lineshape at 202.5 MHz (not shown) and at 121.5 MHz (Magusin and Hemminga, 1993a). In contrast, spectra of 25% and 40% M13 at  $25^\circ\text{C}$  cannot be fitted by sideband patterns of a single chemical shift tensor (Fig. 1 c). Apparently, Herzfeld and Berger's theory does not apply for these cases.

At the  $^{31}\text{P}$  NMR frequency of 202.5 MHz the MAS NMR spectrum of 30% (w/w) TMV shows two resolved sideband patterns with an overall intensity ratio of approximately 2:1 separated by  $3.9 \pm 0.3$  ppm with a linewidth of  $2.5 \pm 0.3$  ppm (Figs. 1 a and 2). The same intensity ratio and almost the same peak separation has been observed in the  $^{31}\text{P}$  NMR spectrum of dry TMV at 121.5 MHz, but the linewidth at 121.5 MHz, 1.5 ppm, is less (Hemminga et al., 1987). The two sideband patterns can be compared with the "ideal" sideband patterns of static chemical shift tensors with various

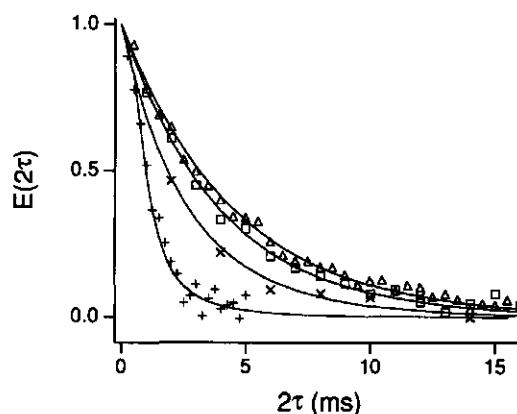


FIGURE 4 Transversal relaxation decay for 70% M13 at 202.5 MHz obtained at spinning rates of 0 kHz ( $+$ ), 1 kHz ( $\times$ ), 2 kHz ( $\square$ ), and 4 kHz ( $\triangle$ ).

tensor values. The sideband pattern of a chemical shift tensor with relative tensor values  $\sigma_{11} - \sigma_o = 79$ ,  $\sigma_{22} - \sigma_o = 18$ , and  $\sigma_{33} - \sigma_o = -97 \pm 2$  ppm fits well to the pattern of major peak and a good fit to the minor peak pattern is obtained for a chemical shift tensor with tensor values 85, 18, and  $-103 \pm 2$  ppm (Fig. 1 c). These tensor values are slightly reduced as compared with the values obtained from MAS NMR spectra of dry TMV (Hemminga et al., 1987).

We have also investigated the transversal relaxation time  $T_{2e}$  of several M13 gels under MAS conditions (Fig. 3). In general, the centerband and sidebands decay exponentially as a function of the echo time and a  $T_{2e}$  value may be obtained by fitting a single exponential to each of these decays. No significant  $T_{2e}$  differences among the centerband and the sidebands have been found and the shape of the bands does not change at increasing echo time.  $T_{2e}$  values obtained at spinning rates greater than 2 kHz are systematically larger than those obtained from static experiments on the same samples and the value of  $T_{2e}$  is somewhere in between at a

rate of 1 kHz (Figs. 3 and 4). It was impossible to measure  $T_{2c}$  in the range of spinning rates less than 1 kHz, because the spinner rotation time became too long a sampling time with respect to  $T_{2c}$  to be measured. Similar to the outcome of nonspinning experiments,  $T_{2c}$  increases with decreasing water content and  $^{31}\text{P}$  NMR frequency (Fig. 5). At 202.5 MHz, the  $T_{2c}$  values determined for the major and the minor peak in the 4-kHz MAS NMR spectrum of 30% TMV are 2.4 and 2.9 ms, respectively. Longitudinal  $^{31}\text{P}$  NMR relaxation times  $T_1$  of M13 gels at 202.5 MHz were generally in the order of seconds, thus three orders of magnitude larger than the  $T_{2c}$  values measured at high spinning rates.

## DISCUSSION

### Analysis of sideband intensities

As reported previously,  $^{31}\text{P}$  NMR lineshapes and transversal relaxation of nonspinning samples of M13 and TMV cannot be interpreted consistently in terms of a single type of motion, like the rotation of the rod-shaped virions about their length axis alone. Instead, a fast type of restricted motion with a frequency greater than  $10^5$  Hz seems to be superimposed on the slow overall motion of the virions (Magusin and Hemminga, 1993a). The occurrence of motions can also explain the fact that Herzfeld and Berger's theory does not apply to the sideband intensities of dilute M13 gels. By analogy with motional narrowing under nonspinning conditions (Magusin and Hemminga, 1993b), it may be reasonably assumed that motions with frequencies less than  $10^3$  would not be able to significantly alter the sideband pattern caused by the  $^{31}\text{P}$  chemical shift anisotropy with a "size"  $(\omega_a/2\pi)|\sigma_{33} - \sigma_{11}|$  of 34 kHz at 202.5 MHz. In contrast, dramatic line-broadening effects would be expected for motions in the  $10^3$  Hz region, because their frequencies would be in the order of the spinning rates applied (Schmidt et al., 1986; Schmidt and Vega, 1987). As all M13 spectra recorded at various spinning rates, temperatures, and water contents contain well resolved sidebands, the motions that modify the sideband intensities should therefore have frequencies greater than  $10^4$  Hz.

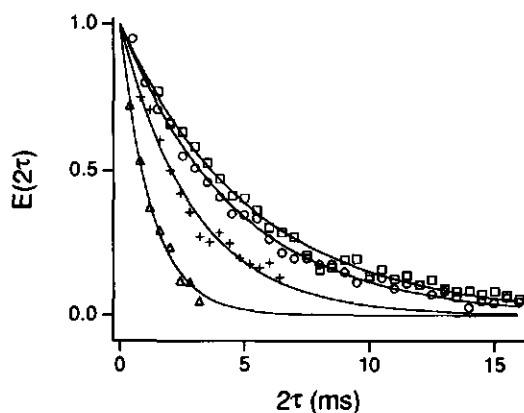


FIGURE 5 Transversal relaxation decay at spinning rates of 4 kHz for 70% M13 at 202.5 MHz ( $\circ$ ), 40% M13 at 202.5 MHz ( $+$ ), and 121.5 MHz ( $\square$ ); decay of 25% M13 at 202.5 MHz at a rate of 5 kHz ( $\triangle$ ).

To extract motional information from the sideband pattern more quantitatively, the previously used model (Magusin and Hemminga, 1993b), in which the fast motions of the nucleic acid phosphodiester are collectively described as restricted rotation about the virion length axis, is extended to MAS NMR experiments (Eq. 2). Quickly summarizing our previous discussion (Magusin and Hemminga, 1993a), we do not wish to pretend that uniaxial rotation about the viral axis is a realistic model for the various types of backbone motion that the nucleic acid molecule inside M13 or TMV may undergo simultaneously. Judging from the complex dynamics observed for "naked" nucleic acids in solution (Alam and Drobny, 1991), we actually believe that, as a result of steric constraints and concerted motions, the dynamics of the nucleic acids encapsulated in TMV and M13 are likely to be much more complicated. By employing the uniaxial diffusion model we simply want to characterize the spatial restriction of nucleic acid backbone motion by a single "cumulative amplitude"  $\lambda$ , much like the general order parameter  $S$  used in Model Free analyses of relaxation measurements to characterize the amount of motional anisotropy (Lipari and Szabo, 1982a; 1982b). In fact, the functions  $\text{sinc}(\lambda)$  and  $\text{sinc}(2\lambda)$  in Eq. 2 can be shown playing a role similar to  $S$  in the (simplified) autocorrelation functions (see Appendix). In our opinion, a more realistic model for nucleic acid backbone motion would involve too many parameters, which would lead to overinterpretation of the experimental data or require additional, questionable assumptions. This would especially be the case for M13, because hardly anything is known about the geometry of its internal DNA molecule. For M13, the nonspecific character of our simple model is actually enhanced by the assumption that the phosphodiester are randomly oriented within the virus particles, which themselves are randomly oriented within the gel. As long as no correlation between the orientation of the phosphodiester and the local axes of backbone motion exists and the effect of slow overall motion about the length axis of the virus is negligible, our model describing phosphodiester motion in terms of uniaxial motion about the viral axis, is theoretically equivalent to any other model that involves uniaxial diffusion about one or more axes not parallel to the viral axis.

Sideband patterns calculated using Eq. 2 for restriction half-angles  $\lambda$  equal to multiples of  $9^\circ$  between  $0^\circ$  and  $90^\circ$ , have been compared with various  $^{31}\text{P}$  MAS NMR spectra of M13. Spectra simulated for  $\lambda = 27^\circ \pm 5^\circ$  fit well to MAS NMR spectra of 40% M13 at 202.5 MHz at spinning rates of 4 and 5 kHz (Fig. 1) and almost the same  $\lambda$  value,  $36^\circ \pm 5^\circ$ , produces the best fit to the 4-kHz MAS NMR spectrum of the same gel at 121.5 MHz. The 4-kHz MAS NMR spectrum of 70% M13 at 202.5 MHz is best reproduced for  $\lambda = 9^\circ$ , and a  $\lambda$  value of  $45^\circ$  is extracted from the 5-kHz MAS NMR spectrum of 25% M13 at 202.5 MHz. These restriction half-angles agree with the values of  $27^\circ$  and  $0^\circ$  obtained by simulating the nonspinning  $^{31}\text{P}$  NMR lineshape of the 40% and 70% M13 sample at 202.5 MHz (not shown) and are also consistent with the values  $52^\circ$  and  $43^\circ$  obtained by analysis



of nonspinning lineshapes of 15% and 30% M13 at 121.5 MHz (Magusin and Hemminga, 1993a). A relation may exist between the increase of motional amplitude and the swelling of M13 at increasing hydration (Dunker et al., 1974). At increasing diameter of the hollow tube inside the rod-shaped phage, nucleic acid backbone motion may increase by the reduction of steric hindrance. When comparing the  $\lambda$  value of about  $30^\circ$  obtained for 40% M13 gels with, for example, backbone fluctuations of  $\pm 27^\circ$  in the gigahertz range reported earlier for DNA (Hogan and Jardetzky, 1980), it should be realized that our model is presumably too simple. Diffusion models involving more angle fluctuations would probably result in smaller restriction angles per fluctuating angle than the  $\lambda$  values found above. Recently, we could further improve the simulated  $^{31}\text{P}$  NMR powder lineshapes of M13 at 121.5 MHz by assuming that the backbone of M13 DNA consists of 83% immobile and 17% mobile phosphodiester. A similar, 5:1 two-component model produces a better simulation of the nonspinning spectrum of 40% M13 at 202.5 MHz as well (not shown), but the two-component model does not significantly improve the simulated MAS NMR spectra.

For TMV, a three-component model is reasonable, because three sets of binding sites exist within the virion. Nonspinning  $^{31}\text{P}$  NMR lineshapes of 30% TMV provide strong indications that one of these three sets is more mobile than the other two, but the question which the mobile set is, cannot be solved unambiguously due to the overlap of their broad powder lines (Magusin and Hemminga, 1993a). The fact that one of the three resonance lines in  $^{31}\text{P}$  NMR spectra of oriented TMV solutions is much broader than the other two, indicates a high level of disorder for one of the three sets of phosphodiester in TMV (Cross et al., 1983a), which seems to support our conclusion that one of the three sets of phosphodiester is less rigidly bound. Cross et al. have speculatively assigned this resonance line to a specific binding site labeled 3 in the computer-refined crystal structure presented by Stubbs and Stauffacher (1981). Using this structure we have recalculated the chemical shift positions of the resonance lines in the oriented spectrum, however, and differently assigned the broad line to site 2 (Magusin and Hemminga, 1993a). Given the ambiguity in the spectral assignment, the question of which binding site could actually be less rigidly bound still remains to be answered.

Because MAS NMR spectra of TMV show two resolved, potentially motion-affected sideband patterns, they offer an extra possibility for assigning mobility to the three sites more specifically. Interpretation of the two sideband patterns in terms of "ideal" MAS behavior shows that the apparent chemical shift anisotropy of the minor resonance is larger than the anisotropy of the major resonance. This was also found for dried TMV samples (Hemminga et al., 1987) and can be observed in the MAS NMR spectrum of 10% TMV solution (Cross et al., 1983a) as well, although this effect was not mentioned in the text of this paper. Taking bond angle and arginine binding effects into account, we assign the minor sideband pattern to site 1, as labeled by Stubbs and Stauff-

facher (1981), and the major sideband pattern to sites 2 and 3 (see Analysis of Lineshapes). The fact that the apparent anisotropy of the major resonance is reduced relative to the minor resonance would then be consistent with our hypothesis to be discussed in Analysis of Lineshapes, that site 2 is less rigidly bound than the other two.

Indeed, a three-component simulation using Eq. 2 produces a good fit, when identical tensor values of 83, 25, and  $-108$  ppm are assumed for the three sites and restriction half-angles are taken as  $18^\circ$ ,  $45^\circ$ , and  $18^\circ$  for sites 1, 2, and 3, respectively (Fig. 1). These values may be compared with the respective half-angles  $9^\circ$ ,  $86^\circ$ , and  $17^\circ$  obtained from the analysis of the nonspinning  $^{31}\text{P}$  NMR lineshape of another sample of 30% TMV at 121.5 MHz (Magusin and Hemminga, 1993a). The difference between these two sets of angular amplitudes shows the difficulty of extracting motional parameters for each site separately from nonspinning spectra due to the strong overlap of their resonances. The presence of motional narrowing in nonspinning and MAS NMR spectra of 30% TMV recorded at 121.5 and 202.5 MHz, respectively, is difficult to reconcile with the absence thereof in spectra of 10% TMV solutions at 60.9 MHz (Cross et al., 1983a). This may be caused by differences in the methods employed by Cross et al. to prepare TMV samples and record their spectra. Because the NMR spectrum-recording method is insufficiently described in their paper, a more specific explanation would only be highly speculative.

### Analysis of transversal relaxation

The observed dependence of  $T_{2e}$  on the spinning rate less than 2 kHz (Fig. 3) indicates a contribution by slow phosphodiester reorientation to transversal relaxation. Because  $T_{2e}$  becomes shorter as the M13 gel becomes more fluid, we tentatively assign this slow phosphodiester reorientation to the overall rotation of the rod-shaped virus particles about their length axis. At spinning rates greater than 2 kHz,  $T_{2e}$  approaches an upper limit, indicating that another relaxation mechanism, which is independent of the spinning rate, becomes more important. Other features of this relaxation mechanism are that it is sensitive to hydration and depends on the magnetic field strength (Figs. 3 and 5). In principle, the observed  $T_{2e}$  increase at decreasing hydration (Table 1) could simply result from the removal of mobile water protons in the vicinity of  $^{31}\text{P}$ , because water protons could increase  $^{31}\text{P}$  relaxation by causing fast fluctuating dipolar interactions. Such  $^1\text{H}$ - $^{31}\text{P}$  dipolar contribution to longitudinal and transversal  $^{31}\text{P}$  relaxation may be estimated by using general equations presented elsewhere (Wittebort and Szabo, 1978). As learned from these equations, the fact that  $T_1$  is three orders of magnitude larger than  $T_2$ , as observed in our experiments, is typical for motions with frequencies which are one or two orders of magnitude lower than the angular resonance frequencies of  $^{31}\text{P}$  and  $^1\text{H}$ . Indeed, transversal relaxation of  $^{31}\text{P}$  nuclei by protons which undergo motions in this frequency range ( $10^7$ – $10^8$  Hz) is not affected by the 30-kHz proton decoupling used in our experiments. The general

**TABLE 1** Restriction half-angles and diffusion coefficients for local backbone motion of the DNA molecule inside M13 and the influence of backbone motion on the homogeneous and the inhomogeneous linewidth.

[M13]	$\nu_0$	$\lambda$	$T_{2e}$	$D'_{app}$	$T_{2e}^{CSA}$	$D'$	$\Delta\nu_{1/2}$	$\Delta\nu_{hom}$	$\Delta\nu_{inh}$
%	(MHz)	(°)	(ms)	(kHz)	(ms)	(kHz)	(Hz)	(Hz)	(Hz)
70	202.5	$9 \pm 5$	4.8	40	6.8	$60 \pm 50$	780	70	710
40	202.5	$30 \pm 5$	2.9	250	3.5	$300 \pm 80$	640	105	535
40	121.5	$30 \pm 5$	6.1	190	9.8	$300 \pm 80$	330	60	270
25	202.5	$45 \pm 5$	1.3	210	1.4	$240 \pm 40$	780	250	530

[M13], weight fraction of M13 in the gel;  $\nu_0$ , <sup>31</sup>P NMR frequency;  $\lambda$ , restriction half-angle for local backbone motion derived from the sideband pattern;  $T_{2e}$ , relaxation time for the part of transversal relaxation that is independent of the spinning rate;  $D'_{app}$ , apparent diffusion coefficient calculated from  $T_{2e}$  by using Eq. 7;  $T_{2e}^{CSA}$ , transversal relaxation time due to fast phosphodiester reorientation, calculated from  $T_{2e}$  by correcting for an additional  $\nu_0$  independent  $T_{2e}^{DIP}$  of 16 ms;  $D'$ , diffusion coefficient calculated from  $T_{2e}^{CSA}$  by using Eq. 7;  $\Delta\nu_{1/2}$ , full linewidth at half-height of the centerband and the sidebands;  $\Delta\nu_{hom}$ , homogeneous linewidth;  $\Delta\nu_{inh}$ , inhomogeneous linewidth.

equations, however, also predict  $T_{2e}$  to be independent of the magnetic field strength in this frequency range and thus fail to explain the difference between the  $T_{2e}$  values measured for 40% M13 at 121.5 and 202.5 MHz.

Alternatively, the same fast backbone motions that are responsible for the motional modification of the sideband intensities, could also cause transversal relaxation due to the chemical shift anisotropy of the <sup>31</sup>P nuclei. Such relaxation mechanism would provide a qualitative explanation for the observed dependence on the magnetic field. As noticed under Analysis of Sideband Intensities, hydration affects the amplitude of nucleic acid backbone motions, which could explain qualitatively the observed  $T_{2e}$  trend at increasing hydration. Assuming that phosphodiester reorientation by slow, overall rotation of the virion and by fast restricted backbone motion is the main cause of transversal relaxation, we have used Eq. 8 to explain the observed dependence of  $T_{2e}$  on the spinning rate. Indeed, sigmoid curves, as predicted by Eq. 8, fit well to the  $T_{2e}$  values obtained for spinning rates of 1 kHz and higher at 202.5 MHz and reasonably to  $T_{2e}$  values measured at 121.5 MHz (Fig. 3). Obviously, the model fails to predict correct  $T_{2e}$  values for static samples. This is due to the assumption implicit in Eq. 5 that the decay of echoes is sampled at even multiples of the rotation time  $T_r$ , which goes to infinity as the spinning rate drops to zero.

Diffusion coefficients  $D$  for the rotational diffusion of the virus particles about their length axis may be estimated from the best fits in Fig. 3 and the half-angles  $\lambda$  estimated from the sideband intensities (see Analysis of Sideband Intensities). Using  $\lambda$  values of 9° and 30° for 70% and 40% M13, we find  $D$  values of 1.4 and 4.4 Hz for 70% and 40% M13 at 202.5 MHz and 5.2 Hz for 40% M13 at 121.5 MHz, respectively. These values are mutually consistent within experimental error and also agree with the values reported previously for 15% and 30% M13 gels (Magusin and Hemminga, 1993a). The  $\omega_r$ -independent part of transversal relaxation may also be estimated from the curves in Fig. 3. For example, for 70% M13, this part of transversal relaxation is characterized by a  $T_{2e}$  value of 4.8 ms. Actual echo decays simulated by multiplication of Eq. 5 for  $D = 1.4$  Hz and an exponential decay with  $T_{2e} = 4.8$  ms fit well to the experimental decays obtained for 70% M13 at the spinning rates applied (Fig. 4). Apparently, the multiexponential decay in Eq. 5 is indeed reasonably approximated by a single expo-

ponential with relaxation time  $T_{2e}^{SOR}$  as described by Eq. 6. The static relaxation decay measured for 70% M13, can also be simulated for  $D = 1.4$  Hz by using a previously discussed model (Magusin and Hemminga, 1993b). This shows that the outcome of spinning and nonspinning relaxation experiments can be interpreted consistently in terms of our models. The ratio between the static  $T_{2e}$  values 1.06 and 0.85 ms at 121.5 and 202.5 MHz closely approximates 1.4, as expected from the  $(\omega_0)^{-2/3}$  dependence of transversal relaxation by ultra-slow diffusion under nonspinning conditions (Magusin and Hemminga, 1993b).

From the  $\omega_r$ -independent part of transversal relaxation, an apparent diffusion coefficient  $D'_{app}$  for the fast phosphodiester reorientation can be calculated directly by using Eq. 7. Different  $D'_{app}$  values, however, are found for 40% M13 at 121.5 and 202.5 MHz in this way (Table 1). This inconsistency may be eliminated by also taking into account another relaxation mechanism, which is independent of both  $\omega_r$  and  $\omega_0$ . Such a type of relaxation could be caused by fluctuating dipolar interactions between <sup>31</sup>P and other nuclei in its vicinity, like <sup>1</sup>H, <sup>14</sup>N, or other <sup>31</sup>P nuclei. For 40% M13, the  $\omega_r$ -independent  $T_{2e}$  values 6.1 and 2.9 ms determined at 121.5 and 202.5 MHz could result from a  $\omega_0$ -independent contribution  $T_{2e}^{DIP}$  of 16 ms superimposed on  $T_{2e}^{CSA}$  values of 9.8 and 3.5 ms, respectively. Similarly, we derived  $T_{2e}^{CSA}$  from the spinning rate independent  $T_{2e}$  values of 70% and 25% M13 gels, assuming  $T_{2e}^{DIP}$  to be the same. The diffusion coefficients  $D'$  which follow from these "corrected"  $T_{2e}^{CSA}$  values by using Eq. 7 are in the order of 10<sup>5</sup> Hz (Table 1).  $D'$  values determined for 25% and 40% M13 are the same within the error caused by the  $\pm 5^\circ$  uncertainty in  $\lambda$ , indicating that in this concentration range the amplitudes of the backbone motions are more sensitive to small hydration changes than their frequencies. More extreme dehydration, however, also influences the frequency of backbone motions, as illustrated by the lower  $D'$  value found for 70% M13. The finding that the major peak in the MAS NMR spectrum of TMV decays faster than the minor peak indicates that the average mobility of the two binding sites giving rise to the major peak, is larger than the mobility of the binding site causing the minor peak. This is consistent with the  $\lambda$  values obtained from the sideband pattern in the previous section.

The effective diffusion coefficient  $D'$  determined by using our simple model is only a qualitative measure which indi-

cates if the backbone motions dominating transversal relaxation at spinning rates greater than 2 kHz become faster or slower under varying conditions. Its value may not even be realistic by order of magnitude, e.g., when the cumulative amplitude  $\lambda$  actually reflects several types of backbone motion, whereas transversal relaxation is dominated by only the slowest one. However, a minimum and a maximum order of magnitude may be estimated from relaxation measurements. On the one hand, the invariance of  $T_{2e}$  at different spinning rates between 2 and 5 kHz, shows that the backbone motions dominating transversal relaxation at these rates are in the order of  $10^4$  Hz or faster. On the other hand, the three orders of magnitude difference between  $T_1$  and  $T_{2e}$  at  $^1\text{H}$  and  $^{31}\text{P}$  resonance frequencies in the order of  $10^9$  rad/s, sets an upper limit of  $10^7$ – $10^8$  Hz, as may be estimated from more general equations presented elsewhere (Wittebort and Szabo, 1978).

### Analysis of lineshapes

Line broadening caused by sample preparation has been suggested as an explanation for the large MAS NMR linewidths generally observed for dried and lyophilized biological materials as compared with solution linewidths (Hemminga et al., 1987). Indeed, it is conceivable, that as a consequence of the dehydration process, the material partly decomposes, or susceptibility heterogeneity is introduced. Such effects, however, are less likely explanations for the broad lines observed for M13 samples frozen at temperatures of  $-140^\circ\text{C}$  and less, because these are homogeneous lumps of ice pressed rigidly against the inner wall of the MAS spinner. At a macroscopic level, there are no visible differences between M13 ice at  $-40^\circ\text{C}$  and  $-140^\circ\text{C}$ , nor do the tuning properties of M13 samples change greatly on changing the temperature between those values, indicating that no phase transition occurs in this temperature trajectory. Nevertheless, the linewidth strongly increases as the sample is cooled down from  $-40^\circ\text{C}$  to  $-140^\circ\text{C}$ . It has been suggested that the difference between the shift position of the major and the minor peak in  $^{31}\text{P}$  MAS NMR spectra of TMV reflects conformational differences among the three types of binding sites (Hemminga et al., 1987). Because the  $^{31}\text{P}$  MAS NMR linewidth measured for M13 at  $-140^\circ\text{C}$  and less is comparable with the isotropic shift range observed for TMV at room temperature (Fig. 2), a spread of static phosphodiester conformations in a similar range as in TMV could offer a possible explanation for the observed M13 lineshape. At higher temperatures the linewidth in MAS NMR spectra of M13 is less. It gradually decreases to a minimum value of 3.0 ppm as the sample becomes more fluid and the amount of internal DNA backbone motion within the virions increases, going from frozen samples at  $-100^\circ\text{C}$  and  $-40^\circ\text{C}$  to viscous gels of 70% and 40% M13 at  $25^\circ\text{C}$ . Apparently, the isotropic shift range becomes narrower as temperature or hydration increases.

Beside influencing the sideband intensities and transversal relaxation by their reorientational character, fast backbone motions could also cause fast fluctuation of the phosphodiester conformations, which may lead to "conformational av-

eraging" of the isotropic shift. Such conformational averaging due to nucleic backbone motions could offer a possible explanation for the reduction of the linewidth at increasing hydration and temperature. In contrast, transversal relaxation tends to broaden the centerband and the sidebands at increasing hydration by adding an increasing homogeneous linewidth to the inhomogeneous linewidth. Indeed, the increased linewidth observed for 25% M13 gels, as compared with 40% M13, could be caused mainly by the increased homogeneous linewidth alone, superimposed on an inhomogeneous width of 2.7 ppm (Table 1).

To test the hypothesis that a distribution of phosphodiester conformations underlies the observed gaussian lineshapes observed in  $^{31}\text{P}$  MAS NMR spectra, the lineshapes of the centerband and the sidebands in MAS NMR spectra of M13 have been simulated by use of Eq. 9, which takes into account a spread of values for the two types of angles that affect the isotropic shift most strongly, i.e., the RO-P-OR' bond angles  $\Phi$ , supposed to be static in our model, and the dihedral angles  $\theta_1$  and  $\theta_2$ , assumed to be quickly fluctuating. Homogeneous line broadening is added as a third broadening factor (Fig. 2). The five model parameters involved in the simulation cannot be unequivocally determined from the measured lineshapes alone, and external arguments are necessary to estimate their values. For the lineshapes at  $25^\circ$ , the homogeneous linewidth  $1/\pi T_{2e}$  is calculated from  $T_{2e}$  measured at spinning rates of 4 and 5 kHz (Fig. 3). For the frozen M13 samples, homogeneous line broadening is neglected. As mentioned under Theory, the static  $\theta_k$  distribution parameter  $v$  is taken as  $20^\circ$ , which represents a realistic spread of dihedral angles in various phosphodiester compounds (Giessner-Prettre et al., 1984). For parameter  $G$ , the isotropic chemical shift change per unit bond angle change, we use a value of 2 ppm per degree, as indicated by empirical data (Gorenstein, 1981). Because the observed linewidth reaches a minimum for 40% M13, we assume the  $\theta_k$  contribution to be completely averaged at this hydration, so that a gauss fit to the lineshape that is left after deconvolution with the homogeneous line directly provides the static  $\Phi$  distribution parameter  $w$  as  $0.9^\circ$  (Fig. 2), which seems realistic as compared with the  $3^\circ$  range of  $\Phi$  in TMV. In contrast, the lineshape at  $-140^\circ\text{C}$  is assumed to be completely static, from which the dihedral shift range parameter  $b$  may be estimated to be  $-2.0$  ppm, in agreement with the range of 3.2–3.8 ppm calculated for the  $\theta_k$  contribution to the isotropic shift (Giessner-Prettre et al., 1984). With these parameter values, we obtain good fits for 18% M13 at  $-100^\circ\text{C}$  and  $-40^\circ\text{C}$  and 70% M13 at  $25^\circ\text{C}$ , for restriction half-angles  $\mu$  of  $17^\circ$ ,  $37^\circ$ , and  $40^\circ$ . When interpreting these large  $\mu$  values it should be realized that the description of conformational fluctuations in terms of only the two dihedral angles  $\theta_k$  is probably too simple. A more sophisticated model with more fluctuating conformational parameters would probably result in smaller restriction angles per parameter. The  $\mu$  values found above should probably be regarded most safely as upper limits rather than as realistic values. Furthermore, factors other than conformational averaging may play a role in the observed effect of

temperature and hydration on the MAS NMR lineshape. Conformational averaging is only a possible explanation, but not the only one. Comparison of the restriction angles estimated from the lineshapes and the sideband intensities above seems to indicate that under conditions which suppress phosphodiester reorientation, e.g., in frozen samples at  $-40^\circ\text{C}$ , some of the conformational parameters may still fluctuate considerably.

Recently, the major and the minor sideband pattern in the MAS NMR spectrum of TMV were assigned on the basis of the  $\text{C}_3'-\text{O}_3'-\text{P}-\text{O}_5'$  and  $\text{O}_3'-\text{P}-\text{O}_5'-\text{C}_5'$  torsional angles (Hemminga et al., 1987). An alternative assignment, however, can be made if the  $\text{RO}-\text{P}-\text{OR}'$  bond angles  $\Phi$  are taken into account, to which the isotropic chemical shift of phosphodiesters is more sensitive (Gorenstein, 1981). A bond angle increase of only  $5^\circ$  already causes the isotropic shift to decrease 7 ppm (Giessner-Pretre et al., 1984). Because  $\Phi$  is  $103^\circ$ ,  $103^\circ$ , and  $100^\circ$  for sites 1, 2, and 3, respectively, as calculated from model coordinates (Stubbs and Stauffacher, 1981), we would expect the occurrence of a major peak belonging to sites 1 and 2, about 4 ppm upfield of a minor peak belonging to site 3 (Fig. 6 b). Because this does not agree with the observed spectrum (Fig. 6 a), even if torsional angle effects of about 1.5 ppm would be involved as well, we have also taken the influence of arginine bonding into account.

In RNA-protein interaction models for TMV, two sites are generally interacting closely with arginine residues, whereas no arginine is close to a third one. The less bound site, however, seems to be assigned differently in different papers. For example, in the paper of Stubbs et al. (1977) it is site 2 (taking into account a change of labels between sites 1 and 2 as compared with our labeling, which follows other papers (Stubbs and Stauffacher, 1981; Namba and Stubbs, 1986)), whereas in the model of Namba and Stubbs in 1986 site 3 is the one without close arginine contact. Similar to the effect

caused by binding of a water molecule to a phosphodiester group (Ribas Prado et al., 1979), a 3.5-ppm decrease of the isotropic shift could be expected due to arginine-phosphate interaction. Assuming on the one hand, that sites 1 and 2 are tightly bound to arginine residues, the spectrum predicted above on the basis of  $\Phi$  differences alone, should be modified by shifting the major peak even 3.5 ppm further upfield. This would increase the predicted separation between the minor and the major peak to 7.5 ppm, and their shift order would still disagree with the experimental spectrum (Fig. 6 c). If, on the other hand, sites 1 and 3 were bound, the resonances belonging to sites 1 and 3 would shift 3.5 ppm upfield, so that resonance of site 3 would be located 0.5 ppm downfield of the position of site 2 (Fig. 6 d). The resulting spectrum would agree with the experimental spectrum by containing a major peak belonging to the overlapping resonances of site 2 and 3, about 3.8 ppm downfield of a minor peak belonging to site 1. It should be noticed that such assignment is only speculative, because the effect of arginine binding on the isotropic chemical shift of  $^{31}\text{P}$  inside TMV is unknown and other factors, not accounted for in our model, can also influence the isotropic chemical  $^{31}\text{P}$  shift. The supposed absence of close contacts between site 2 and an arginine residue, however, would be consistent with our earlier suggestion that this site is more mobile than the other two (Magusin and Hemminga, 1993a). This is also confirmed by our analysis of the sideband patterns and transversal relaxation of the two peaks.

Recently, we reported that in MAS NMR spectra of lyophilized TMV samples, the major and minor sideband patterns are not resolved (Hemminga et al., 1987). A possible explanation for this effect is provided by our model. The absence of conformational averaging of the isotropic chemical shift at extremely low hydration probably spoils the resolution of the peaks in the MAS NMR spectrum of lyophilized TMV, much like the broad peak observed for frozen M13 samples at  $-140^\circ\text{C}$ . Using the M13 model parameters  $\nu = 20^\circ$  and  $b = -2.0$  ppm for 30% TMV at  $25^\circ$  as well, and taking a homogeneous linewidth of 130 Hz for both peaks, a good fit to the major and minor peak is obtained for  $\mu = 40^\circ$ , if the resonances of sites 2 and 3 are assumed to be located 3.1 and 4.2 ppm downfield of the resonance of site 1, respectively (Fig. 2).

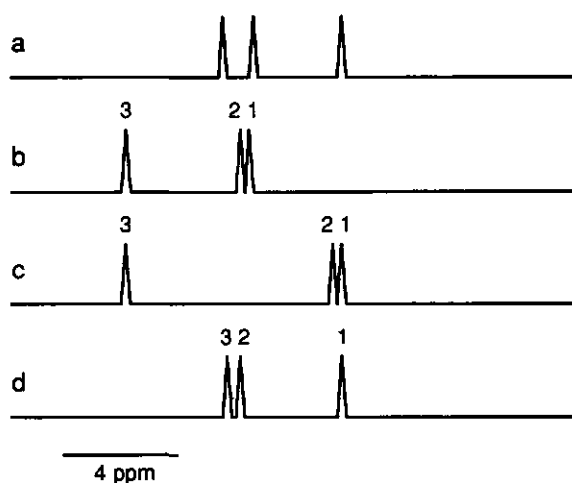


FIGURE 6 Stick spectra illustrating the assignment of the peaks in MAS NMR spectra of TMV; unassigned stick spectrum derived from the experimental lineshape (a), hypothetical spectrum based on the  $\Phi$  angle effects only (b), spectra also taking arginine binding into account to either sites 1 and 2 (c) or sites 1 and 3 (d).

## CONCLUSION

The model of phosphodiester motion in gels of M13 and TMV, which recently emerged from analyses of  $^{31}\text{P}$  NMR lineshapes and transversal relaxation of static NMR samples (Magusin and Hemminga, 1993a), is also consistent with the effects of motion on sideband spectra and transversal relaxation under MAS conditions. Overall rotation of the rod-shaped virions about their length axis and local backbone motions of the encapsulated nucleic acid molecules are responsible for the various deviations from "ideal" MAS behavior. Sideband intensities seem to be influenced by fast restricted reorientation of the phosphodiester groups, caused by nucleic acid backbone motions. Sideband patterns and

transversal relaxation observed for 25% and 40% M13 are consistent with angular amplitudes of 30° and 45°. These amplitudes should be regarded as cumulative motional parameters of whole classes of motions, rather than as realistic amplitudes of specific motions alone, because the description of the complicated backbone dynamics as only one type of uniaxial diffusion is probably too simple. The increase of motional amplitudes at increasing hydration could perhaps be related to swelling of the M13 virions. Effective frequencies of the backbone motions in the order of 10<sup>5</sup> kHz can be estimated from the spinning rate independent part of transversal relaxation, which is measured at spinning rates above 2 kHz, but these values can hardly be related to actual microscopic rate constants due to the cumulative character of the model. By causing the conformation of the phosphodiester groups to fluctuate, fast restricted backbone motions could also offer a possible explanation for the observed narrowing of the centerband and sidebands at high temperatures and hydration. Slow rotation of the virus particles about their length axis only contributes significantly to transversal relaxation at spinning rates less than 2 kHz. This contribution even becomes dominant under nonspinning conditions, which further justifies the neglect of other relaxation mechanisms in our analysis of nonspinning relaxation measurements (Magusin and Hemminga, 1993a).

This research was supported by the Netherlands Foundation of Biophysics with financial aid of the Netherlands Organization for Scientific Research (NWO). We are grateful to Gerda Nachtegaal and Leon ter Beek for experimental assistance, to Arno Kentgens for his program to analyze "ideal" sideband patterns, and to Johan Kijlstra for his survey of the literature about <sup>31</sup>P isotropic chemical shifts. We are especially indebted to the SON solid-state NMR facility in Nijmegen (the Netherlands), where the MAS NMR experiments were conducted.

#### APPENDIX: COMPARISON OF THE CUMULATIVE MOTIONAL AMPLITUDE $\lambda$ AND THE GENERAL ORDER PARAMETER $S$

The description of the complex dynamic behavior of the encapsulated backbone using a nonspecific "cumulative amplitude"  $\lambda$  as a measure of the spatial restriction of the motion may be compared with the use of the generalized order parameter  $S$  in the Model Free analysis of longitudinal and transversal relaxation times (Lipari and Szabo, 1982a). In the Model Free approach  $S$  is defined as the limiting value  $S^2$  of the simple correlation function for internal motion  $C_1(t) = S^2 + (1 - S^2)\exp(-t/\tau_c)$  as  $t \rightarrow \infty$ . Similarly, in our combined diffusion model the sinc functions in Eq. 2 also appear in the limiting values  $\text{sinc}^2(\lambda)$  and  $\text{sinc}^2(2\lambda)$  for the correlation functions

$$\frac{1}{2}\langle D_{n1}^2(\Omega(0))[D_{n1}^2(\Omega(t))]^* \rangle$$

and

$$\frac{1}{2}\langle D_{n2}^2(\Omega(0))[D_{n2}^2(\Omega(t))]^* \rangle.$$

Like  $S^2$ ,  $\text{sinc}^2(\lambda)$  and  $\text{sinc}^2(2\lambda)$  approximate 1 in the case of

extremely limited motion ( $\lambda \approx 0$ ) and vanish if the motion is unrestricted ( $\lambda = \pi$ ).

#### REFERENCES

- Alam, T. M., and G. P. Drobny. 1991. Solid-state NMR studies of DNA structure and dynamics. *Chem. Rev.* 91:1545-1590.
- Banner, D. W., C. Nave, and D. A. Marvin. 1981. Structure of the protein and DNA in fd filamentous bacterial virus. *Nature*. 289:814-816.
- Cross, T. A., S. J. Opella, G. Stubbs, and D. L. D. Caspar. 1983a. Phosphorus-31 nuclear magnetic resonance of the RNA in tobacco mosaic virus. *J. Mol. Biol.* 170:1037-1043.
- Cross, T. A., P. Tsang, and S. J. Opella. 1983b. Comparison of protein and deoxyribonucleic acid backbone structures in fd and Pf1 bacteriophages. *Biochemistry*. 22:721-726.
- DiVerdi, J. A., and S. J. Opella. 1981. Phosphorus-31 nuclear magnetic resonance of fd virus. *Biochemistry*. 20:280-284.
- Dufourc, E. J., C. Mayer, J. Stohrer, G. Althoff, and G. Kothe. 1992. Dynamics of phosphate head groups in biomembranes. Comprehensive analysis using phosphorus-31 nuclear magnetic resonance lineshape and relaxation time measurements. *Biophys. J.* 61:42-57.
- Dunker, A. K., R. D. Klausner, D. A. Marvin, and R. L. Wiseman. 1974. Filamentous bacterial viruses X. X-ray diffraction studies of the R4 A-protein mutant. *J. Mol. Biol.* 81:115-117.
- Edmonds, A. R. 1960. Angular Momentum in Quantum Mechanics. Princeton University Press, Princeton, NJ. 146 pp.
- Giessner-Prettre, C., B. Pullman, and F. Ribas Prado. 1984. Contributions of the PO Ester and CO torsion angles of the phosphate group to <sup>31</sup>P-nuclear magnetic shielding. *Biopolymers* 23:377-388.
- Gorenstein, D. G. 1981. Nucleotide conformational analysis by <sup>31</sup>P nuclear magnetic resonance spectroscopy. *Annu. Rev. Biophys. Bioeng.* 10: 355-386.
- Haeberlen, U. 1976. High Resolution NMR in Solids: Selective Averaging. Academic Press, New York. 208 pp.
- Hemminga, M. A., P. A. De Jager, J. Krüse, and R. M. J. N. Lamerichs. 1987. Magic-angle-spinning NMR on solid biological systems. Analysis of the origin of the spectral linewidths. *J. Magn. Reson.* 71:446-460.
- Herzfeld, J., and A. E. Berger. 1980. Sideband intensities in NMR spectra of samples spinning at the magic angle. *J. Chem. Phys.* 73:6021-6030.
- Hogan, M. E., and O. J. Jardetzky. 1980. Internal motions in deoxyribonucleic acid II. *J. Am. Chem. Soc.* 102:3460-3468.
- Lipari, G., and A. Szabo. 1982a. Model-free approach to the interpretation of nuclear magnetic resonance relaxation in macromolecules. 1. Theory and range of validity. *J. Am. Chem. Soc.* 104:4546-4559.
- Lipari, G., and A. Szabo. 1982b. Model-free approach to the interpretation of nuclear magnetic resonance relaxation in macromolecules. 2. Analysis of experimental results. *J. Am. Chem. Soc.* 104:4559-4570.
- Magusin, P. C. M. M., and M. A. Hemminga. 1993a. Analysis of <sup>31</sup>P NMR lineshapes and transversal relaxation of bacteriophage M13 and Tobacco Mosaic Virus. *Biophys. J.* 64:1861-1868.
- Magusin, P. C. M. M., and M. A. Hemminga. 1993b. A theoretical study of rotational diffusion models for rod-shaped viruses: the influence of motion on <sup>31</sup>P NMR lineshapes and transversal relaxation. *Biophys. J.* 64:1851-1860.
- Marvin, D. A., R. L. Wiseman, and E. J. Wachtel. 1974. Filamentous bacterial viruses XI. Molecular architecture of the class II (Pf1, Xf) virion. *J. Mol. Biol.* 82:121-138.
- Mehring, M. 1983. Principles of High Resolution NMR in Solids. Springer-Verlag, Berlin. 342 pp.
- Namba, K., and G. Stubbs. 1986. Structure of tobacco mosaic virus at 3.6 Å resolution: implications for assembly. *Science* 231:1401-1406.
- Pauls, K. P., A. L. MacKay, O. Söderman, M. Bloom, A. K. Tanjea, and R. S. Hodges. 1985. Dynamic properties of the backbone of an integral membrane polypeptide measured by deuterium NMR. *Eur. Biophys. J.* 12:1-11.
- Ribas Prado, F., C. Giessner-Prettre, B. Pullman, and J.-P. Daudey. 1979. Ab initio quantum mechanical calculations of the magnetic shielding tensor of phosphorus-31 of the phosphate group. *J. Am. Chem. Soc.* 101: 1737-1742.

- Schmidt, A., S. O. Smith, D. P. Raleigh, J. E. Roberts, R. G. Griffin, and S. Vega. 1986. Chemical exchange effects in NMR spectra of rotating solids. *J. Chem. Phys.* 85:4248–4253.
- Schmidt, A., and S. Vega. 1987. NMR line shape analysis for two-site exchange in rotating solids. *J. Chem. Phys.* 87:6895–6907.
- Slichter, C. P. 1978. *Principles of Magnetic Resonance*. Springer-Verlag, Berlin. 397 pp.
- Stubbs, G., and C. Stauffacher. 1981. Structure of the RNA in tobacco mosaic virus. *J. Mol. Biol.* 152:387–396.
- Stubbs, G., S. Warren, and K. Holmes. 1977. Structure of RNA and RNA binding site in tobacco mosaic virus from 4 Å map calculated from x-ray fiber diagrams. *Nature*. 267:216–221.
- Thomas, G. J., Jr., B. Prescott, S. J. Opella, and L. A. Day. 1988. Sugar pucker and phosphodiester conformations in viral genomes of filamentous bacteriophages: fd, If1, IKe, Pf1, Xf, and Pf3. *Biochemistry*. 27: 4350–4357.
- Wittebort, R. J., and A. J. Szabo. 1978. Theory of NMR relaxation in macromolecules: restricted diffusion and jump models for multiple internal rotations in amino acid side chains. *J. Chem. Phys.* 69: 1722–1736.

## **CHAPTER 5**

### **2D-Exchange $^{31}\text{P}$ NMR spectroscopy of bacteriophage M13 and tobacco mosaic virus**

(published in 1995, Biophys. J. 68, final manuscript version)

## 2D-Exchange $^{31}\text{P}$ NMR Spectroscopy of Bacteriophage M13 and Tobacco Mosaic Virus

Pieter C.M.M. Magusin and Marcus A. Hemminga

From the Department of Molecular Physics, Agricultural University, Dreijenlaan 3, 6703 HA Wageningen, The Netherlands

**ABSTRACT** Two-dimensional exchange  $^{31}\text{P}$  nuclear magnetic resonance spectroscopy is used to study the slow overall motion of the rod-shaped viruses M13 and TMV in concentrated gels. Even for short mixing times, observed diagonal spectra differ remarkably from projection spectra and one-dimensional spectra. Our model readily explains this to be a consequence of the  $T_{2\rho}$  anisotropy caused by slow overall rotation of the viruses about their length axis. 2D-exchange spectra recorded for 30% (w/w) TMV with mixing times below 1 sec do not show any off-diagonal broadening, indicating that its overall motion occurs in the sub-Hertz frequency range. In contrast, the exchange spectra obtained for 30% M13 show significant off-diagonal intensity for mixing times of 0.01 sec and higher. A log-Gaussian distribution around 25 Hz of overall diffusion coefficients mainly spread between 1 and  $10^3$  Hz, faithfully reproduces the 2D-exchange spectra of 30% M13 recorded at various mixing times in a consistent way. A small, but notable change in diagonal spectra at increasing mixing time, is not well accounted for by our model and is probably caused by  $^{31}\text{P}$  spindiffusion.

### INTRODUCTION

In the past few years, two-dimensional (2D) exchange nuclear magnetic resonance (NMR) spectroscopy has proven its value for studying motion in a broad range of systems, such as synthetic polymers (Schmidt-Rohr and Spiess, 1991), lipids (Fenske and Jarrell, 1991), liquids (Kimich and Fischer, 1994) and liquid-gas interfaces (Tomasselli et al., 1993). Some processes, such as exchange of nuclear spins between different chemical or physical environments, translation of spins in a field gradient, or reorientation of nuclei with chemical shift anisotropy (CSA) with respect to the magnetic field, can correlate different resonance positions in the NMR spectrum through time. By use of 2D-exchange NMR spectroscopy, this correlation can be made visible as a cross-peak, or, more generally, off-diagonal intensity in 2D NMR spectra, which are therefore easy to interpret, at least in a qualitative manner. Quantitatively, 2D-exchange spectra dominated by specific reorientational processes have been analyzed in terms of combined subspectra representing different reorientation angles (Wefing et al., 1988). The possibility to extract the distribution of reorientation angles directly from the spectrum is especially useful for studying amorphous materials containing internal motions without sharply defined restriction angles and correlation times.

In previous work, we have presented analyses of one-dimensional (1D)  $^{31}\text{P}$  NMR spectra and transversal relaxation decays of bacteriophage M13 and tobacco mosaic virus (TMV). M13 and TMV are rod-shaped viruses with a length of ~900 and 300 nm and a diameter of ~9 and 18 nm, respectively. Intact virus particles largely consist of a protein coat protecting the encapsulated viral genome, which contributes only a small part of the particle weight. Because the coat proteins of M13 and TMV do not contain  $^{31}\text{P}$  nuclei, selective information about the structure and dynamics of the phosphodiester in the encapsulated nucleic acid molecule

can be obtained by use of  $^{31}\text{P}$  NMR spectroscopy. The way in which  $^{31}\text{P}$  NMR powder lineshapes and transversal relaxation observed for M13 and TMV are influenced by motion, cannot be explained consistently by simple models, like e.g. isotropic rotational diffusion or rotation of the rod-shaped virions about their length axis alone (Magusin and Hemminga, 1993a). Instead, a combination of fast, restricted nucleic acid backbone motion and slow overall motion of the virions is found. Fast, restricted backbone motion also explains the fact that sideband intensities in magic angle spinning (MAS) spectra of dilute M13 gels (Magusin and Hemminga, 1994) deviate from the values predicted by standard theory (Herzfeld and Berger, 1980). The spinning-rate dependence of MAS transversal relaxation has successfully been assigned to slow overall rotation of the virions as a whole (Magusin and Hemminga, 1994). To test and refine this model further, we have investigated the slow overall motion of the rod-shaped viruses in concentrated gels using 2D-exchange  $^{31}\text{P}$  NMR spectroscopy. The results of this investigation are presented and analyzed in this paper.

### THEORY

To calculate the effect of rotational diffusion of the rod-shaped virions about their length axis on  $^{31}\text{P}$  two-dimensional exchange spectra, the orientation of a  $^{31}\text{P}$  chemical shift tensor is first expressed by use of the Euler angles  $\Omega = (\alpha, \beta, \gamma)$  in an axis system fixed to the virion with its  $z$  axis parallel to the length axis of the virion. The orientation of this rotor axis system in the laboratory frame with the  $z$  axis parallel to the magnetic field, in turn, is given by  $\Omega' = (\phi, \theta, \psi)$ . If interactions between  $^{31}\text{P}$  and other nuclei are negligible, transversal and longitudinal  $^{31}\text{P}$  magnetization can be calculated from the positive and negative-helicity components  $\mu_{\pm}(\Omega, \Omega', t)$  of the spindensity operator  $\rho(\Omega, \Omega', t)$  and its longitudinal component  $\mu_z(\Omega, \Omega', t)$ . In the



presence of only Zeeman interaction, chemical shift and rotational diffusion, the relevant equations for these three components derived from the Stochastic Liouville Equation are represented in the rotating frame by

$$\frac{d\mu_z(\Omega, \Omega', t)}{dt} = \left( \pm i\omega(\Omega, \Omega') + D \frac{\partial^2}{\partial \psi^2} \right) \mu_z(\Omega, \Omega', t) \quad (1a)$$

and

$$\frac{d\mu_x(\Omega, \Omega', t)}{dt} = D \frac{\partial^2}{\partial \psi^2} \mu_x(\Omega, \Omega', t) \quad (1b)$$

where  $D$  denotes the diffusion coefficient for the overall virion motion and  $\omega(\Omega, \Omega')$  represents the chemical shift interaction, expressed in terms of the Wigner functions  $D_{m' m}^2(\alpha\beta\gamma) = \exp(im'\gamma) d_{m' m}^2(\beta) \exp(im\alpha)$  (Edmonds, 1960; Haeblerlen, 1976) as

$$\omega(\Omega, \Omega') = \omega_0 \sigma_0 + \omega_0 \sum_{m'=-2}^2 D_{m' 0}^2(\Omega') \times \\ \times [F_0 D_{0 m'}^2(\Omega) + F_2 (D_{2 m'}^2(\Omega) + D_{-2 m'}^2(\Omega))] \quad (2a)$$

where  $\omega_0 = \gamma B_0$  is the Zeeman angular frequency,  $\sigma_0 = (\sigma_{11} + \sigma_{22} + \sigma_{33})/3$ ,  $F_0 = (\sigma_{33} - \sigma_0)$  and  $F_2 = (\sigma_{11} - \sigma_{22})/\sqrt{6}$  for a chemical shift tensor with tensor values  $\sigma_{11}$ ,  $\sigma_{22}$  and  $\sigma_{33}$ . In our previous analyses of  $^{31}\text{P}$  powder lineshapes and magic angle spinning spectra of M13 and TMV, we have described the net effect of fast, restricted backbone motions of the encapsulated nucleic acid molecule in a simplified way, as the effect caused by fast, restricted diffusion of the phosphodiester about the length axis of the virions. Also here, we will assume that the phosphodiester undergoes uniaxial diffusion restricted to angles  $\alpha \in [\alpha_0 - \lambda, \alpha_0 + \lambda]$ , fast enough to allow us to replace  $D_{n' m'}^2(\Omega)$  ( $n = 0, \pm 2$ ) in eq. 2a by the average  $D_{n' m'}^2(\Omega) \text{sinc}(m'\lambda)$ , where  $\Omega_0 = (\alpha_0, \beta, \gamma)$  and  $\text{sinc}(m'\lambda)$  denotes the function  $\sin(m'\lambda)/m'\lambda$ , which yields

$$\omega_\lambda(\Omega_0, \Omega') = \omega_0 \sigma_0 + \omega_0 \sum_{m'=-2}^2 d_{m' 0}^2(\theta) e^{im'(\psi - \psi_0)} \times \\ \times [F_0 d_{0 m'}^2(\beta) + F_2 (d_{2 m'}^2(\beta) e^{2i\gamma} + d_{-2 m'}^2(\beta) e^{-2i\gamma})] \text{sinc}(m'\lambda) \quad (2b)$$

The development of transversal coherence  $\mu_\pm(\Omega, \Omega', t)$  would follow from the solution of Eq. 1a. Unfortunately, this equation cannot be solved analytically. For very slow rotational diffusion with a coefficient  $D$  much smaller than the static linewidth of about  $\omega_0 |\sigma_{33} - \sigma_{11}|$ , however, spindensity may be assumed to stay close to its initial orientation within times in the order of the decay time of the free induction decay and it is then justified to linearize Eq. 1a by approximating  $\omega_\lambda(\Omega_0, \Omega')$  for orientations closely around any orientation  $\Omega'_0 = (\phi, \theta, \psi_0)$  as  $\omega_\lambda(\Omega_0, \Omega'_0) + g_\lambda(\Omega_0, \Omega'_0) (\psi - \psi_0)$ , where  $g_\lambda(\Omega_0, \Omega'_0)$  denotes the derivative  $\partial \omega_\lambda / \partial \psi$  for  $\psi = \psi_0$ . The linearized eq. 1a may be solved similarly to the case of spins diffusing in a linear field gradient (Slichter, 1978), from which the two transversal components of spindensity at orientations infinitely close to  $\Omega'_0$  may be derived as

$$\mu_\pm(\Omega_0, \Omega'_0, t) = \exp[-Dr_\lambda(\Omega_0, \Omega'_0)t^2 \pm i\omega_\lambda(\Omega_0, \Omega'_0)t] \mu_\pm(\Omega_0, \Omega'_0, 0) \quad (3a)$$

where

$$r_\lambda(\Omega_0, \Omega'_0) = [g_\lambda(\Omega_0, \Omega'_0)]^2 / 3 \quad (3b)$$

Analogously, a  $\pi$  pulse at time  $\tau$  after the excitation pulse produces an echo at time  $2\tau$  given by

$$E_\pm(\Omega_0, \Omega'_0, 2\tau) = \exp[-Dr_\lambda(\Omega_0, \Omega'_0)2\tau^2] \mu_\pm(\Omega_0, \Omega'_0, 0) \quad (4)$$

Eq. 4 shows that in a first approximation very slow overall diffusion causes a type of transversal relaxation that is non-exponential, non-fluctuating and anisotropic. An apparent relaxation time  $T_{2e}$  may be defined as the time  $2\tau$  at which the powder echo  $\langle E_\pm(\Omega_0, \Omega'_0, 2\tau) \rangle$  decays to  $e^{-1}$  of its initial value. It follows from Eq. 4 that  $T_{2e}$  is inversely proportional to the cube root of  $D$ .

In the absence of  $T_1$  relaxation and spindiffusion, the development of longitudinal coherence  $\mu_z(\Omega, \Omega', t)$  is only determined by the overall motion of the rod-shaped virions. Therefore, from a given longitudinal coherence distribution  $\mu_z(\Omega, \Omega', t_1)$  at a specific time  $t_1$ , the coherence distribution  $\mu_z(\Omega, \Omega', t_1 + t_m)$  at a later time  $t_1 + t_m$  can be calculated by integrating the fraction of coherence associated to each virion orientation  $\Omega'_1 = (\phi_1, \theta_1, \psi_1)$  that is transferred to the orientation  $\Omega'_2 = (\phi_2, \theta_2, \psi_2)$  between  $t_1$  and  $t_1 + t_m$

$$\mu_z(\Omega, \Omega', t_1 + t_m) = \int P(\Omega'_2 | \Omega'_1, t_m) \mu_z(\Omega, \Omega'_1, t_1) d\Omega'_1 \quad (5)$$

where  $P(\Omega'_2 | \Omega'_1, t_m)$  may also be regarded as the conditional probability density of finding a virion in orientation  $\Omega'_2$  provided that its orientation was  $\Omega'_1$  a time  $t_m$  before. For uniaxial rotational diffusion of the rod-shaped virions about their length axis,  $P(\Omega'_2 | \Omega'_1, t_m)$  follows from Eq. 1b as

$$P(\Omega'_2 | \Omega'_1, t_m) = \frac{\delta(\phi_2 - \phi_1) \delta(\theta_2 - \theta_1)}{(4\pi Dt_m)^{1/2}} \times \\ \times \sum_{k=-\infty}^{\infty} \exp\left[-\frac{(\psi_2 - \psi_1 - 2k\pi)^2}{4Dt_m}\right] \quad (6)$$

where  $\delta(\phi_2 - \phi_1)$  and  $\delta(\theta_2 - \theta_1)$  represent Dirac's delta functions and the summation over  $k$  has been included in the definition of  $P(\Omega'_2 | \Omega'_1, t_m)$  to let the integration boundaries in Eq. 3a be standard ones, more specifically  $0 < \psi_1 < 2\pi$ . If  $t_m$  reduces to 0,  $P(\Omega'_2 | \Omega'_1, t_m)$  becomes the three-dimensional delta function  $\delta(\phi_2 - \phi_1) \delta(\theta_2 - \theta_1) \delta(\psi_2 - \psi_1)$ , as expected.

The pulse sequence employed in our experiments to record 2D-exchange NMR spectra is depicted in Fig. 1. Transversal  $^{31}\text{P}$  magnetization is first created from  $^1\text{H}$  magnetization using cross-polarization. During the following evolution time  $t_1$  the orientations of the virions are indirectly probed by labeling  $^{31}\text{P}$  magnetization with the anisotropic chemical shift. After  $t_1$ , the  $x$  or  $y$ -component is rotated along the  $z$ -direction and during the following mixing time  $t_m$ , the orientations of the virus particles are allowed to change. To probe the new orientations, the  $z$ -magnetization of the  $^{31}\text{P}$  magnetization is rotated back to the transversal plane and the echo

produced by a  $\pi$  pulse at a short time  $\Delta$  after back-rotation is measured during the detection time  $t_2$ . The NMR signal that results from the pulse sequence in Fig. 1 depends on the phase shifts between the rf-pulses. By varying these phase shifts different NMR signals can be generated which in combination produce a purely amplitude modulated signal

$$S(t_1, t_2 | t_m) = (8\pi^2)^{-3} \iiint d\Omega_0 d\Omega'_1 d\Omega'_2 P(\Omega'_2 | \Omega'_1, t_m) \times \exp[-D r_\lambda(\Omega_0, \Omega'_1) t_1^3] \cos(\omega_\lambda(\Omega_0, \Omega'_1) t_1) \times (7) \\ \times \exp[-D r_\lambda(\Omega_0, \Omega'_2) (2\tau^3 + t_2^3)] \cos(\omega_\lambda(\Omega_0, \Omega'_2) t_2)$$

as can be derived by use of Eqs. 3a, 3b, 4a and 4b.

In principle, 2D-exchange spectra  $I(\omega_1, \omega_2 | t_m)$  may be simulated for various diffusion coefficients  $D$  by Fourier transformation of the 2D signals  $S(t_1, t_2 | t_m)$  generated by use of Eq. 7. The integration over chemical shift tensor orientations  $\Omega_0$ , virus orientations  $\Omega'_1$  and  $\Omega'_2$ , and diffusion coefficients  $D$ , however, makes such calculations too lengthy to be of practical use. The calculation time may strongly be reduced by making some approximations. First, lineshape effects caused by transversal relaxation during short echo delays  $2\tau$  are only small. This has been experimentally observed for M13 and is also calculated theoretically for uniaxial diffusion of M13 as a whole, if it is assumed that phosphodiester are randomly oriented within the phage (Magusin and Hemminga, 1993b). The angular dependent relaxation factor  $\exp[-D r(\Omega_0, \Omega'_2) 2\tau^3]$  in Eq. 7 may then be approximated by an isotropic factor  $\exp[-D \langle r^2 \rangle 2\tau^3]$ , which can be drawn outside the angular integrals. This makes Eq. 7 symmetric with respect to exchange between  $t_1$  and  $t_2$ , so that  $S(t_1, t_2 | t_m)$  needs only be calculated for  $t_1 \leq t_2$ , which halves the calculation time.

A further reduction of calculation time is possible if one single set of subspectra generated only once, can be used in different combinations to simulate 2D-exchange spectra for various diffusion coefficients and mixing times. A similar procedure to analyse 2D-exchange spectra in terms of jump angle distributions has been presented elsewhere (Wefing et al., 1988; Wefing and Spiess, 1988).  $P(\Omega'_2 | \Omega'_1, t_m)$  (Eqs. 6 and 8) depends on the rotation angle  $\Delta\Omega' = \Omega'_2 - \Omega'_1$  rather than on the orientation angles  $\Omega'_2$  and  $\Omega'_1$  separately. After Fourier transformation, we therefore apply the coordinate transform  $(\Omega'_1, \Omega'_2) \rightarrow (\Omega'_1, \Delta\Omega')$  to Eq. 7, substitute  $P(\Omega'_1 + \Delta\Omega' | \Omega'_1, t_m)$  by  $P(\Delta\Omega' | t_m)$ , and finally approximate the integral over  $\Delta\Omega'$  by a summation over a set of subspectra  $I_n(\omega_1, \omega_2 | \Delta\Omega'_n)$  for a series of equidistant values  $\Delta\Omega'_n$  to obtain

$$I(\omega_1, \omega_2 | t_m) = \sum P(\Delta\Omega'_n | t_m) I_n(\omega_1, \omega_2 | \Delta\Omega'_n) \quad (8)$$

Strictly mathematically, subspectra  $I_n(\omega_1, \omega_2 | \Delta\Omega'_n)$  still depend on the diffusion coefficient  $D$  through transversal relaxation (Eq. 7), so that different sets of subspectra would still have to be calculated to simulate 2D-exchange spectra for different diffusion coefficients. For long mixing times  $t_m \gg t_1, t_2 > T_2^*$ , however, the effect of transversal relaxation during  $t_1$  and  $t_2$  on the off-

diagonal intensity is generally negligible with respect to the off-diagonal intensity caused by the large orientational changes taking place during  $t_m$ . As a consequence, subspectra generated for some specific  $D$  value can actually well be used to simulate exchange spectra for a complete range of diffusion coefficients. In our calculations we therefore make an artificial distinction between rotational diffusion with diffusion coefficient  $D_0$  taking place during  $t_1$  and  $t_2$  and diffusion with coefficient  $D$  during  $t_m$ . A value for  $D_0$  can be independently estimated from transversal  $^{31}\text{P}$  relaxation measurements (Magusin and Hemminga, 1993a), so that only the diffusion coefficient  $D$  remains to be determined from 2D-exchange NMR spectra. The subspectra are then given by

$$I_n(\omega_1, \omega_2 | \Delta\Omega'_n) = (8\pi^2)^{-2} \exp[-D_0 \langle r^2 \rangle 2\tau^3] \int dt_1 e^{i\omega_1 t_1} \int dt_2 e^{i\omega_2 t_2} \quad (9)$$

$$\int d\Omega_0 d\Omega'_1 \exp[-D_0 r_\lambda(\Omega_0, \Omega'_1) t_1^3] \cos(\omega_\lambda(\Omega_0, \Omega'_1) t_1) \times \exp[-D_0 r_\lambda(\Omega_0, \Omega'_1 + \Delta\Omega'_n) t_2^3] \cos(\omega_\lambda(\Omega_0, \Omega'_1 + \Delta\Omega'_n) t_2)$$

Because  $P(\Delta\Omega' | t_m)$  does not depend on the sign of the rotation (Eq. 6), the summation in Eq. 8 may be further simplified by combining subspectra for positive and negative  $\Delta\Omega'_n$  beforehand, yielding

$$I_n^+(\omega_1, \omega_2 | \Delta\Omega'_n) = \begin{cases} I_n(\omega_1, \omega_2 | \Delta\Omega'_n) + I_n(\omega_1, \omega_2 | -\Delta\Omega'_n), & \text{if } \Delta\Omega'_n \neq 0 \\ I_n(\omega_1, \omega_2 | 0), & \text{if } \Delta\Omega'_n = 0 \end{cases} \quad (10)$$

In the derivation of Eq. 8 it is assumed that all virions in the gel undergo rotational diffusion with the same diffusion coefficient  $D$ . However, local viscosity differences in the concentrated gels could exist, causing variations in rotational diffusion. To include the effect of motional inhomogeneity, it is assumed in the model that

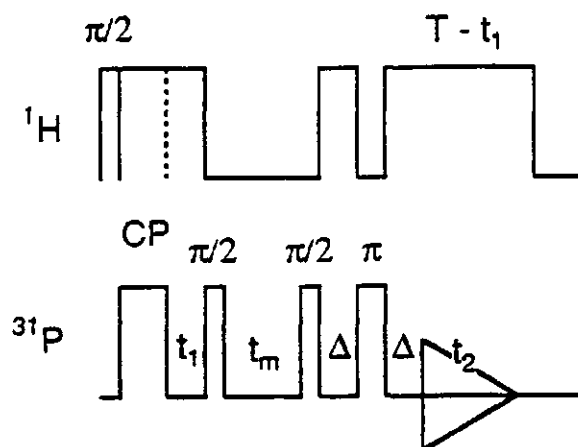


FIGURE 1: pulse sequence with  $^1\text{H}$  and  $^{31}\text{P}$  pulses (above and below, respectively) used for 2D-exchange  $^{31}\text{P}$  NMR spectroscopy. CP denotes the cross-polarization contact time. A  $\pi$  pulse creates the echo measured during detection time  $t_2$ . High-power proton-decoupling is on during the evolution time  $t_1$ , refocusing delays  $\Delta$  and detection time  $t_2$ . By decreasing the length of the final decoupling pulse at increasing  $t_1$ , proton decoupling is on during a constant time  $T$ , so that the sample-heating caused by it is kept constant to prevent temperature drift.

the logarithmic values  $\log(D)$  of the diffusion coefficients  $D$  are symmetrically distributed around some central value  $\log(D_c)$  according to a Gaussian density function with characteristic width  $W$  (Wefing et al., 1988). For simplicity, rotational diffusion during  $t_1$  and  $t_2$  is considered to be homogeneous and independent from diffusion during  $t_m$ . For the case of inhomogeneous diffusion,  $P(\Delta\Omega'|t_m)$  in Eq. 8 must be replaced by

$$P(\Delta\Omega'|t_m) = \frac{\delta(\Delta\phi)\delta(\Delta\theta)}{2\pi(Wt_m)^{1/2}} \times \int_{-\infty}^{\infty} \exp\left[-\left\{\frac{\log(D) - \log(D_c)}{W}\right\}^2\right] \times \frac{1}{D^{1/2}} \sum_{k=-\infty}^{\infty} \exp\left[-\frac{(\Delta\psi + 2k\pi)^2}{4Dt_m}\right] d\log(D) \quad (11)$$

where  $\Delta\phi = \phi_2 - \phi_1$ ,  $\Delta\theta = \theta_2 - \theta_1$  and  $\Delta\psi = \psi_2 - \psi_1$ . For  $W$  approaching 0, Eq. 8 reduces to Eq. 6 again.

## MATERIAL AND METHODS

### Experimental Procedures

M13 and TMV were grown, purified and concentrated to 30% (w/w) as described previously (Magusin and Hemminga, 1993a). NMR spectra were recorded on a Bruker CXP300 spectrometer operating at a  $^{31}\text{P}$  NMR frequency of 121.5 MHz. 2D-exchange  $^{31}\text{P}$  NMR spectra were recorded using the pulse sequence depicted in Fig. 1, which involves cross-polarization to create transversal  $^{31}\text{P}$  magnetization and a Hahn echo producing  $\pi$  pulse to remove the effect of probe ringing on the weak signal. Because of the dielectric properties of wet M13 and TMV gels, the  $\pi/2$  pulse was set to 5  $\mu\text{s}$  on the weak  $^{31}\text{P}$  NMR signal of the samples itself. The Hartmann-Hahn condition necessary for cross-polarization was found by measuring the  $^1\text{H}$   $\pi/2$  pulse length directly on the water signal and setting it equal to the  $^{31}\text{P}$   $\pi/2$  pulse length. The dwell time was 5  $\mu\text{s}$  and the carrier frequency was set to the center of the  $^{31}\text{P}$  resonance. To record spectra of M13,  $t_1$  was systematically incremented by 5  $\mu\text{s}$ . For TMV the  $t_1$ -increment was 10  $\mu\text{s}$ . CYCLOPS phase alternation was employed to remove the effects of pulse imperfections and Time Proportional Phase Incrementing (TPPI) was used to acquire the spectra in the phase-sensitive mode (Marion and Wüthrich, 1983). Phase-cycling of the first proton pulse suppressed the effect of direct  $^{31}\text{P}$  excitation on the signal. Signals were recorded with 256 data points. To avoid truncation effects and to obtain the best signal to noise ratio within the measuring time available, the number of  $t_1$ -increments (NE) and the number of scans per  $t_1$ -increment (NS) were chosen differently for different mixing times  $t_m$ . M13 spectra for  $t_m = 0.1$  and 1.0 sec were recorded with NE = 64 and NS = 1024. For  $t_m = 0.01$  sec these numbers were both 128. TMV spectra were acquired with NE = 128 and NS = 512. The repetition time was 1.1 sec. Two dummy scans were used to get the spinsystem in a steady state. High power proton decoupling was on during cross-polarization (1.0 ms), the

variable evolution time  $t_1$ , refocussing delays  $\tau$  and acquisition time  $t_{\text{acq}}$  (1.4 ms). An extra decoupling delay at the end of the pulse sequence was shortened at increasing  $t_1$ , so that the total decoupling time per experiment was kept constant at approximately 3 ms. In this way, the temperature could be kept constant at 30  $^\circ\text{C}$  throughout the experiment by use of a Bruker temperature unit, as checked using a fluoroptic thermometer as described previously (Magusin and Hemminga, 1993a). Sample tubes were sealed with a two-component glue to keep the water content in the gel constant which was checked by weighing and spectrophotometry.

### Simulation Procedures

2D-exchange  $^{31}\text{P}$  NMR spectra at 121.5 MHz were simulated for M13 using Fortran programs derived from the equations in this paper. For the chemical shift tensor of  $^{31}\text{P}$  nuclei in M13 the relative tensor values  $\sigma_{11} - \sigma_0 = 77$  ppm,  $\sigma_{22} - \sigma_0 = 18$  ppm and  $\sigma_{33} - \sigma_0 = -95$  ppm (where  $\sigma_0$  is the isotropic shift) were taken (Magusin and Hemminga, 1993a, Magusin and Hemminga, 1994). In the simulations it was assumed that a random distribution of shift tensor orientations exists within M13. To analyse experimental spectra, a set of 16 subspectra was first generated in a numerical way approximating Eq. 9 for a series of jump angles  $\Delta\Omega'_n = (0, 0, \Delta\psi_n)$  with  $\Delta\psi_n$  being multiples of 0.2 rad between 0.0 and 3.0 rad. Next, these subspectra were combined according to Eq. 8 with  $P(\Delta\Omega'|t_m)$  or  $P'(\Delta\Omega'|t_m)$  calculated for various mixing times and diffusion coefficients. These linear combinations were fitted to the experimental spectrum allowing height of the simulated spectrum to vary. The best fitting linear combination was found by comparing the variance between the theoretical spectra and the observed spectrum.

## RESULTS

Fig. 2 shows contour plots of the 2D-exchange  $^{31}\text{P}$  NMR spectra of 30% M13 and 30% TMV recorded with a mixing time  $t_m = 1$  sec. To facilitate comparison between the two, the contour in the TMV spectrum has been drawn at the same relative intensity level, 23%, as the middle contour in the M13 spectrum. For TMV, this contour lies practically on the diagonal, indicating that most phosphodiesteres in TMV do not undergo large reorientations at the timescale of seconds. In contrast, the 23% contour in the spectrum of M13 illustrates a large spread of spectral intensity in the frequency plane. The approximately hexagonal shape of the 10% contour reflects the three discontinuities in the one-dimensional  $^{31}\text{P}$  powder lineshape. At shorter mixing times, these discontinuity features of the 10% contour become less prominent. Narrower, elliptically shaped contours are observed in spectra recorded with  $t_m = 0.1$  sec. The width of this ellipse further reduces as  $t_m$  decreases to 0.01 sec and for  $t_m \leq 0.001$  sec, only a narrow diagonal ridge is visible in 2D-exchange NMR spectra of 30% M13.

Theoretical studies have pointed out that homogeneous jumplike motions would often cause characteristic ridge patterns to show up in 2D-exchange spectra (Wefing and Spiess, 1988; Wefing et al., 1988). No such ridge patterns are present in 2D-exchange spectra of M13. Instead,

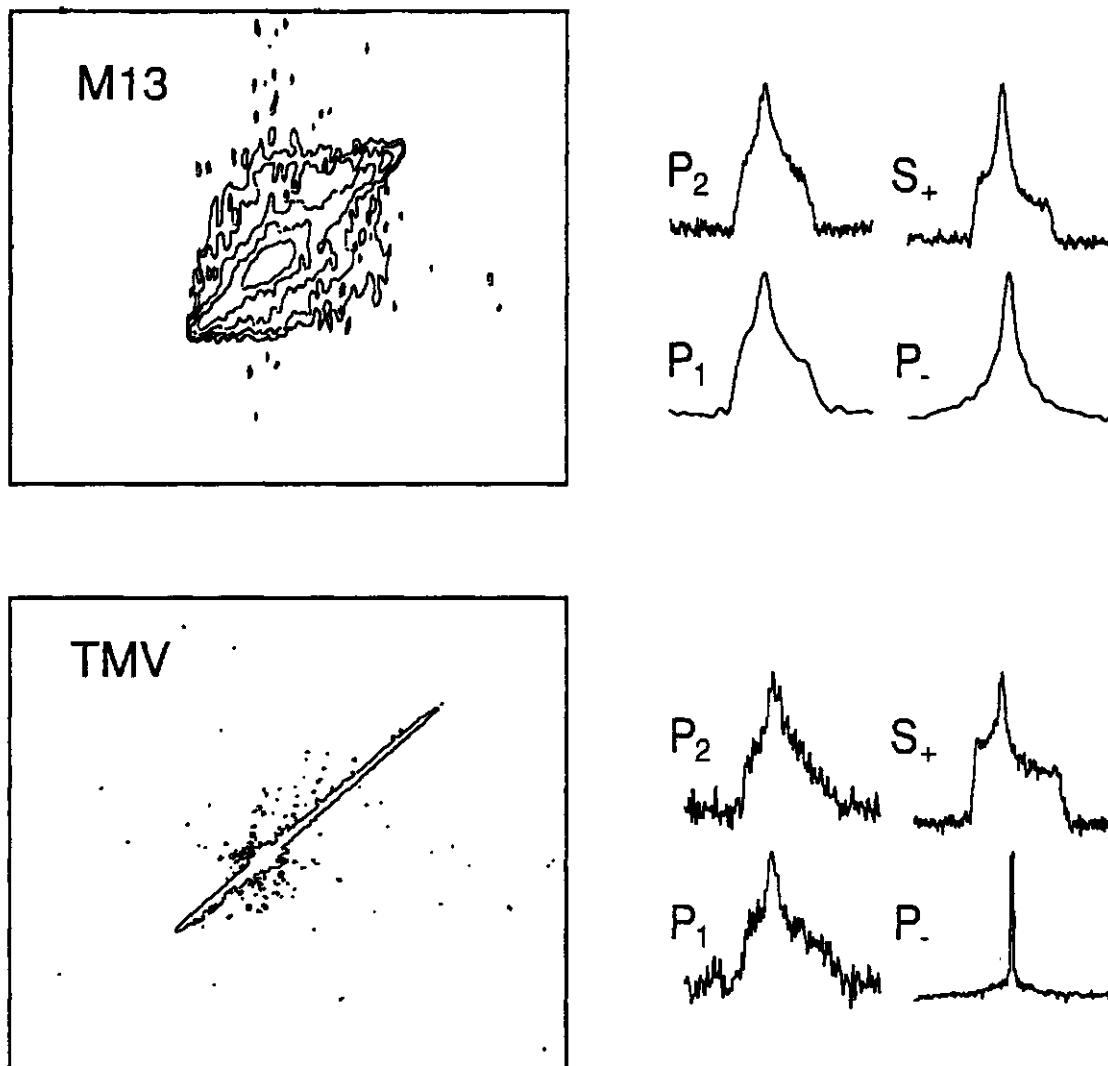


FIGURE 2: 2D-exchange spectra of M13 and TMV for  $t_m = 1$  sec. The contours shown for M13 represent levels of 10, 15, 23, 33 and 50% with respect to the highest intensity at the  $\sigma_{22}$  position on the diagonal. Only the 23%-contour is shown for TMV.  $P_2$  and  $P_1$  are the spectral projections on the  $\nu_2$ - and  $\nu_1$ -axis, respectively,  $S_+$  denotes the spectral cross-section along the diagonal and  $P_-$  is the projection on the anti-diagonal. Frequency ranges shown are 50 kHz for  $P_2$  and  $P_1$ ,  $50 \times \sqrt{2}$  kHz for  $S_+$  and  $50 / \sqrt{2}$  kHz for  $P_-$ . No filtering or symmetrization has been used to create the figure.

intensity curves in spectral cross-sections taken at right angles with respect to the spectrum diagonal, generally have gaussian shapes, gradually broadening at increasing  $t_m$ . Such type of anti-diagonal broadening is indicative for rotational diffusion dominating 2D-exchange (Wefing et al., 1988). Interestingly, 2D-exchange spectra of 15% M13 recorded with mixing times of 0.001 and 0.01 sec (not shown) are very similar to the 30% M13 spectra recorded with mixing times of 0.01 and 0.1 sec, respectively (Fig. 3). This directly indicates that, if one type of motion mainly underlies the observed off-diagonal broadening at both concentrations, this motion should be about ten times faster in 15% than in 30% M13 gels. This, in turn, would agree with the factor 8 difference between the diffusion coefficients, which we estimated

previously by interpreting transversal relaxation in terms of slow overall rotation of the rod-shaped M13 virions about their length axis (Magusin and Hemminga, 1993a). Remarkably, the diagonal cross-section  $S_+$  in 2D-exchange spectra of M13 and TMV recorded even at vanishing mixing times (10  $\mu\text{s}$ ) strongly differs from the corresponding 1D  $^{31}\text{P}$  NMR spectra. Discontinuities are generally more pronounced in  $S_+$  than in the projection  $P_2$  on the  $\nu_2$  axis, which represents the Fourier transform of the time-domain cross-section  $S(0, t_2|t_m)$ . In the absence of  $T_1$  anisotropy,  $P_2$  should be similar to the 1D spectrum. This phenomena cannot be explained by the experimental asymmetry of the  $t_1$  and  $t_2$  time domains with regard to the Hahn-echo pulse-sequence preceding  $t_2$ , but not  $t_1$  (Fig. 1). The absence of a true  $t_1 = 0$

measurement would distort the projection  $P_1$  on the  $\nu_1$  axis more, than the lineshape in the diagonal spectrum  $S_+$ , which would be some average between the  $P_1$  and  $P_2$  lineshapes. Obviously this is not the case, because  $P_1$  and  $P_2$  are practically the same, whereas  $S_+$  differs from  $P_1$  and  $P_2$  significantly (Fig. 2). It will be shown below, that  $T_{2e}$  anisotropy provides an explanation for the observed lineshape in the diagonal spectrum. Less pronounced than the difference between  $S_+$  and  $P_2$ , but still well visible, is the lineshape change in  $S_+$  as a function of  $t_m$  (Fig. 4). Especially for TMV, the spectral intensity around the  $\sigma_{22}$  chemical shift position is observed to shrink with respect to the lineshape as a whole at increasing  $t_m$ . Below, this effect will be tentatively assigned to anisotropic spindiffusion.

## DISCUSSION

As demonstrated previously, a combination of slow overall motion of the rod-shaped viruses M13 and TMV about their viral axis and fast restricted backbone motion of the encapsulated nucleic acid molecule can provide a consistent explanation for the motional effects on the observed  $^{31}\text{P}$  NMR powder lineshapes and transversal relaxation (Magusin and Hemminga, 1993a; Magusin and Hemminga, 1994). We have employed two-dimensional  $^{31}\text{P}$  exchange NMR spectroscopy to investigate the slow overall rotation of the rod-shaped virions about their length axis in more detail. The absence of off-diagonal broadening in exchange spectra recorded for TMV with mixing times  $t_m \leq 1$  sec, immediately shows that the diffusion coefficient  $D_0$  for overall motion of 30% TMV is below the upperlimiting value of 3 Hz, which we have previously estimated from nonspinning transversal relaxation assuming it to be caused by slow overall motion only (Magusin and Hemminga, 1993a). MAS  $T_{2e}$

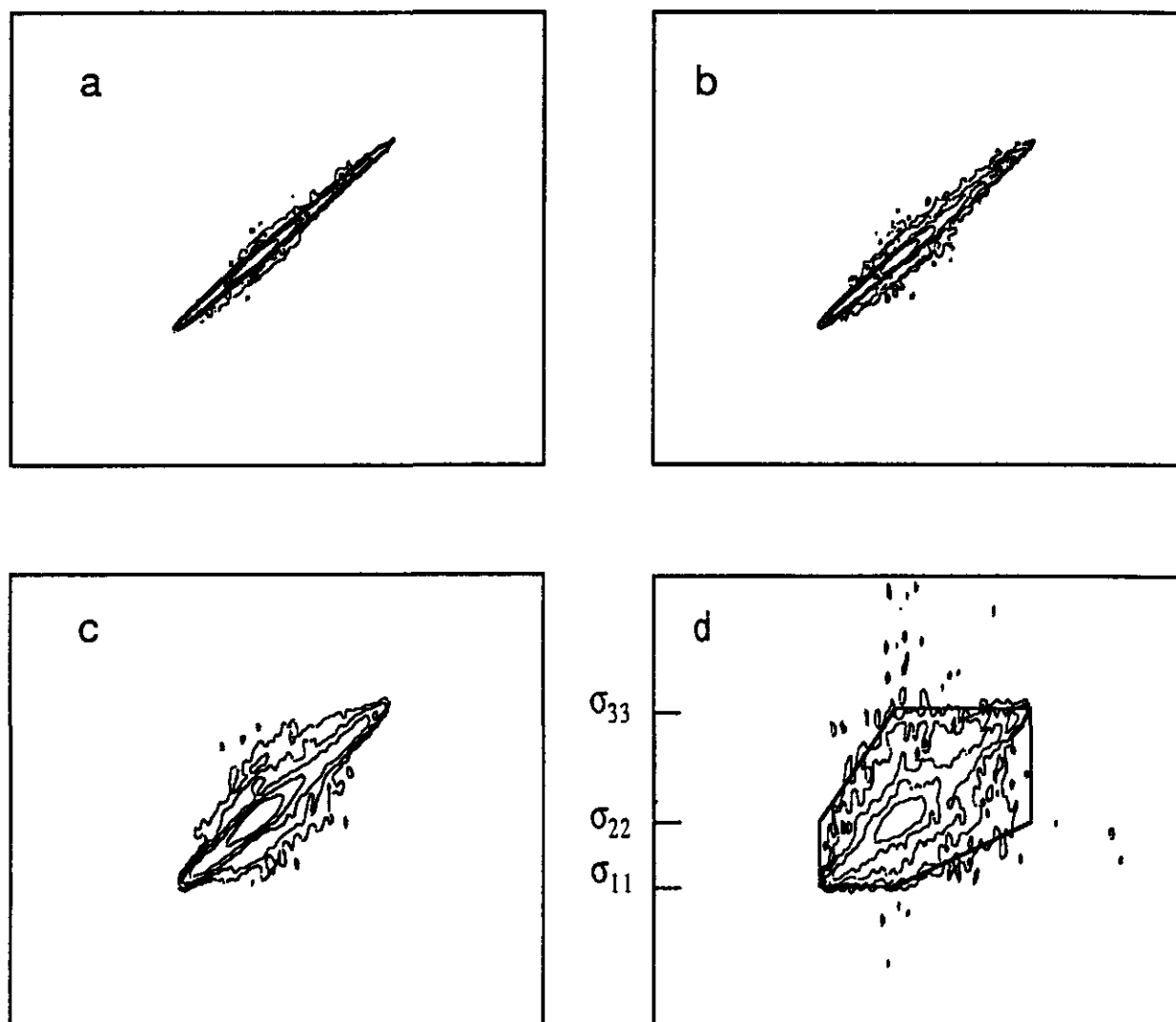


FIGURE 3: Contour plots of the spectra recorded for  $t_m = 0.001$  (a), 0.01 (b), 0.1 (c) and 1 sec (d) respectively. Contour levels are the same as in Fig. 2. The hexagon reflecting the chemical shift tensor values  $\sigma_{11}$ ,  $\sigma_{22}$  and  $\sigma_{33}$  (see text), is also illustrated in Fig. 3d.

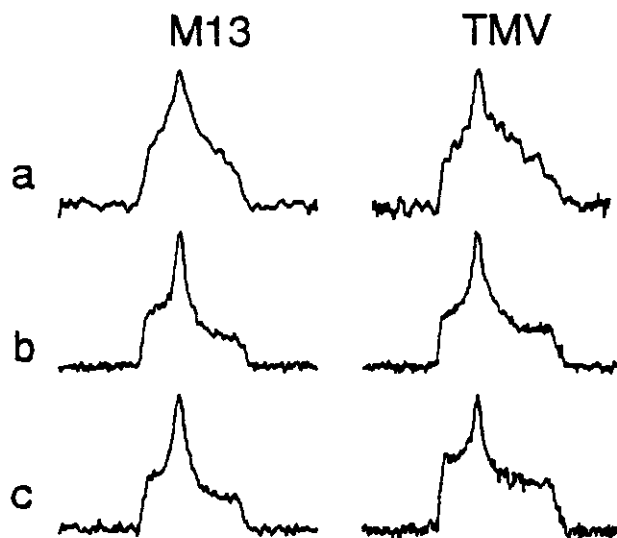


FIGURE 4: 1D spectra (row a) and diagonal spectra for  $t_m = 0.01$  sec (row b) and 1 sec (row c) for M13 and TMV, respectively.

studies have revealed the presence of an additional relaxation mechanism, perhaps related to fast backbone motions of the encapsulated RNA molecule (Magusin and Hemminga, 1994), which could well be responsible for half of the observed nonspinning relaxation. Because  $T_{2e} \propto D_o^{-1/3}$  (see definition below Eq. 4), this would indicate that  $D_o$  is actually in the order of  $10^{-1}$  Hz. Indeed, slow overall rotation in the sub-Hertz range would be consistent with the absence of broadening in exchange spectra recorded with  $t_m = 1$  sec. In contrast to TMV, the exchange spectra obtained for M13 already start to broaden for  $t_m = 0.01$  sec, which roughly agrees with the 50 Hz estimated for overall motion from nonspinning relaxation.

To extract quantitative information from the experimental results obtained for M13, the previous model for nonspinning samples (Magusin and Hemminga, 1993b) has been extrapolated to 2D-exchange NMR experiments. In both the previous and present model, the motions of the nucleic acid phosphodiester are collectively described as fast, restricted rotation about the virion length axis characterized by a single "cumulative amplitude"  $\lambda$ , which may be compared to the general order parameter  $S$  in Model Free relaxation analyses (Lipari and Szabo, 1982a, Lipari and Szabo, 1982b). Off course, uniaxial rotation about the viral axis is a simplified model to describe the net effects of the various types of constrained and concerted backbone motions that occur inside M13 or TMV. The cumulative amplitude  $\lambda$  may be regarded as a parameter characterizing the pseudo-static motional narrowing of one- and two-dimensional  $^{31}\text{P}$  powder lineshapes caused by fast backbone motions. In the analysis of the 2D-exchange spectra presented in this paper,  $\lambda$  is not treated as a variable fitting parameter, but is fixed to the value previously estimated on the basis of the observed 1D lineshape (Magusin and Hemminga, 1993a). Another simplification is that our model distinguishes between overall diffusion of the virus particles during the mixing time  $t_m$ , and virion diffusion during the evolution time  $t_1$  and acquisition time  $t_2$ . As mentioned under *Theory*, this artificial distinction speeds up the spectral analysis, because various 2D-exchange

spectra can be simulated using a single set of subspectra generated for an *a priori* selected value for the overall diffusion coefficient  $D_o$  during  $t_1$  and  $t_2$ .  $D_o$  has already been determined independently on the basis of  $T_{2e}$  measurements (Magusin and Hemminga, 1993a). *A posteriori*,  $D_o$  and the overall diffusion coefficient extracted from off-diagonal broadening during  $t_m$  will be compared. Despite its relatively simple character, our model still contains quite a number of parameters. In our analysis of 2D-exchange spectra, however,  $\lambda$ ,  $D_o$  and the chemical shift tensor values  $\sigma_{11}$ ,  $\sigma_{22}$  and  $\sigma_{33}$  are treated as constants with values based on previous lineshape and relaxation analysis. As will be discussed, the change of the 2D-exchange spectrum at varying  $t_m$  will be solely interpreted in terms of slow overall rotation of the virus particles about their length axis during  $t_m$ , which for homogeneous diffusion is characterized by the coefficient  $D$  as a single fitting parameter only, and for inhomogeneous diffusion by the central diffusion coefficient  $D_c$  and the distribution width  $W$ .

We have used Eqs. 9 and 10 to calculate 16 subspectra  $I_n^{\pm}(\omega_1, \omega_2 | \Delta\Omega'_n)$ , where  $\Delta\Omega'_n = (0, \Delta\psi_n, 0)$ ,  $\Delta\psi_n$  being equidistant multiples of 0.2 rad between 0.0 and 3.0 rad. For the restriction halfangle  $\lambda$  and the overall diffusion coefficient  $D_o$ , the values 0.75 rad and 50 Hz were first selected in accordance with the outcome from previous analyses of 1D  $^{31}\text{P}$  lineshapes and transversal relaxation (Magusin and Hemminga, 1993a). Using this set of subspectra and assuming a Gaussian distribution of rotation angles  $\Delta\Omega'_n$  typical for homogeneous, uniaxial diffusion (Eq. 6), subspectra combinations according to Eq. 8 can be made that fit well to every experimental exchange spectrum recorded for M13 separately. Spectra recorded for mixing times  $t_m = 0.01, 0.1$  and 1 sec are best simulated for different diffusion coefficients  $D = 15, 5$  and 1.7 Hz, respectively (Fig. 5). However, no  $D$  value is found that produces good fits to the three spectra together. In a first attempt, we tried to reduce the difference among the resulting  $D$  values by introducing extra transversal

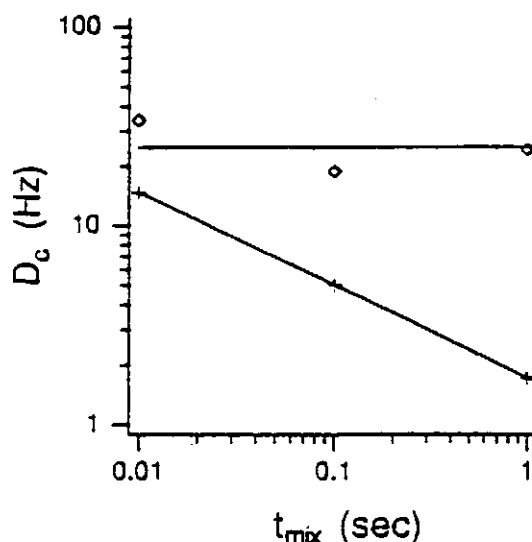


FIGURE 5: Plot of the (central) overall diffusion coefficient estimated from exchange spectra of M13 against  $t_m$ . (+) homogeneous diffusion; (o) a log-Gaussian distribution of diffusion coefficients with  $W = 1.5$  (Eq. 11).

relaxation during  $t_1$  and  $t_2$  into the model. This adds an extra  $t_m$ -independent spectral broadening to simulations, which especially influences the simulated spectra for short mixing times. If, for instance, subspectra are generated for  $D_0 = 400$  Hz instead of  $D_0 = 50$  Hz, the  $t_m$ -independent homogeneous broadening is roughly doubled (see definition of  $T_{2e}$  below Eq. 4). As a result, reduced  $D$  values of 6.9, 3.6 and 1.3 Hz are obtained for  $t_m = 0.01$ , 0.1 and 1 sec, respectively. Indeed, increasing  $D_0$  reduces the  $D$  value resulting from spectral simulation for short  $t_m$  more, than for long  $t_m$  and thereby suppresses the difference among  $D$  values found for different  $t_m$ . However,  $D_0 \geq 400$  Hz would be inconsistent with the diffusion coefficient of 50 Hz found in our previous relaxation analysis (Magusin and Hemminga, 1993a) and would also disagree with the extremely narrow diagonal ridge observed in the exchange spectrum recorded for  $t_m = 10 \mu\text{s}$  (not shown).

Obviously, the simple model employed to analyse 2D-exchange spectra in the above discussion, cannot provide a consistent explanation for the exchange spectra recorded at various mixing times together. To remove this inconsistency, we have tested several model-variants on the basis of some previously expressed, tentative ideas (Magusin and Hemminga, 1993a). For instance, because simulations of the 1D  $^{31}\text{P}$  NMR spectrum of 30% M13 are slightly improved by the assumption that the backbone of M13 DNA consists of 83% immobile and 17% mobile phosphodiester, we have tried both fast- and intermediate-exchange two-component models. Under fast exchange conditions, on the one hand, motional narrowing would cause the contribution by a mobile phosphodiester fraction to the 2D-exchange spectrum to be a narrower intensity pattern close to the diagonal even at long  $t_m$ . Such effect could qualitatively explain why the diagonal ridge observed in M13 spectra recorded with  $t_m = 1$  sec is relatively narrow, as compared to the already quite broad diagonal ridge observed for  $t_m = 0.01$  sec. In the intermediate exchange case, on the other hand, the mobile phosphodiesters undergoing motions in the  $10^4 - 10^5$  Hz frequency range, would contribute a broad, practically  $t_m$ -invariant intensity pattern to the exchange spectrum recorded with  $t_m \geq 10^{-2}$  sec. A broad intensity pattern in the exchange spectrum would lead to an overestimation of the overall diffusion coefficient  $D$ , especially at short  $t_m \approx 10^{-2}$  sec. This could possibly explain the difference between the estimated  $D$  values at various  $t_m$ . We have also checked if 2D-exchange spectra of M13 actually reflect some preferential orientation of the phosphodiesters with respect to the viral axis. An anisotropic distribution of phosphodiester orientations, e.g. such that most  $\sigma_{33}$ -components were parallel to the viral axis, could lead to a narrower intensity pattern at long  $t_m$ , than expected from a random distribution. On the basis of a previous comparison of structural parameters (Magusin and Hemminga, 1993a), a model has been set up, in which 83% phosphodiester is oriented with respect to the viral axis as in B-DNA with respect to the helical axis. Unfortunately, none of the above three model-variants is able to remove the apparent inconsistency between the exchange spectra recorded with various  $t_m$ , or even to

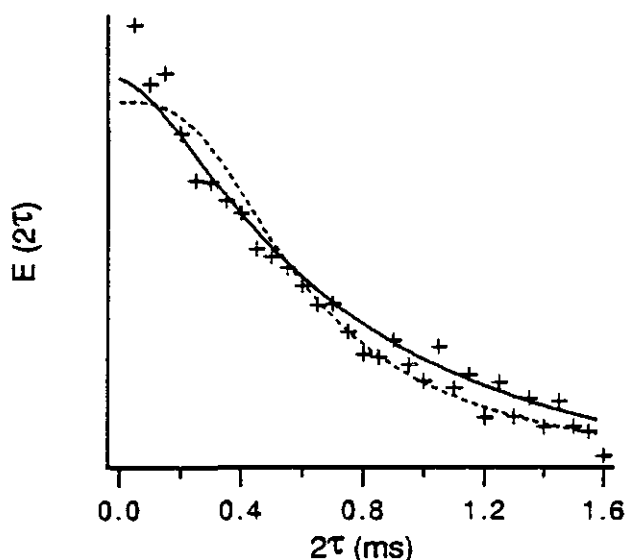


FIGURE 6: Simulation of nonspinning transversal relaxation for a log-Gaussian distribution of diffusion coefficients with  $D_c = 25$  Hz and  $W = 1.5$  (Eq. 11), superimposed on 3-ms exponential relaxation caused by fast nucleic acid backbone motions, as estimated from MAS experiments (see text). The broken line illustrates the previously published simulation for homogeneous overall motion with a diffusion coefficient of 50 Hz (Magusin and Hemminga, 1993a).

produce better simulations for each of the experimental spectra separately. Our previous, tentative assumption that two phosphodiester fractions exist within M13, can neither be justified, nor rejected on the basis of the M13 exchange spectra.

As noticed previously (Magusin and Hemminga, 1993a),  $^{31}\text{P}$  transversal relaxation decays observed for M13 are steeper at short echo times  $2\tau < 0.2$  ms, than the theoretical curves that fit best to the whole set of echoes measured up to  $2\tau = 1.6$  ms (Fig. 6). This could indicate that part of the virions diffuses more rapidly, than expected from the average diffusion coefficient. Such motional inhomogeneity would be characterized by a spread of overall diffusion coefficients. Assuming a log-Gaussian distribution characterized by a central value  $D_c$  and a width parameter  $W$  (Wefing et al., 1988), the spread of rotation angles  $P'(\Delta\Omega' t_m)$  resulting from the overall diffusion of the rod-shaped virions about their length axis can be derived as a function of  $t_m$  (Eq. 11). Using the same sets of subspectra  $I_n^{\pm}(\omega_1, \omega_2 | \Delta\Omega'_n)$  as employed for testing the models discussed above, combinations can be made for different values for  $D_c$  and  $W$  and compared with the experimental spectra. For each of the above discussed models adapted for motional inhomogeneity, a pair of values for  $D_c$  and  $W$  can be obtained which consistently explains the observed M13 spectra recorded with  $t_m = 0.01$ , 0.1 and 1 sec. For instance, using the single component model with  $D_0 = 50$  Hz and  $\lambda = 0.75$  rad, exchange spectra can be simulated for  $D_c = 25$  Hz and  $W = 1.5$  which fit well to the three experimental spectra (Figs. 5 and 7). Most virions in 30% M13 gels thus seem to undergo overall rotational diffusion with coefficients in a range of three decades around 25 Hz, i.e. between 1 and 1000 Hz. An upperlimit of 1000 Hz would still agree with the absence of sideband broadening in the observed MAS spectra (Magusin and Hemminga, 1994). The central

overall diffusion coefficient  $D_c = 25$  Hz estimated from the exchange spectra, is twice as small as the homogeneous overall diffusion coefficient  $D_0 = 50$  Hz determined from transversal relaxation. Because  $T_{2e}$  is inversely proportional to the cube root of the diffusion coefficient, slow overall diffusion seems to be responsible for about  $2^{-1/3} \approx 80\%$  of the observed relaxation. The remaining 20% is indicative for some extra relaxation mechanism with  $T_{2e} \approx 3$  ms at a  $^{31}\text{P}$  resonance frequency of 121.5 MHz. Such value would well agree with the MAS  $T_{2e}$  value of 1.3 ms previously measured at 202.5 MHz for 25% M13, which we ascribed to fast nucleic acid backbone motions (Magusin and Hemminga, 1994). Indeed, if we repeat the previous simulation of the nonspinning transversal relaxation decay while this time taking into account a log-Gaussian distribution with  $W = 1.5$  around  $D = 25$  Hz and extra relaxation with  $T_2 \approx 3$  ms by fast backbone motions, an even better fit is obtained than the previously published simulation (Fig. 6) (Magusin and Hemminga, 1993a). Motional inhomogeneity in gels of M13 is probably caused by the tendency of the bacteriophages to form variously sized aggregates (Day et al., 1988).

The agreement between exchange spectra simulated for  $D_c = 25$  Hz and  $W = 1.5$  and the experimental M13 spectra recorded with various  $t_m$ , is illustrated by the theoretical and experimental  $P_1$  projections,  $P_-$  projections and  $S_+$  sections in Fig. 7.  $P_2$  projections of the experimental spectra are slightly larger than those of the simulated spectra that fit best to the observed 2D spectra as a whole. This could be an experimental artifact caused by the merging of the first two  $^{31}\text{P}$  pulses in the pulse sequence for  $t_1 = 0$  (Fig. 1). The good fit between experimental and simulated spectra indicates that the difference between the

projection spectra and the diagonal spectrum observed for M13 and TMV can mainly be explained by the anisotropy of the transversal relaxation caused by slow overall rotation.  $T_{2e}$  anisotropy could perhaps also explain the fact that the  $^{31}\text{P}$  NMR lineshape of 10% TMV (Cross et al., 1983) seems to be less motionally narrowed than the one observed for 30% TMV observed by us.

The relative shrinking of the  $\sigma_{22}$  discontinuity on the diagonal in 2D-exchange spectra of M13 and TMV with respect to the other two discontinuities for  $t_m > 0.01$  sec, is not well accounted for by our model. We tend to assign this effect to  $^{31}\text{P}$  spindiffusion. Distances between neighbouring phosphodiester in M13 are probably similar to those in TMV, which vary between 5.4 and 7.5 Å (Opella and DiVerdi, 1982; Stubbs and Stauffacher, 1981). Such internuclear distances indicate weak  $^{31}\text{P}$  -  $^{31}\text{P}$  couplings of  $\leq 100$  Hz. Spindiffusion effects would thus indeed be expected in exchange spectra for  $t_m > 0.01$  sec. Effective homonuclear coherence transfer, however, would be limited to neighbouring  $^{31}\text{P}$  nuclei with chemical shifts that differ less than the coupling size, thus 1 ppm at 121.5 MHz, unless motions in the  $10^3$ - $10^4$  Hz range would be present, bridging chemical shift differences across the  $^{31}\text{P}$  powder resonance line. A narrow shift matching condition would be consistent with the narrow ridge observed in exchange spectra of TMV. The shrinking of the  $\sigma_{22}$  discontinuity is most easily explained in a qualitative manner by use of our M13 model, in which the shift tensor orientations of neighbouring  $^{31}\text{P}$  nuclei are assumed to be completely uncorrelated. As illustrated by the powder lineshape itself with its maximum at  $\sigma_{22}$ , any  $^{31}\text{P}$  spin within M13 would have relatively many  $^{31}\text{P}$  spins with a chemical shift close to  $\sigma_{22}$  around itself. Because the effectiveness of spindiffusion between  $^{31}\text{P}$  spins depends upon their chemical shift difference,  $^{31}\text{P}$  spins with a chemical shift close to  $\sigma_{22}$  relax faster than other spins. This would explain the observed shrinking of the  $\sigma_{22}$  discontinuity on the diagonal in exchange spectra of M13. For TMV, a similar explanation would have to include the regular geometry of the encapsulated RNA molecule, which causes the chemical shift tensors of neighbouring phosphodiester not to be randomly oriented with respect to each other. Because motions in the  $10^3$ - $10^4$  Hz range seem to be largely absent in concentrated M13 gels (Magusin and Hemminga, 1994), spindiffusion effects in exchange spectra of M13 are probably concentrated on the diagonal, like for TMV. Therefore, the various observed off-diagonal intensity patterns probably reflect the pure effect of slow overall motion of the rod-shaped viruses only.

## CONCLUSION

2D-exchange  $^{31}\text{P}$  NMR spectroscopy is a powerful technique to study the slow overall motion of the rod-shaped viruses M13 and TMV. Spectra of 30% TMV recorded with  $t_m \leq 1$  sec do not show any off-diagonal broadening, indicating that TMV particles in concentrated gels are extremely immobile, even at a timescale of seconds. For 30% M13, a log-Gaussian distribution around 25 Hz of rotational diffusion coefficients mainly spread between 1 and  $10^3$  Hz must be introduced to reproduce the 2D-exchange NMR spectra recorded at various mixing

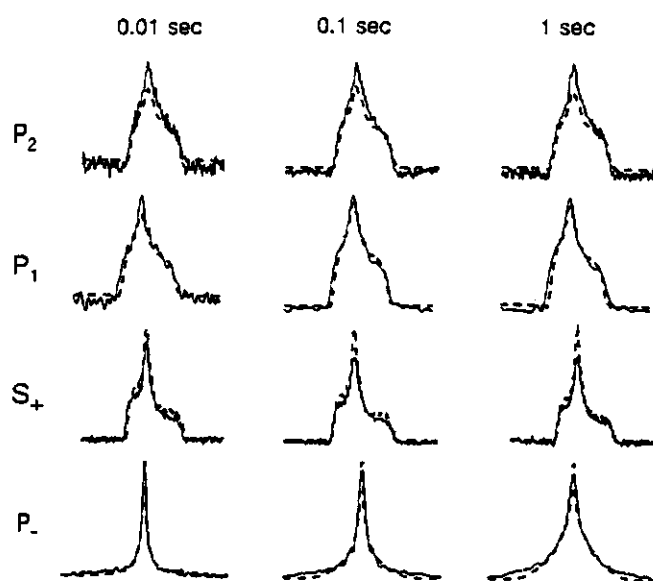


FIGURE 7: Comparison of theoretical (—) and experimental (---) 2D-exchange spectra of M13 for various  $t_m$ , reflected by projection and diagonal spectra (see Fig. 2). Theoretical spectra have been calculated for a distribution of diffusion coefficients with  $D_c = 25$  Hz and  $W = 1.5$  (Eq. 11) and fitted to the experimental 2D-exchange spectra as a whole.



times in a consistent way. Taking this distribution and a minor relaxation contribution caused by fast backbone motion into account, an even better fit to the nonspinning transversal relaxation decay is obtained, than published previously for homogeneous diffusion (Magusin and Hemminga, 1993a). The shrinking of the  $\sigma_{22}$  discontinuity on the diagonal with respect to the lineshape as a whole at  $t_m \geq 0.1$  sec, cannot be explained by slow overall motion, but seems to be caused by spindiffusion between  $^{31}\text{P}$  nuclei with chemical shifts that differ less than 1 ppm.

This paper is the last one in a series of four, in which models have been developed and tested to explain the results of various  $^{31}\text{P}$  NMR experiments observed for intact M13 and TMV virus particles in concentrated gels. At this stage, it is worthwhile to present a brief overview to show advantages and limitations of the specific NMR techniques employed by us, for investigating large nucleoprotein complexes, such as M13 and TMV, in general (Tab. 1). In these systems,  $^{31}\text{P}$  nuclei represent natural NMR labels for studying structural and dynamic properties of the nucleic acid backbone selectively, even when the complex mainly consists of proteins. High-power  $^1\text{H}$ -decoupled 1D  $^{31}\text{P}$  NMR spectra observed for nonspinning samples of these complexes contain a single broad resonance line reflecting the average  $^{31}\text{P}$  chemical shift anisotropy (CSA) typical for phosphodiester in DNA or RNA. The strong CSA-broadening, however, tends to mask the small differences among the phosphodiesters of the complexed nucleic acid (Magusin and Hemminga, 1993a). Such phosphodiester inhomogeneity, indicating e.g. inequivalence among binding sites, is best studied using  $^{31}\text{P}$  MAS NMR spectroscopy (Magusin and Hemminga, 1994).  $^{31}\text{P}$  MAS NMR spectra of TMV show two resolved sideband patterns with an overall intensity ratio of approximately 2, reflecting the three types of phosphodiesters in TMV. In contrast, MAS NMR spectra of M13, only contain a single, relatively broad centerband flanked by sidebands, indicating that a continuous distribution of phosphodiester conformations exists within the phage. Nucleic acid backbone motions perhaps underly the observed decrease of inhomogeneous linewidth at increasing temperature and hydration by partly averaging the conformational differences.

$^{31}\text{P}$  NMR spectroscopy is also a powerful tool to study the mobility of the complexed nucleic acid in a broad frequency range. For the viruses M13 and TMV studied by us, the observed motional narrowing of the  $^{31}\text{P}$  NMR lineshapes is indicative for restricted motion with frequencies in the order of the static linewidth or larger ( $\geq 10^4$  Hz). In contrast,  $^{31}\text{P}$  transversal relaxation measured for nonspinning M13 at various temperatures and hydration percentages, indicates motion in the slow or intermediate frequency region. We have shown by simulation that simple models, such as isotropic and rigid-rod diffusion, cannot reproduce the experimental data. Instead, a consistent description is offered by a combined diffusion model, in which the lineshape is dominated by fast internal DNA motions and transversal relaxation reflects slow overall rotation of the virions about their length axis. The presence of phosphodiester motions with frequencies  $\geq 10^5$  Hz is confirmed by the fact that sideband

intensities in MAS spectra of dilute M13 gels seem to be affected by motions without the sidebands being broadened (Magusin and Hemminga, 1994). The presence of slow motion is confirmed by the fact that  $^{31}\text{P}$  transversal relaxation is strongly suppressed by MAS. From the spinning-rate dependent part of transversal relaxation, overall diffusion coefficients can be extracted in perfect agreement with those obtained from transversal relaxation under nonspinning conditions. The part of transversal relaxation which does not depend on the spinning-rate, is assigned to the same phosphodiester motions which also cause the motional narrowing of the  $^{31}\text{P}$  resonance line.

If the nucleic acid backbone is sufficiently immobilized within a nucleoprotein complex, detailed information about motion of the complex in the sub-kHz range can be obtained by use of 2D-exchange  $^{31}\text{P}$  NMR spectroscopy. Comparison of the off-diagonal intensity patterns in 2D-exchange spectra recorded with various mixing times provides insight in the distribution of motional amplitudes and correlation times involved. 2D-exchange spectra of TMV demonstrate that the virus is less mobile than estimated from transversal relaxation alone (see *Discussion*), indicating that overall motion causes only part of the observed nonspinning  $T_{2e}$ -relaxation. Exchange spectra of M13 obtained for various mixing times suggest that overall diffusion of the virus particles in the sticky gels is inhomogeneous.

Table 1: sorts of information about phosphodiester structure, nucleic acid backbone motion and overall virion motion obtained in our study of M13 and TMV illustrating the use of different  $^{31}\text{P}$  NMR techniques for investigating nucleoprotein complexes, in general. For the rod-shaped M13 and TMV viruses, the observed motional effects on  $^{31}\text{P}$  NMR spectra and transversal relaxation can be explained by a combination of slow rotational diffusion of the virions about their length axis and fast restricted motions of the encapsulated nucleic acid molecules. In contrast to the three distinct types of phosphodiesters in TMV, a continuous distribution of phosphodiester conformations seems to exist in M13.

type of spectroscopy	object of analysis	phosphodiester structure	nucleic acid backbone motion	virion overall motion
nonspinning 1D $^{31}\text{P}$ NMR spectroscopy*	lineshape transversal relaxation	average conformation	cumulative amplitude	average diffusion coefficient
magic angle spinning 1D $^{31}\text{P}$ NMR spectroscopy†	centerband lineshape sideband intensities transversal relaxation	distribution of conformations	conformational fluctuation cumulative amplitude effective frequency	average diffusion coefficient
nonspinning 2D-exchange $^{31}\text{P}$ NMR spectroscopy†	lineshape analysis			distribution of diffusion coefficients

\* Magusin and Hemminga, 1993a

† Magusin and Hemminga, 1994

† this paper

## Acknowledgements

This research was supported by the Netherlands Foundation of Biophysics with financial aid of the Netherlands Organization for Scientific Research (NWO). We are grateful to Ruud Spruijt for isolation of M13 and TMV, Jan Jaap ter Horst for experimental assistance and to Klaus Schmidt-Rohr and Arno Kentgens for helpful discussions.

## REFERENCES

- Cross, T. A., S. J. Opella, G. Stubbs, and D. L. D. Caspar. 1983. Phosphorus-31 nuclear magnetic resonance of the RNA in tobacco mosaic virus. *J. Mol. Biol.* 170:1037-1043.
- Day, L. A., C. J. Marzec, S. A. Reisberg, and A. Casadevall. 1988. DNA packing in filamentous bacteriophages. *Ann. Rev. Biophys. Chem.* 17:509-539.
- Edmonds, A. R. 1960. *Angular Momentum in Quantum Mechanics*. Princeton University Press. Princeton, New Jersey. 146 pp.
- Fenske, D. B., and H. C. Jarrell. 1991. Phosphorus-31 two-dimensional solid-state exchange NMR. Application to model membrane and biological systems. *Biophys. J.* 59:55-69.
- Haeblerlen, U. 1976. *High Resolution NMR in Solids: Selective Averaging*. Academic Press. New York. 208 pp.
- Herzfeld, J., and A. E. Berger. 1980. Sideband intensities in NMR spectra of samples spinning at the magic angle. *J. Chem. Phys.* 73:6021-6030.
- Kimich, R., and E. Fischer. 1994. One- and two-dimensional pulse sequences for diffusion experiments in the fringe field of superconducting magnets. *J. Magn. Res. Ser. A.* 106:229-235.
- Lipari, G., and A. Szabo. 1982a. Model-Free Approach to the Interpretation of Nuclear Magnetic Resonance Relaxation in Macromolecules. 1. Theory and Range of Validity. *J. Am. Chem. Soc.* 104:4546-4559.
- Lipari, G., and A. Szabo. 1982b. Model-Free Approach to the Interpretation of Nuclear Magnetic Resonance Relaxation in Macromolecules. 2. Analysis of Experimental Results. *J. Am. Chem. Soc.* 104:4559-4570.
- Magusin, P. C. M. M., and M. A. Hemminga. 1993a. Analysis of  $^{31}\text{P}$  NMR lineshapes and transversal relaxation of bacteriophage M13 and Tobacco Mosaic Virus. *Biophys. J.* 1861-1868.
- Magusin, P. C. M. M., and M. A. Hemminga. 1993b. A theoretical study of rotational diffusion models for rod-shaped viruses: the influence of motion on  $^{31}\text{P}$  NMR lineshapes and transversal relaxation. *Biophys. J.* 1851-1860.
- Magusin, P. C. M. M., and M. A. Hemminga. 1994. Analysis of  $^{31}\text{P}$  MAS NMR lineshapes and transversal relaxation of bacteriophage M13 and Tobacco Mosaic Virus. *Biophys. J.* 66:1197-1208.
- Marion, D., and K. Wüthrich. 1983. Application of phase sensitive two-dimensional correlated spectroscopy (COSY) for measurements of proton-proton spin-spin coupling constants in proteins. *Biochem. Biophys. Res. Commun.* 113:967-974.
- Opella, S. J., and J. A. DiVerdi. 1982. Properties of the phosphodiester backbone of duplex DNA and filamentous bacteriophage DNA. In *Biochemical Structure Determination by NMR*. A. A. Bothner-By, J. Gluckson, and B. D. Sykes, Eds. Marcel Dekker, New York. 149-168.
- Schmidt-Rohr, K., and H. W. Spiess. 1991. Nature of nonexponential loss of correlation above the glass transition investigated by multi-dimensional NMR. *Phys. Rev. Lett.* 66:3020-3023.
- Slichter, C. P. 1978. *Principles of Magnetic Resonance*. Springer-Verlag. Berlin. 397 pp.
- Stubbs, G., and C. Stauffacher. 1981. Structure of the RNA in tobacco mosaic virus. *J. Mol. Biol.* 152:387-396.
- Tomasselli, M., B. H. Meier, P. Robyr, U. W. Suter, and R. R. Ernst. 1993. Direct measurement of xenon exchange between gas and liquid phase by 2D NMR. *Chem. Phys. Lett.* 214:1-4.
- Wefing, S., S. Kaufmann, and H. W. Spiess. 1988. Two-dimensional exchange NMR of powder samples. II. The dynamic evolution of two-time distribution functions. *J. Chem. Phys.* 89:1234-1244.
- Wefing, S., and H. W. Spiess. 1988. Two-dimensional exchange NMR of powder samples. I. Two-time distribution functions. *J. Chem. Phys.* 89:1219-1233.

## **APPENDIX**

### **Naming of the binding sites in TMV**

## Naming of the binding sites in TMV

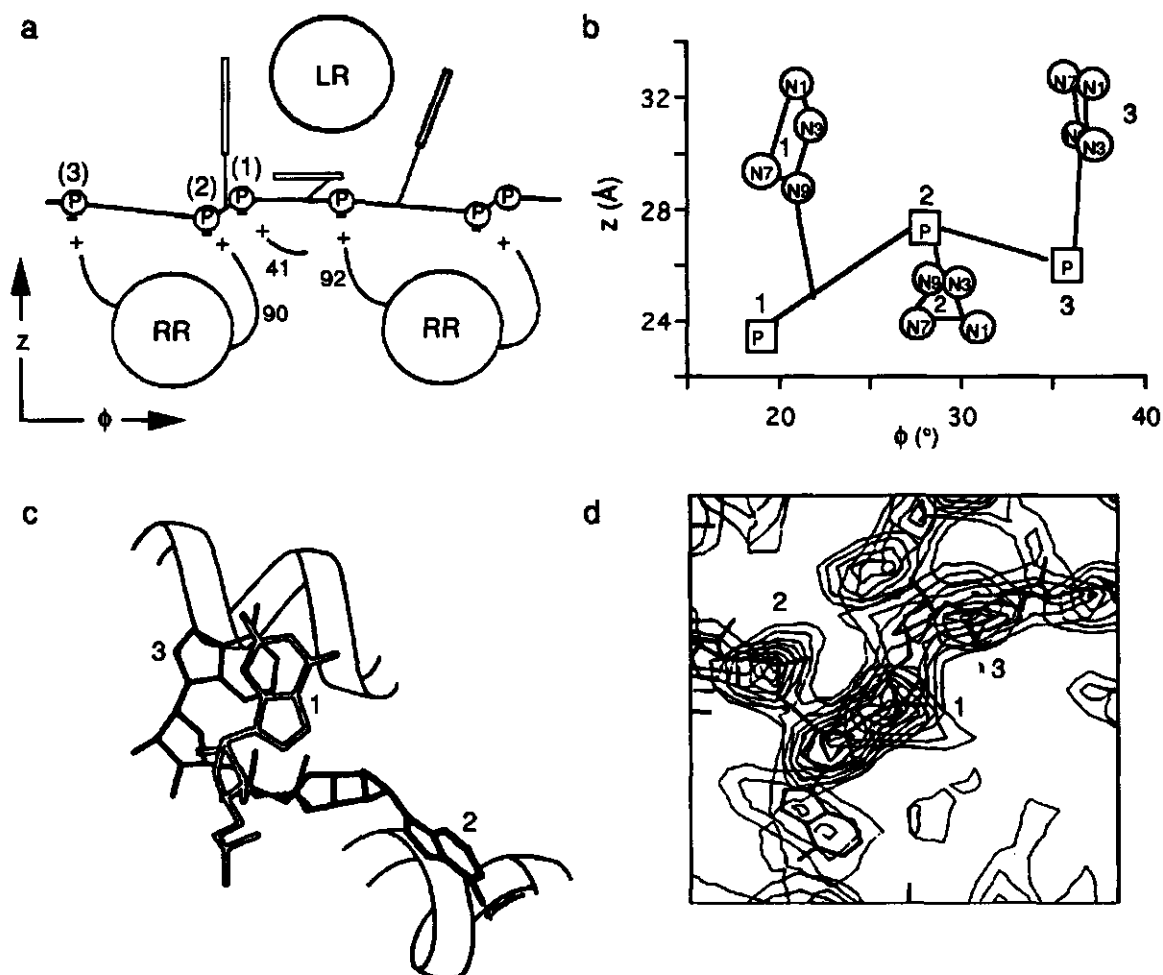


FIGURE 1: adapted figures from (Stubbs et al., 1977) (a), (Namba et al., 1989) (c) and (Cross et al., 1983) (d), and figure based on model coordinates (Stubbs and Stauffacher, 1981) (b), illustrating positions of the phosphates and the bases along the RNA molecule (see text)

Since 1977, a number of publications have appeared, which deal with the structure of the RNA molecule in TMV (Stubbs et al., 1977; Stubbs and Stauffacher, 1981; Cross et al., 1983; Namba et al., 1989). In comparing these papers, we found that the names of the nucleotides are not consistently used. This has already been noted in Chapters 3 and 4 (Magusin and Hemminga, 1993; Magusin and Hemminga 1994). The purpose of this appendix is to exemplify this in more detail.

Fig. 1a is part of a figure published in 1977 (Stubbs et al., 1977) and illustrates the position of the phosphates and the bases along a radius. Because  $\phi$  increases from left to right, the figure may be regarded as a schematic view from a point outside the virus towards the central core. Two bases are sticking up in  $z$ -direction, while the third is pointing away from the central core towards the reader. In this publication, the phosphate near Arg41 is

defined as phosphate 1, while Arg90 and Arg92 are close to the phosphates labeled 2 and 3, respectively. Thus, labeling occurs in the direction of *decreasing*  $\phi$ .

In 1981, Stubbs and Stauffacher published a table with model coordinates for a hypothetical poly-A RNA molecule encapsulated in TMV, based on x-ray diffraction data (Stubbs and Stauffacher, 1981). Using their coordinates, we have constructed Fig. 1b, which shows, for the three binding sites, the positions of the phosphorus atoms and the nitrogens at positions 1, 3, 7 and 9 in the bases. The positions of the phosphates and the orientations of the base planes in Fig. 1b roughly correspond to those in Fig. 1a. However, the phosphates in Fig. 1b are labeled in the direction of *increasing*  $\phi$ . As compared to Fig. 1a, the labels of phosphates 1 and 2 have been interchanged. In this thesis, we standardly use the phosphate labeling illustrated in Fig. 1b. In terms of

this standard phosphate labeling, Fig. 1a thus suggests that Arg90 and Arg92 form salt-bridges with the phosphates 1 and 3, respectively.

Fig. 1c is part of a figure presented by Namba et al. in 1989. The viral axis is vertical, to the left of the figure. Bases 1 and 3 are thus sticking up and base 2 is pointing outward, so that the figure and the base labeling are consistent with Fig. 1b. It seems reasonable to assume therefore, that phosphate labeling is also the same. In contrast to Stubbs et al. in 1977 (Fig. 1a), Namba et al. suggest that Arg90 and Arg92 closely interact with phosphates 1 and 2, respectively, and thus tacitly introduce a change in one of the the salt-bridges.

As indicated in Fig. 1d, yet another phosphate labeling is used by Cross et al. in 1983, who, apart from the phosphate labels, copied their figure from the paper by Stubbs and Stauffacher (Stubbs and Stauffacher, 1981). Fig. 1d represents a view down the z-axis, whereby bases 1 and 3 have been omitted because they protrude out of the plane, towards the reader (Stubbs and Stauffacher, 1981). Note that phosphate labeling occurs in the direction of decreasing  $\phi$ , as opposed to the labeling in the articles by Stubbs and Stauffacher in 1981 (Fig. 1b) and Namba et al. in 1989 (Fig. 1c). Phosphates labeled 1, 2 and 3 in Fig. 1d correspond to the phosphates 3, 2, 1 in Fig. 1b, respectively.

Cross et al. have further labeled the three resonance lines in the  $^{31}\text{P}$  NMR spectrum of oriented TMV solution, from left to right in the spectrum, as A, C, B, which they tentatively assigned to sites 1, 3 and 2, respectively. We have repeated their  $^{31}\text{P}$  chemical-shift calculation on the basis of the model-coordinates presented by Stubbs and Stauffacher in 1981. Based on this calculation, we have alternatively assigned the resonance lines A, C and B to phosphates 1, 2 and 3, respectively, in Chapter 3. Table 1 summarizes the relations between the different ways of nucleotide labeling in the literature.

TABLE 1: Labeling of the three binding sites in TMV in different publications

* , †	‡	§	§
1	2	3	A
2	1	2	C
3	3	1	B

\* Stubbs and Stauffacher, 1981

† this thesis

‡ Stubbs et al., 1977

§ Cross et al., 1983

## REFERENCES

- Cross, T. A., S. J. Opella, G. Stubbs, and D. L. D. Caspar. 1983. Phosphorus-31 nuclear magnetic resonance of the RNA in tobacco mosaic virus. *J. Mol. Biol.* 170:1037-1043.
- Magusin, P. C. M. M., and M. A. Hemminga. 1993. Analysis of  $^{31}\text{P}$  NMR lineshapes and transversal relaxation of bacteriophage M13 and Tobacco Mosaic Virus. *Biophys. J.* 1861-1868.
- Magusin, P. C. M. M., and M. A. Hemminga. 1994. Analysis of  $^{31}\text{P}$  MAS NMR lineshapes and transversal relaxation of bacteriophage M13 and Tobacco Mosaic Virus. *Biophys. J.* 66:1197-1208.
- Namba, K., R. Pattanayek, and G. Stubbs. 1989. Visualization of protein-nucleic acid interactions in a virus. Refined structure of intact tobacco mosaic virus at 2.9 Å resolution by x-ray fiber diffraction. *J. Mol. Biol.* 208:307-325.
- Stubbs, G., and C. Stauffacher. 1981. Structure of the RNA in tobacco mosaic virus. *J. Mol. Biol.* 152:387-396.
- Stubbs, G., S. Warren, and K. Holmes. 1977. Structure of RNA and RNA binding site in tobacco mosaic virus from 4-Å map calculated from x-ray fiber diagrams. *Nature.* 267:216-221.

## Summary

In this thesis, the results of various  $^{31}\text{P}$  NMR experiments observed for intact virus particles of bacteriophage M13 and Tobacco Mosaic Virus (TMV), are presented. To explain the results in a consistent way, models are developed and tested.  $^{31}\text{P}$  nuclei in M13 and TMV are only present in the phosphodiester of the encapsulated nucleic acid molecule. Therefore,  $^{31}\text{P}$  NMR spectroscopy reveals structural and dynamic properties of the nucleic acid backbone selectively without isotope labeling, even though the virus particles largely consist of coat proteins. In the Introduction (Chapter 1), it is discussed that the  $^{31}\text{P}$  chemical shift is sensitive to local nucleic acid backbone geometry and that the  $^{31}\text{P}$  NMR relaxation is dependent on the isolated and collective backbone motions. As shown in Chapter 3, high-power  $^1\text{H}$ -decoupled one-dimensional  $^{31}\text{P}$  NMR spectra observed for nonspinning samples of M13 and TMV contain a single, broad line dominated by the  $^{31}\text{P}$  chemical shift anisotropy (CSA), which masks any structural inequivalence among the encapsulated phosphodiesters. However, these spectra do contain interesting mobility information. On the one hand, they show that the nucleic acid molecule in each of the viruses is strongly immobilized in comparison to free nucleic acids in solution, as a result of interactions with the protein coat. On the other hand, the  $^{31}\text{P}$  resonance lineshapes show clear signs of motional narrowing, which is indicative for (restricted) motion with frequencies in the order of the static linewidth or larger ( $\geq 10^4$  Hz). In contrast, the nonspinning  $^{31}\text{P}$  transversal relaxation measured for M13 indicates motion in the slow or intermediate frequency region as compared to the static linewidth ( $\leq 10^4$  Hz), because  $T_{2e}$  becomes shorter as the viscosity of the gel decreases.

To analyze the results in a more quantitative manner, three different rotational diffusion models for the phosphorus motion are developed in Chapter 2. These models are first tested at a theoretical level to get a feeling for their accuracy and to check their correspondence with standard theories under appropriate limiting conditions. Simulations show that a clear distinction between the effect of motional amplitude and frequency cannot be made within experimental error on the basis of one-dimensional spectra or transversal relaxation alone. However, these parameters can be extracted from the combined data. For fast motions, the transversal  $^{31}\text{P}$  NMR relaxation predicted by our models is consistent with standard Redfield relaxation theory. The relaxation effects caused by ultra-slow rotational diffusion closely resemble the effects of *translational* diffusion of water protons in an inhomogeneous magnetic-field gradient. It is discussed in Chapter 3, that simple models, like isotropic and rigid-rod diffusion cannot reproduce the experimental data. Instead, a consistent description is offered by a combined diffusion model, in which the  $^{31}\text{P}$  NMR lineshape is dominated by

fast internal DNA or RNA motions, and transversal relaxation reflects slow overall rotation of the rod-shaped virions about their length axis.

To obtain more specific structural information, magic angle spinning (MAS) NMR spectroscopy is employed, which breaks up the broad  $^{31}\text{P}$  NMR lineshape into a sharp centerband at the isotropic chemical shift position flanked by rotational sidebands (Chapter 4). MAS  $^{31}\text{P}$  NMR spectra of TMV show two resolved sideband patterns with an overall intensity ratio of approximately 2, which are assigned to the three types of phosphodiesters in TMV on the basis of RO-P-OR' bondangles and supposed arginine bonding effects. In contrast, MAS  $^{31}\text{P}$  NMR spectra of M13, only contain a single, relatively broad centerband flanked by sidebands, indicating that a continuous distribution of phosphodiester conformations, rather than a few distinguishable, exists within the phage. The observed decrease of inhomogeneous linewidth at increasing temperature and hydration could perhaps be caused by some sort of "conformational averaging" as a consequence of nucleic acid backbone motion. This is illustrated by use of a simple model, which shows the lineshape effects caused by fast restricted fluctuation of the dihedral angles between the POC and the OCH planes on both sides of the  $^{31}\text{P}$  nucleus in the nucleic acid backbone. The presence of internal phosphodiester motions with frequencies  $\geq 10^5$  Hz, as concluded from the motional narrowing of nonspinning  $^{31}\text{P}$  NMR lineshapes in Chapter 3, is confirmed by the deviation of sideband intensities in MAS  $^{31}\text{P}$  NMR spectra of dilute M13 gels from the theoretical values for solid powders. No dramatic broadening of the sidebands is observed, indicating that motions with frequencies in the order of the spinning rates applied ( $10^3$  Hz) are absent. Backbone motions also seem to be the main cause of transversal relaxation measured at spinning rates of 4 kHz or higher. At spinning rates below 2 kHz, transversal relaxation is significantly faster. This dependence of  $T_{2e}$  on the spinning rate is assigned to slow, overall rotation of the rod-shaped M13 phage about its length axis.

Both nonspinning and MAS  $^{31}\text{P}$  NMR spectra are analyzed in Chapter 2 and 3, respectively, to study possible mobility differences among the phosphodiesters in M13 and TMV. The nonspinning lineshape of 30% TMV is best simulated, if it is assumed that one of the three binding sites is more mobile than the other two. It is shown that this is compatible with the reduced CSA reflected by the major sideband pattern in MAS spectra of TMV as compared to the minor one. A large mobility of one of the three binding sites would agree with structural models based on x-ray diffraction data, in which two of the binding sites are interacting with arginine residues, whereas no arginine is close to the third one. Two-component analysis of the nonspinning  $^{31}\text{P}$  NMR data of 30% M13 suggests that the encapsulated DNA molecule

perhaps contains 83% immobile and 17% mobile phosphodiester. This would shed new light on the nonintegral ratio 2.4:1 between the number of nucleotides and protein coat subunits in the phage: if 83% of the viral DNA is less mobile, the binding of the DNA molecule to the protein coat would actually occur at the integral ratio of two nucleotides per protein subunit. However, MAS NMR spectra provide no additional evidence for such a two-component model.

Finally, in Chapter 5, the slow overall motion of M13 and TMV is investigated using 2D-exchange  $^{31}\text{P}$  NMR spectroscopy. 2D-exchange  $^{31}\text{P}$  NMR spectra recorded for TMV with mixing times  $t_m \leq 1$  sec do not show any off-diagonal broadening indicating that the value of 3 Hz for the overall motion of TMV determined in Chapter 3 from nonspinning transversal relaxation, is an overestimation. For 30% M13, a log-Gaussian distribution around 25 Hz

of coefficients mainly spread between 1 and  $10^3$  Hz must be introduced to reproduce the 2D-exchange spectra recorded at various mixing times in a consistent way. Motional inhomogeneity in gels of M13 is probably caused by the tendency of the bacteriophages in solutions to form variously sized aggregates. Taking the same coefficient distribution and a minor relaxation contribution caused by fast backbone motion into account, nonspinning transversal relaxation can even be better simulated for inhomogeneous overall motion, than it was done for homogeneous motion in Chapter 3. The shrinking of the  $\sigma_{22}$ -discontinuity on the diagonal with respect to the lineshape as a whole for  $t_m \geq 0.1$  sec, cannot be explained by slow overall motion, but seems to be caused by restricted spindiffusion between  $^{31}\text{P}$  nuclei with chemical shifts that differ less than 1 ppm.

## Samenvatting

Dit proefschrift handelt over de met behulp van fosforkernspinresonantie ( $^{31}\text{P}$  NMR) spectroscopie verkregen resultaten voor intacte virusdeeltjes van bacteriofaag M13 en tabaksmozaïekvirus (TMV). Om deze resultaten consistent te kunnen verklaren, zijn er in dit proefschrift verschillende modellen opgezet en uitgetest. Fosforkernen in M13 en TMV komen slechts voor in de fosfodiester groepen van het DNA of RNA, dat de beide virussen respectievelijk bevatten. Daardoor verschaft  $^{31}\text{P}$  NMR-spectroscopie selectief informatie over de structuur en beweging van de in M13 en TMV ingekapselde nucleïnezuren, hoewel deze virussen, qua gewicht, voor het grootste deel uit eiwitten bestaan. In de Algemene Introductie (hoofdstuk 1) wordt erop gewezen, dat de  $^{31}\text{P}$  chemische verschuiving gevoelig is voor de locale structuur in het nucleïnezuur-molecuul, en dat de  $^{31}\text{P}$  NMR-relaxatie afhangt van locale en collectieve bewegingen in het nucleïnezuur. Zoals aangetoond in hoofdstuk 3, komt er in proton-ontkoppelde  $^{31}\text{P}$  NMR-spectra van stilstaande M13- en TMV-gels slechts één enkele brede resonantielijns voor, die gedomineerd wordt door de richtingsafhankelijkheid van de chemische verschuiving. Deze chemische-verschuivingsanisotropie maskeert eventuele structurele verschillen tussen de fosfodiesteren van de ingekapselde nucleïnezuren. Desalniettemin, bevatten deze spectra interessante bewegingsinformatie. Enerzijds, laten ze zien dat het nucleïnezuurmolecuul in elk van de twee virussen weinig beweeglijk is, althans vergeleken met vrije, ongebonden nucleïnezuren in verdunde oplossingen. Anderzijds, vertonen de  $^{31}\text{P}$  NMR lijnen toch duidelijke sporen van beperkte, maar snelle beweging. In tegenstelling tot de  $^{31}\text{P}$  NMR-lijnen, duiden de uitkomsten van  $^{31}\text{P}$  NMR relaxatie-metingen juist op de aanwezigheid van *langzame* beweging: de gemeten transversale relaxatietijd ( $T_{2e}$ ) wordt immers korter naarmate de beweeglijkheid in de gels toeneemt.

Voor een meer kwantitatieve analyse van deze resultaten, worden in hoofdstuk 2 drie rotatie-diffusie modellen ontwikkeld voor mogelijke bewegingen van de fosforkernen. Met behulp van deze modellen zijn eerst uitgebreid simulaties verricht, om een gevoel te krijgen voor hun nauwkeurigheid en om, in bepaalde limietgevallen, hun overeenstemming met elders gepubliceerde theorieën te controleren. Simulaties brengen aan het licht, dat op grond van eendimensionale  $^{31}\text{P}$  NMR-spectra, of transversale relaxatie alléén, geen duidelijk onderscheid gemaakt kan worden tussen effecten veroorzaakt door de grootte, danwel de snelheid van de beweging. Uit de combinatie van beide gegevens kunnen deze parameters echter wél worden afgeleid. Voor snelle bewegingen, stemmen de ontwikkelde modellen overeen met de algemene relaxatietheorie van Redfield. Voor langzame bewegingen, lijken de effecten van rotationele diffusie op  $^{31}\text{P}$  NMR-relaxatie precies op proton-relaxatie veroorzaakt door translationele diffusie van water in een inhomogene

veldgradiënt. Zoals besproken in hoofdstuk 3, kunnen de meest eenvoudige modellen, zoals langzame, isotrope beweging van het nucleïnezuur of uniaxiale beweging van de staafvormige virusdeeltjes om hun lengteas, de experimentele resultaten niet afdoende verklaren. Een consistente verklaring wordt geboden door een gecombineerd diffusie model, waarin de  $^{31}\text{P}$  NMR-lijnvorm vooral door snelle, interne nucleïnezuurbewegingen wordt beïnvloed, terwijl  $T_{2e}$ -relaxatie vooral veroorzaakt wordt door de langzame beweging van de virusdeeltjes als geheel om hun lengteas.

Om meer inzicht te krijgen in structuur-verschillen tussen de verschillende fosfodiesteren in de ingekapselde nucleïnezuren, is gebruik gemaakt van een techniek die in het Engels "magic angle spinning" (MAS) genoemd wordt. Bij deze techniek roteert men het te meten materiaal in de spectrometer onder een bepaalde hoek met het magneetveld, de "magische hoek" (in een kubus gelijk aan die tussen de lichaamsdiagonaal en een ribbe). MAS middelt de anisotropie van de chemische verschuiving (gedeeltelijk) uit, hetgeen leidt tot een opsplitsing van de brede  $^{31}\text{P}$  NMR-lijnvorm in een centrale resonantie band omgeven door een aantal gelijkvormige zijbanden (hoofdstuk 4). MAS  $^{31}\text{P}$  NMR-spectra van TMV vertonen twee onderscheiden zijbandpatronen die zich, qua intensiteit, verhouden als ongeveer 2:1. In hoofdstuk 4 worden deze twee zijbandpatronen op basis van RO-P-OR' bindingshoeken en veronderstelde arginine-bindingseffecten toegekend aan de drie fosfodiester types in TMV. In tegenstelling tot bij TMV, vertonen MAS  $^{31}\text{P}$  NMR-spectra van M13 slechts een enkele, relatief brede centrale resonantie-lijn met een bij benadering Gaussische vorm. Waarschijnlijk komen er in M13 geen duidelijk te onderscheiden fosfodiester types voor, maar is er daarentegen sprake van een continue distributie van allerlei fosfodiesterconformaties binnen een bepaalde conformatie ruimte. Een soort "conformationele uitmiddeling", als gevolg van nucleïnezuurbewegingen, zou mogelijk ten grondslag kunnen liggen aan de waargenomen afname van de inhomogene lijnbreedte bij toenemende temperatuur en watergehalte. Dit wordt aannemelijk gemaakt met behulp van een eenvoudig model dat het effect van snelle fluctuatie van twee torsiehoeken aan weerszijden van de fosfodiester groep in de het nucleïnezuurmolecuul laat zien. De aanwezigheid van snelle fosfodiesterbewegingen, waartoe in hoofdstuk 3 op grond van de  $^{31}\text{P}$  NMR-spectra van stilstaande virus gels geconcludeerd wordt, wordt bevestigd door de geconstateerde afwijkingen tussen de zijband intensiteiten in MAS  $^{31}\text{P}$  NMR-spectra van verdunde M13 gels en de theoretisch af te leiden intensiteiten voor rigide poedervormige materialen. Dramatische lijnbreedte effecten zijn niet waargenomen, wat erop duidt dat fosforbewegingen met frekwenties in de orde van de gehanteerde rotatie frekwenties ( $10^3$  Hz) in M13 en TMV ontbreken. Snelle nucleïnezuurbewegingen



zijn waarschijnlijk ook verantwoordelijk voor de transversale relaxatie die bij rotatie frekwenties van 4 kHz en hoger gemeten wordt. Bij rotatie frekwenties onder de 2 kHz, is transversale relaxatie significant sneller. Deze afhankelijkheid van de transversale relaxatie van de rotatie frekwentie duidt op de aanwezigheid van langzame bewegingen van M13 virusdeeltjes als geheel, om hun lengteas.

$^{31}\text{P}$  NMR-spectra van zowel stilstaande, als roterende gels van M13 en TMV zijn in, respectievelijk, hoofdstuk 2 en 3 nader geanalyseerd om eventuele onderlinge beweeglijkheidsverschillen tussen de fosfodiësters van de ingekapselde nucleïnezuuren vast te stellen. De beste simulatie voor de waargenomen  $^{31}\text{P}$  NMR-lijnvorm van een stilstaande TMV-gel wordt bereikt, indien wordt aangenomen dat één van de drie types fosfodiësters in TMV beweeglijker is dan de andere twee. Een dergelijke interpretatie biedt ook een verklaring voor de verschillen tussen de twee zijband patronen in MAS  $^{31}\text{P}$  NMR-spectra van TMV. Een grotere beweeglijkheid van één van drie fosfodiëstertypes zou overeenstemmen met de op röntgen-diffractie gebaseerde structuurmodellen voor de eiwit nucleïnezuur-interacties in TMV, waarin twee van de drie fosfodiësters per manteleiwit monomeer, daadwerkelijk een zoutbrug aangaan met een arginine residu en de derde minder direct gebonden is. Een tweecomponenten analyse van de resultaten verkregen voor stilstaande M13-gels, biedt een aanwijzing dat het ingekapselde DNA-molecuul misschien 83% onbeweeglijke en 17% beweeglijke fosfodiësters zou bevatten. Dit zou nieuw licht werpen op de vreemde verhouding 2,4 : 1 tussen het aantal nucleotides en manteleiwit-monomeren in de faag: als slechts 83% van de fosfodiësters in M13 daadwerkelijk

gebonden is, zouden er bij de nucleoproteïne binding eigenlijk twee (en niet 2,4) fosfodiësters per manteleiwit betrokken zijn. Echter, MAS  $^{31}\text{P}$  NMR-spectra bieden geen aanvullend bewijs voor (noch tegen) een dergelijke hypothese.

In hoofdstuk 5 wordt tenslotte de langzame beweging van M13- en TMV-virusdeeltjes als geheel, onderzocht m.b.v. tweedimensionale (2D-) exchange  $^{31}\text{P}$  NMR-spectroscopie. Geen van de 2D-exchange  $^{31}\text{P}$  NMR-spectra van 30% TMV vertoont enige spectrale intensiteit buiten de spectrum-diagonaal. Dit duidt erop, dat TMV nog minder beweeglijk is, dan de toch al lage schatting (3 Hz) in hoofdstuk 3 op basis van transversale relaxatie doet vermoeden. De verschillende 2D-exchange  $^{31}\text{P}$  NMR-spectra voor 30% M13 kunnen slechts op een consistente manier verklaard worden m.b.v. een continue (log-Gaussische) distributie van diffusiecoëfficiënten tussen de 1 en de  $10^3$  Hz. Inhomogene beweging zou het gevolg kunnen zijn van de neiging van de staafvormige virussen om aan elkaar te klitten en zo clusters van verschillende groottes te vormen. Met behulp van dezelfde distributie van coëfficiënten en een geringe bijdrage aan de transversale relaxatie door interne nucleïnezuurbewegingen, kan een nog betere simulatie van transversale relaxatie verkregen worden, dan op basis van het homogene bewegingsmodel van hoofdstuk 3. Het relatief inkrimpen van de  $\sigma_{22}$ -discontinuïteit op de spectrum diagonaal bij langere wachttijden kan niet met langzame virus beweging worden verklaard, maar is mogelijk het gevolg van beperkte homonucleaire spindiffusie tussen naburige fosforkernen, die minder dan 1 ppm in chemische verschuiving van elkaar verschillen.

## Curriculum Vitae

Petrus Cyrillus Methodius Maria Magusin werd op 29 maart 1963 geboren te Nijmegen. In 1981 legde hij het eindexamen Gymnasium- $\beta$  af, waarna hij Scheikunde ging studeren aan de Katholieke Universiteit te Nijmegen. Na het cum laude behalen van zijn fysisch georiënteerde kandidaatsexamen Scheikunde S3, maar tevens uitgebreid met Biochemie, heeft hij twee hoofdvakstages verricht. Tijdens de eerste hoofdvakstage bij de afdeling Biofysische Chemie van prof. dr. C.W. Hilbers, heeft hij onderzoek gedaan naar de binding van het cytostaticum Bleomycine aan DNA m.b.v. UV/Vis spectroscopie en  $^1\text{H}$  NMR-spectroscopie. Tevens was hij betrokken bij het opzetten van 2D-heteronucleaire  $^1\text{H}$  -  $^{15}\text{N}$  NMR-experimenten. Zijn tweede hoofdvakstage Biochemie bij prof. dr. H.P.J. Bloemers betrof de bepaling van de nucleotidevolgorde van een DNA-fragment van 2400 baseparen, dat in het humane genoom vlak naast het zogenaamde fcs-gen, een proto-oncogen, gelegen is. Tijdens zijn studie was Magusin twee jaar secretaris van de Scheikunde-onderwijscommissie en drie jaar lid van de sectieraad Scheikunde. In 1987 werd het doctoraalexamen afgelegd.

Van december 1987 tot december 1991 verrichtte hij als Onderzoeker-in-Opleiding in dienst van de Stichting van Biofysica (NWO), het onderzoek, dat aan dit proefschrift ten grondslag ligt. Het onderzoek werd uitgevoerd bij de door prof. dr. T.J. Schaafsma beheerde vakgroep Moleculaire Fysica van de Landbouwniversiteit te Wageningen. Onder begeleiding van dr. M.A. Hemminga, bestudeerde Magusin intacte virusdeeltjes van de bacteriofaag M13 en het plantenvirus TMV met behulp van vaste-stof  $^{31}\text{P}$  NMR-spectroscopie. Een deel van de analyse en interpretatie van de resultaten werd uitgevoerd in 1992.

Van april 1993 tot en met mei 1994 werkte Magusin als vervangend dienstplichtige en stagiair bij de hoofdafdeling Midden- en Oost-Europa van het ministerie van Economische Zaken. Als lid van de Nederlandse delegatie in het Beheerscomité was hij betrokken bij de hulpprogramma's van de Europese Unie voor Midden- en Oost-Europa. Vanaf maart 1995 is Magusin werkzaam als post-doc medewerker bij de vakgroep Physikalische Chemie van prof. dr. ir. W.S. Veeman van de Universiteit van Duisburg in Duitsland.